ABSTRACT

Title of Document: PREDICTION OF HEAT TRANSFER AND
                      PRESSURE DROP OF CONDENSING
                      REFRIGERANT FLOW IN A HIGH ASPECT
                      RATIO MICRO-CHANNELS

                      Ebrahim AL-Hajri, Doctor of Philosophy, 2009

Directed By: Professor, Michael Ohadi, Department of
                      Mechanical Engineering

This thesis presents a detailed study of parametric characterization of two-phase condensing flow of two selected refrigerants R134a and R-245fa in a single water-cooled micro-channel of 0.4 mm X 2.8 mm cross-section (0.7 mm hydraulic diameter and 7:1 aspect ratio) and 190 mm in length. To avoid flow mal-distribution associated with typical micro-channel tube banks, a single micro-channel was fabricated utilizing an innovative approach and used for the present study experiments. The study investigated the effects of variations in saturation temperature ranging from 30 ^{o}C to 70 ^{o}C, mass flux from 50 to 500 kg/m^{2}s, and inlet super heat from 0 ^{o}C to 15 ^{o}C on the average heat transfer and overall pressure drop coefficient of the micro-channel condenser. In all cases the inlet vapor quality was kept at 100% quality (saturated vapor) and the outlet condition was always kept at 0% quality (saturated liquid). Accuracy of the fabricated channel geometry with careful design

and choice of instrumentation of the test setup resulted in energy balance and average heat transfer coefficient uncertainties within +/-11% and +/-12%, respectively. It is observed that saturation temperature and mass flux have a significant effect on both heat transfer coefficient and overall pressure drop coefficient, where as the inlet super heat has little effect. This study provides further understanding of the potential micro-scale effects on the condensation phenomenon for the tube geometry and the dimensions investigated in the present study combined with flow visualization study. No previous study has addressed the unique single micro-channel geometry being investigated in the present work combined with the two-phase flow visualization of the flow regimes in the present micro-channel geometry. The letter was a major undertaking of the present work and represents one of the main contributions of the present work. The results of the present work shall prove useful in contributing to better understanding of any micro-scale effects on the condensation flow of the two selected refrigerants (one commonly used high pressure refrigerant, R134a) and the other a new low pressure refrigerant (R245fa). It is also expected that the results of this study will lead to future work in this area, realizing the fast penetration of the micro-channel technology in various compact/ultra compact heat exchangers, including refrigeration, petrochemical, electronics, transportation, and process industries.

PREDICTION OF HEAT TRANSFER AND PRESSURE DROP OF
CONDENSING REFRIGERANT FLOW IN A HIGH ASPECT RATIO MICRO-
CHANNELS

By

Ebrahim S AL-Hajri

Dissertation submitted to the Faculty of the Graduate School of the
University of Maryland, College Park, in partial fulfillment
of the requirements for the degree of
Doctor of Philosophy
2009

Advisory Committee:
Professor Michael Ohadi, Chair/Advisor
Professor Reinhard Radermacher
Professor Marino di Marzo
Professor Gary A. Pertmer
Assistant Professor Bao Yang

Dedication

To my parents, my wife and my kids for their sacrifices, support and unconditional

love.

Acknowledgements

Table of Contents

List of Tables

List of Figures

Nomenclature

$\dot{m}$	mass flow rate, kg/s
A	area, m^2
c	empirical constant
C_o	dimensionless parameter defined by Shah for the density ratio model
c_p	specific heat, j/kg ^{o}C
D_h	hydraulic diameter, m
f	friction factor, dimensionless
F_{den}	viscosity correction factor for rotameter, dimensionless
G	mass flux, kg/m^{2}s
g_g	gravitational acceleration, 9.81 m/s^2
h	heat transfer coefficient, kg/m^{2}K
k	thermal conductivity, W/m.K
p_c	critical pressure, psi
p_{red}	reduced pressure, P_{sat}/p_c
Pr_l	Prandtl number of liquid, dimensionless
P_{sat}	saturation pressure, psi
Q	total heat transfer, W
q''	heat flux, W/m^2
Re_l	Reynolds number assuming all mass flowing as liquid, dimensionless
T	temperature, ^{o}C
x	quality, dimensionless
Z	dimensionless parameter defined by Shah for the reduced pressure model
z	horizontal direction
ΔP	pressure drop, kPa
R	the R value indicates how well the model fits the data in regression analysis, dimensionless
f_o	friction factor for adiabatic two-phase, dimensionless
S	slip ratio, dimensionless
V	velocity, m^2/s
n	tube roughness, dimensionless
f_{int}	interfacial friction factor, dimensionless
a, b, c & d	empirical constants in Churchill equation (5.62)
F, H, E, Z & W	parameters defined by Cavallini
j_v	superficial vapor velocity, dimensionless
A_{SM}	property coefficient used in the Smith (1969) fraction equation (6.2)

Greek Letters

δ	liquid film thickness, m
ε	vapor void fraction
ε_h	homogenous void fraction, dimensionless
ε_{ra}	Rouhani-Axelsson void fraction
μ	dynamic viscosity, N s/m^2
ρ	density, kg/m^3
ρ_{fl}	Density of float material, kg/m^3
τ	wall thickness
Φ	two-phase pressure drop multiplier, dimensionless
φ	two-phase, notation
χ_{tt}	Martinelli parameter
ϵ	error of regression analysis, dimensionless
Γ	Chisholm property coefficient, dimensionless
β_o	intercept term in regression analysis, dimensionless
βp	unknown parameters in regression analysis, dimensionless
σ	surface tension, N/m
α	void fraction, dimensionless
Ψ	surface tension parameter, dimensionless
e	energy, Joule

Subscripts and Superscripts

avg	average
dens	density
des	design (or manufacturer calibration) condition of rotameter scale e.g. water at temperature of 20 ^{o}C
f	friction
g	gravitational
l	liquid
m	momentum
n	empirical constant
ref	refrigerant
sat	saturation
th	Theoretical calculation (at measurement conditions)
tp	two-phase
v	vapor
evap	evaporator
lo	liquid only flows in the tube
vo	vapor only flows in the tube

CHAPTER 1: INTRODUCTION

1.1 *Background*

Many technologies, including the oil and gas, HVAC, energy generation, and chemical processes rely on innovative techniques to improve system performance and to reduce or eliminate harm to the environment. One significant area of innovation in these industries has been the introduction of micro-fluidics and micro-based heat exchangers, which can introduce substantial savings in weight and volume of the devices, leading to saving the high cost of materials and shipping costs as well as reducing the carbon foot print. The benefits of micro-based heat exchangers and energy devices have driven researcher to develop a foundation of understanding of micro-scale transport phenomena, particularly in micro-scale flow. Researchers have been studying flows inside micro-channels for over 100 years and they have recorded the advantages over conventional tubes and channels; however, microfabrication technologies at the commercial scale have appeared only in the last couple of decades. The need for microfabrication technologies was driven by the need for miniaturization of system components while enhancing the system performance; this need has increased substantially especially in electronics, micro-reactors, and micro-fuel cell and space/aerospace applications. The drive to miniaturization of systems is redirecting research and development from the macro-scale to the micro-scale. Researchers in this field have been reporting some significant outcomes especially in multi-phase processes (Bergles, et al. 2003). However, the fundamental

understanding of fluid flow and heat transfer in complex two-phase flow systems is still far from being well understood.

Existing empirical results of two-phase flows in micro channels are often limited to out dated refrigerants and/or highly uncertain data. To design accurate micro-devices, it is necessary to know the behavior of the fluid flow and values of the transport parameters as precisely as possible (Bontemps 2005). A considerable amount of research has been performed on the evaporation phenomena in micro-channels, but relatively research has been directed on condensation in micro-channels. One might argue that these two phenomenon are based on similar physics. However, the fact that in condensation nucleation sites are not present, this fact alone can cause substantial changes in the physics.

In recent years the phenomenon of condensation in micro-channels has been investigated by several researchers: J. Thome (2003), S. Garemilla (2003, 2004 and 2005), R. Cavallini (2002), Cohlmen, R. L. Webb (1998), M. Zhang (1999 and 2001), and Wang et al. (1999 and 2002) to name a few. Some of these researchers have focused only on the heat transfer aspect of the condensation, while others have reviewed the pressure drop part of the phenomena, while still others have looked at both. They have also evaluated different channel sizes and shapes using a wide range of fluids. However, only a few have examined condensation in high aspect ratio micro-channels. In addition, the majority of the studies have been done on multiple channels where flow mal distributions can occur.

1.2 Objectives of the Present Study

Condenser design using micro-channels requires a great understanding of both heat transfer coefficient and pressure drop for condensation in micro-channels. Therefore, this study was carried to fulfill these needs. In-line with this need, the current study of the phenomenon in micro-channels was guided by the following objectives:

1) Utilizing an innovative fabrication technique the single high-aspect micro channel needs to be fabricated such that it meets the required objectives for accuracy of the energy balance and heat transfer and pressure drop coefficients.

2) Generate experimental comparisons of heat transfer rates and pressure drops of two-phase flow for two selected refrigerants in a flat plate, single-micro-channel condenser with macro-scale correlations of heat transfer rates and pressure drop.

3) Develop correlations of heat transfer and pressure drop coefficients using the experimental data obtained in this study together with the data obtained in the literature.

4) Use two different refrigerants that are commercially available as the working fluid to conduct experiments.

5) Determine whether or not there is any deviation in heat transfer and pressure drop trends when compared to macro-scale, conventional tubes, and if there is, quantify it.

6) Through flow visualization experiments provide a better understanding of the condensation phenomena in the current high-aspect ratio micro channel. This represented a major undertaking and was the first study of its kind based on available literature.

1.3 *Organization of Dissertation*

The thesis is organized into seven chapters. Chapter 1 is a general introduction. Chapter 2 gives a literature review of single-phase and two-phase condensation in micro-channels. The experimental setup, fabrication, measurements and instrumentation, data reduction, experimental procedures, and uncertainty analysis are the subject matters of Chapter 3. The choice and comparison of the refrigerants used in this study are also included in Chapter 3, as well as modifications made to the test setup throughout the duration of the investigation to improve the accuracy of the results.

The results of condensation heat transfer coefficient and pressure drops for both refrigerants are presented in Chapter 4. Among other findings the results quantify the effects of mass flux, saturation temperature, and inlet super heat on heat transfer coefficient and pressure drops.

Chapter 5 incorporates the correlations obtained from the literature and explains the physical phenomenon and methodology employed in each correlation. A comparison of the data obtained from experiments with the predictions from the correlations is shown in this chapter.

The classification of visualization results of two-phase flow and two-phase flow regime mapping are discussed in Chapter 6.

The conclusion of this work and suggestions for future work are given in Chapter 7, which is then followed by the references cited in the present work.

CHAPTER 2: LITERATURE REVIEW

2.1 *Condensation in Mini and Micro-Channels*

There is considerable research on the evaporation phenomenon in micro-channels, but there is little on condensation in micro-channels. One might argue that these two phenomena are based upon the same physics. This might be true; however, in condensation nucleation sites are not present and this fact alone can cause substantial changes in the physics of the phenomenon. To design accurate micro-devices, it is necessary to know the behavior of the fluid flow and values of certain key transport parameters as precisely as possible (Bontemps 2005). Therefore, researchers have touched on the issue of condensation for years to accurately quantify the heat transfer coefficient and pressure drop. This section will present some of those investigations, which all seem to agree that heat transfer and pressure drop are very much dependent on the flow regime inside the channel. The objective of this chapter is to document selected relevant previous work and the contributions they have offered, and from there establish the need for the present study and the contributions it offers to the advancement of knowledge for condensation heat transfer and pressure drops in high-aspect ratio micro-channels.

2.1.1 Heat Transfer

Heat transfer in condensing flows in large channels has been evaluated for a long time, but only recently efforts have been made to understand condensation in micro-channels. The existing empirical results of two-phase flows in micro-channels

are limited to out dated refrigerants and, are often subjected to highly uncertain data collection, thus lacking conclusive findings on the basic physics of the phenomena.

Riehl et al. (1998) preformed a literature survey of single-phase and two-phase flow heat transfer coefficients of experimental data obtained for micro-channels and compared them to the available analytical models. The comparisons showed large discrepancies; the models were not able to predict the experimental data. Furthermore, the correlations for micro-channel convective flow also showed wide discrepancies. Riehl et al. (2002) presented experimental results of condensation for miniature systems with restricted heat dissipation areas and using methanol as the working fluid. The experiments were conducted for two different saturation temperatures, a range of heat dissipation rate from 20 to 350 W and four micro-channel condensers with channel diameters between 0.5 to 1.5 mm. All the channels had aspect ratios of 1. They also developed an empirical Nusselt number correlation that was able to predict 95% of their data within a 25% error band.

Garimella et al. (2003 and 2005) experimentally evaluated different shapes and sizes of micro and mini-channels for pressure drop and heart transfer of a condensing flow. The channels hydraulic diameters ranged from 0.4 to 5 mm for qualities ranging from 0% to 100% and mass fluxes between 150 kg/m^{2}s and 750 kg/m^{2}s. They developed a model for pressure drop that was able to predict 90% of the measured data within 28% error band; however, as the model depends on flow visualization information, which is not often practical for use as a general correlation for condenser design.

El Hajal et al. (2003) studied condensation of 15 different fluids amongst which were pure refrigerants and refrigerant blends. The tests were conducted at 40 $^{\circ}$C saturation temperature and mass fluxes ranging from 16 to 1532 kg/m^{2}s and the tube diameter ranging from 3.14 to 21 mm. They used the studies of evaporating refrigerants of Kattan et al. (1998-I; 1998-II; 1998-III) to develop a flow regime map and a heat transfer model. They defined several regimes, namely bubbly flow, intermittent, annular, stratified wavy, fully stratified and mist. They claimed that heat transfer occurred due to two types of mechanisms: film condensation and convective condensation. Their correlation for heat transfer coefficient was governed by the interfacial friction factor, the Prandtl number and the Reynolds number.

Baird et al. (2003) experimentally investigated local heat transfer coefficient of condensation inside 0.92 mm and 1.95 tube diameters. Then developed a model that agreed with their experimental data more than other models by using a simple shear-driven annular flow model to predict the condensation heat transfer coefficient.

Other researchers (Kim et al. (2003) and Wang et al. (2002)) suggested that the condensation phenomenon in mini-channels may differ from that in macro-channels. Kim et al. (2003) found that the existing heat transfer correlations fell short in predicting their experimental investigation data of R134a condensing inside a single round tube with an inner diameter of 0.691 mm. At low mass fluxes the disagreement was more obvious. The existing correlations that Wang et al. (2002) tested over-predicted the heat transfer in a horizontal rectangular multi-channel condenser of 1.46 mm hydraulic diameter.

2.1.2 *Pressure Drop*

The correlations of condensation pressure drop developed by Lcokhart and Martinelli (1949), Chisholm (1973), and Friedel (1979) are being used to this day. The majority of the newly developed pressure drop correlations in condensation are based on these models or compared against them. However, these correlations do not represent the actual phenomena due to the assumptions that were made to develop these correlations in the first place; these assumptions lead to large inaccuracies in estimating the actual pressure drop inside the channel. For example, Lockhart and Martinelli (1949) developed the Martinelli multiplier, which relates the pressure drop of only liquid flowing inside the channel to the pressure drop of only vapor flowing inside the channel. This assumption does not take into account the pressure drop due to the interaction of the two-phases; nor does it take into account the pressure drop due to deceleration caused by the change in density of the liquid.

Cavallini et al. (2002) and Mitra (2005) have improved on the Friedel correlation, which uses liquid only two-phase multiplier, by modifying the empirical constants and the exponents. Cavallini et al. (2002) investigated condensation of R123a, R125, R410a, R32, R236ea and R22 inside a round tube with 8 mm inner diameter while varying mass flux from 100 to 750 kg/m2s. The study was intended to improve Friedel's (1979) correlation in the annular regime. They also used the dimensionless vapor velocity to distinguish between the different flow-regimes that exist in condensation. New constant were fitted to Friedel's correlation from the study of the annular regime and due to the insignificant effect of gravitational forces in the annular flow regime, the Froude number was not accounted for in the two-phase

multiplier correlation. However, these predictions cannot be applied at flow transitions.

Chen et al. (2001) conducted experiment of pressure drop using air-water in 1.02, 3.17, 5.05 and 7.02 mm tube diameter and using R410a in 3.17, 5.05, 7.02 and 9 mm diameters. In an attempt to fit their data, they modified the Friedel pressure drop correlation by adding a two-phase multiplier. They also modified the exponent of both the Webber number, which account for surface tension, and the Bond number, which accounts for mass flux. Their correlation predicts the data with an average deviation of 87%.

Zhang and Webb (2001) conducted pressure drop studies on circular channels of diameter 3.25 mm and 6.25 mm and a multi-port heat exchanger of hydraulic diameter of 2.13 mm. They concluded that the dependent of Friedel (1979) correlation on Webber and Froude number is weak; therefore, they modified the Friedel (1979) correlation by using the reduced pressure definition rather than the ratios of density and viscosity, then they were able to predict the data.

Wheeler et al. (1993) compared two-phase and single-phase flows for space applications. Their experiments were carried out on a reduced gravity aircraft. The scope of their test was to record the annular flow pressure drops at acceleration levels close to 0.05 g, in a tube with an inner diameter of 10.41mm and a length of 1.251m. The data they collected for 0.05 g acceleration could not be predicted by the 1.0 g acceleration models.

In their study of pressure drop, Wilson et al. (2003) recommended the use of a circular tube liquid only two-phase multiplier correlation of Jung and Radermacher

(1989). They studied the effect of aspect ratio by flattening an 8.91 mm diameter circular tube. Their correlation uses the definition of the turbulent Martinelli parameter, which cannot be used in this study because the flow inside the channel is laminar in all the testing conditions. Wilson et al. (2003) concluded that pressure drop increases as the channel approaches a rectangular shape.

Based on experimental adiabatic data of air-water of an upward flow in vertical tubes with diameter ranging from 1 to 4 mm, Mishima and Hibiki (1996) developed a modified Lockhart and Martinelli–Chisholm constant C as a function of inner diameter. The correlation was in a good agreement with the transition criteria of Mishima and Ishii (1984).

Lee and Lee's (2001) study of pressure drop of air-water flows in rectangular tubes showed the dominant effect of surface tension. They modified the Chisholm parameter to include the effects of the ratio of viscous and surface tension, the ratio of liquid viscosity to density effect, and the effect of the slug Reynolds number. Garimella et al. (2005) used Lee and Lee's (2001) non-dimensional surface tension parameter to develop a pressure drop model for dispersed/mist/annular flows. The model also included an interfacial friction factor correlation and the liquid-phase Reynolds number. The predicted results were in a good agreement with Garimella et al. (2005) experimental results.

Souza et al. (1993) developed a correlation for two-phase pressure drop by conducting experimental investigation on a horizontal tube with 10.9 mm diameter using R123a and R12 as the working fluids. The two-phase multiplier that was used

was based on the mixture quality, the Martinelli parameter (the turbulent liquid film and turbulent vapor core definition of Martinelli parameter), and the Froude number.

Zhang and Kwon (1999) developed a pressure drop correlation using the two-phase liquid-only multiplier. Their model was developed based on Friedel correlation, where they modified the Friedel correlation to fit their data, and then they replaced the property groupings with the reduced pressure and applied theoretical limits of the mixture.

Tran et al. (2000) investigated flow boiling of R134a, R12 and R113 inside circular tubes with diameters of 2.46 and 2.92 mm and inside a rectangular tube (4.06 mm x 1.7 mm) with mass fluxes ranging from 69 to 704 kg/m^{2}s. They compared their experimental results of the annular region with large tube correlations. They noted that most of the correlation under-predicted their results. They related the increase of pressure drop in small channels to the additional friction related to the bubbles that were confined, elongated, and that slide over a thin liquid due to the size of the channel. They further noted bubble movements in the large tubes were less confined. They used the two-phase Martinelli parameter to correlate their experimental pressure drop. Then they introduced the confinement number N_{conf} (the ratio of surface tension to buoyancy forces) that was defined by Cornwell and Kew (1993), in their correlation. Only then they were able to fit their data well with the correlation.

Garimella et al. (2005) presented a multiple flow-regime model for pressure drop during the condensation of refrigerant R134a in horizontal micro-channels. They measured two-phase pressure drops in five circular channels ranging in hydraulic diameter from 0.5 mm to 4.91 mm. In each test, pressure drop measurements were

first taken over the entire range of qualities from 100% vapor to 0% vapor for five

different refrigerant mass fluxes between 150 kg/m^{2}s and 750 kg/m^{2}s. With the data

available, they were able to develop a comprehensive model that addresses the entire

progression of the condensation process from the vapor phase to the liquid phase. The

correlation even included the overlap and transition regions between the respective

regimes using interpolation technique. The model over-predicts their data by 35% on

average.

2.1.3 *Flow Visualization*

It is known that both heat transfer and pressure drop are dependent on the flow

regime that exists inside the channels. Therefore, many investigators have studied the

flow inside the channels using visualization techniques to help improve their models

and also to understand this complicated phenomenon better. The majority of these

investigations have resulted in flow regime maps. Some of the early developed

theoretical models to determine flow regime transition in two-phase flow for large

tubes are those developed by Baker (1954) and Mandhane (1974), Taitel and Dukler

(1976), and Weisman et al. (1979). Baker (1954) used air-water and air-oil data to

develop the first two-phase flow regime maps for large tubes. He used superficial

liquid mass flux times a fluid property scaling factor on the horizontal axes; whereas

for the vertical axes he used the vapor superficial mass flux times another fluid

property scaling factor. Mandhane et al. (1974) also developed a map using more than

5900 air-water data points in horizontal large tubes. Instead of the superficial mass

fluxes used by Baker (1954), they used superficial liquid velocity in the vertical axes

and superficial vapor velocity in the horizontal axes.

Suo and Griffith (1964) investigated flow regimes in small diameter tubes and capillaries. They used air-water, helium-heptane, nitrogen-water and nitrogen heptane fluid pairs to study elongated bubble flow in small tubes with diameters ranging from 1 to 1.6 mm. By using a dimensionless bubble velocity and the ratio of average liquid volume flow rate to the total volume flow rate, they were able to define the transition from slug flow to annular flow and bubbly slug flow.

Griffith and Lee (1964) investigated the transition from annular to slug flow in a capillary tube with 1 mm diameter. They proposed that surface tension forces at the liquid-vapor interface pull the interfacial liquid waves in the annulus towards the tube center that eventually block the vapor passage, and hence form slugs.

Taitel and Dukler (1976) used the Lockhart-Martinelli parameter in the horizontal axis and a modified Froude rate times a transition criteria on the vertical axes to develop a theoretical flow regime map for gas-liquid mixtures for horizontal and near-horizontal pipe flow. They were able to define five basic flow regimes: smooth-stratified, wavy stratified, intermittent (slug and plug), annular with dispersed liquid and dispersed bubble.

Breber et al. (1980) conducted experimental investigation of condensing flow of R11, R12, R113, steam and n-Pentane inside circular tubes with diameters ranging from 4.8 to 50.8 mm. They developed a flow regime map based on the condensation data and defined four different regimes: annular and annular mist, bubble, wavy and stratified and slug and plug flow in their flow regime map. They used the Martinelli parameter and the superficial gas velocity to determine the transition from one regime

to another. They compared their experimental results with Taitel and Dukler's (1976) work showing a good agreement, except at small diameters.

Troniewski and Ulbrich (1984) investigated two-phase flow patterns of air and sugar-water mixtures in rectangular channels with hydraulic diameter ranging from 7.4 to 13.3 mm in vertical and horizontal orientations. In vertical channels, they observed bubble, plug-slug, annular, and mist flow patterns. In horizontal channels, bubble, plug-slug, stratified, wavy, semi-annular, annular, and mist flow patterns were observed. They proposed geometry correction factors based on the single phase velocity profiles in rectangular channels to the co-ordinate axes on the Baker (1954) map.

Steiner (1993) used quality on the horizontal axis and mass flux on the vertical axis to develop his flow regime map. This type of flow regime maps is widely used by researchers now a day (Thome et al. (2003), El Hajal et al. (2003), Garimella et al. (2003) and Garimella (2004)). However, some of these researchers noted that more than one flow regimes seem to exist near the boundaries when using this type of flow regime maps.

Coleman and Garimella (1999) and Triplett et al. (1999) conducted studies on tube diameter and shape effects on flow patterns and flow regime transitions for air-water flow in small diameter channels with diameters ranging from 1.3 to 5.5 mm. They noted regimes such as bubble, dispersed, elongated bubble, slug, stratified, slug-annular, wavy, annular wavy, and annular. They concluded that tube diameter and surface tension are important parameters that should be considered when determining flow patterns and transitions but their study did not consider fluid properties.

Yang and Shieh (2001) study of flow patterns for the refrigerant R134a and air-water mixtures at adiabatic conditions in horizontal tube with diameters ranging from 1 to 3 mm and concluded that the transition from slug to annular flow occurs earlier in the air-water case and that flow regime transitions are affected by surface tension.

Coleman and Garimella (2000-I, 2000-II and 2003) identified wavy, intermittent and dispersed flow regimes in their study of condensation inside round and square tubes channels with hydraulic diameter ranging from 1 to 5 mm, using R134a as the condensing fluid. They extracted equation for transition criteria and concluded that the intermittent and annular flow regime areas in their flow regime map increases as the tube diameter decreases, while the wavy flow regime disappears gradually.

El Hajal et al. (2003) and Thome et al. (2003) developed a flow pattern map for condensation based on a prior map developed for evaporation by Kattan *et al.* (1998-I; 1998-II; 1998-III). The flow regimes they identified were: fully-stratified, stratified-wavy, intermittent, annular, mist and bubbly flow. The flow map incorporates a new definition of the logarithmic mean void fraction: for high reduced pressures, the homogeneous void fraction model is proposed; at low reduced pressures, the model by Rouhani and Axelsson (1970) is used. For intermediate pressures, both models were combined to obtain a logarithmic mean void fraction. The flow map was built on a data bank of twenty different fluids (including R410A and R404A), with reduced pressures ranging from $0.02 < P_r < 0.8$ and tube diameters

ranging from 3.14 to 21.4 mm. This study was also used to develop a new heat transfer model.

Recently, Jassim and Newell (2006) developed a unique flow map based on probabilistic void fraction model for R410A, R134a, and air water in 6-port micro-channels at 10 $^{\circ}$C saturation temperatures, qualities from 0 to 100%, and mass fluxes varying from 50 to 300 kg/m^{2}s. In their probabilistic model they defined time fractions models and pressure drop models for each existing regime, and then they multiplied the corresponding time fraction to the pressure drop model of each regime to obtain the predicted overall pressure drop. Then they developed a flow regime map with the vapor quality on the x-axes and the time fraction on the y-axes. The probabilistic flow map models developed were found to accurately predict void fraction and pressure drop for the entire quality range and for all three fluids.

2.1.4 Summary

In summary the literature review above, presents a wide range of studies of flow condensation in macro, mini and micro-scale channels. From the above reviews it is clear that some of the researchers focused only on the heat transfer aspect of the condensation, while others reviewed the pressure drop part of the phenomena, while some looked at both. They also evaluated different channel sizes and shapes using a wide range of fluids. However, few or even none have examined condensation in high aspect ratio micro-channels. In addition, the majority of the heat transfer coefficient and pressure drop measurement studies were done on multiple channels (bank of channels) where flow mal distributions can occur, which introduces flow instability. This present work, therefore, provides a comparison of condensing R134a and

R245fa heat transfer and pressure drop coefficients in a micro-channel with hydraulic diameter of 0.7 mm and an aspect ratio of 7:1. Additionally the present work conducted flow visualization experiments that are vitally important to the better understanding of the flow fluid and heat transfer mechanisms in the channel. A brief summary of the literature review presented in this chapter is given in Table 2-1. It is obvious from the comparison in the table that so far no study of heat transfer coefficient and pressure drop including flow visualization and flow mapping for a micro-channel with aspect ratio 7:1 has been carried.

Table 2-1 Summary of reviewed literature

Researcher	Channel Type	Fluid	D_h (mm)	T_{sat} (^{o}C)	G (kg/m^{2}s)
Breber et al. (1980)	Circular	Steam, n-Pentane, R-11, R-12 and R-113	4.8 to 22	-	17 to 990
Cavallini et al. (2002)	Circular	R-123a, R-125, R-410a, R32, R-236ea and R22	8	-	100 to 750
Coleman and Garimella (1999)	Rectangular and circular	Air-water	1.3 to 5.5	52	50 to 750
Coleman and Garimella (2000-I; 2000-II and 2003)	Rectangular, square and circular	R-134a	1 to 4.91	-	150 to 750
Dobson and Chato (1998)	Circular	Near-azeotropic belnds of R-32/R-125, R-12, R-22 and R-134a	3.14 to 7.04	35 to 60	25 to 800
El Hajal et al. (2003)	Circular	15 different fluids	3.14 to 21	40	16-1532
Garimella et al. (2003 & 2005)	Micro & mini channels	R-134a	0.4 to 5	52	150-700
Kim et al. (2003)	Circular	R-134a	0.691	-	200 to 600
Lee and Lee (2001)	Rectangular	Air/water mixture	0.4 to 4	-	-
Mitra (2005)	Circular	R410a	6.22 and 9.4	-	200 to 800
Riehl et al. (1998) & (2002)	Micro-channel	Methanol	0.5 to 1.5	-	-

Researcher	Channel Type	Fluid	D_h (mm)	T_{sat} (^{o}C)	G (kg/m^{2}s)
Shah (1979)	Circular	R11, R12, R22, R113, Methanol, ethanol, benzene, toluene and tricholoroethylene	7 to 40	11 to 211	7 to 40
Suo and Griffith (1964)	Circular	Air-water, helium-heptane, nitrogen-heptane and nitrogen-water	1 to 1.6	25	-
Tandon et al. (1982)	Circular	Steam, R-113 and R-12	4.8 to 15.9	-	-
Tran et al. (2000)	Circular and rectangular	R113, R12 and R134a	2.46, 2.92 and (4.06x1.7)	-13 to 127	69 to 704
Triplett et al. (1999)	Circular, rectangular and semi-triangular	Air-water	1 to 5.5	-	50 to 750
Troniewski and Ulbrich (1984)	Rectangular	Air/Sugar water	7.4 to 13.3	25 to 35	200-1600
Yang and Shieh (2001)	Circular	Air-water and R134a	1 to 3	25-30	300-1600

CHAPTER 3: EXPERIMENTAL APPARATUS AND PROCEDURE

The present work expands upon the recent studies in our Smart and Small Thermal System (S2TS) laboratory involving design, fabrication, instrumentation and characterization testing of novel micro-channel heat exchangers including micro-channel evaporators, gas coolers and condensers with applications in refrigeration/HAVC and related industries. Experiments for the current study were carried out in an experimental loop consisting of the test section module, a coolant loop with accessories, and a data acquisition system. The experiments were conducted for the parametric ranges listed in Table 3-1 for two different refrigerants to investigate the effect of superheating, saturation temperature and mass flux on average heat transfer coefficient and overall pressure drop.

Table 3-1 Experimental parametric study table

Test	$T_{ref\text{-}sat}$	Mass Flux kg/m^{2}s	Superheating	Remarks
1		200	0 C	Study effects of superheating
2			5 C	
3			10 C	
4			15 C	
5		300	0 C	
6			5 C	
7	50 C		10 C	
8			15 C	
9		50	0 C	Study effects of mass fluxes
10		100		
11		200		
12		300		
13		400		
14		500		
15		50	10 C	
16		100		
17		200		
18		300		
19		400		
20		500		
21	30 C	200	0 C	Study effects of saturation temperature
22	40 C			
23	50 C			
24	60 C			
25	70 C			
26	30 C		10 C	
27	40 C			
28	50 C			
29	60 C			
30	70 C			
31	30 C	300	0 C	
32	40 C			
33	50 C			
34	60 C			
35	70 C			
36	30 C		10 C	
37	40 C			
38	50 C			
39	60 C			
40	70 C			

3.1 *Test Section Design and Fabrication*

3.1.1 *Refrigerant loop*

The experimental set-up along with associated instruments was assembled in a way that heat losses were minimal as per requirement of the project. A schematic diagram of the test facility is shown in Figure 3-1. The testing apparatus consist of

two loops: (1) the refrigerant loop and; (2) the water-chilling loop. The refrigerant loop consists of a high precision Coriolis flow meter, variable-speed gear pump, a pre-heater, a heater (evaporator), a test section (condenser), a reservoir, and a sub-cooler. The refrigerant is circulated by the gear pump with precise flow rate control and then is passed through a flow meter where the refrigerant flow rate is measured. The use of a gear pump instead of a compressor allows testing a pure refrigerant without the influence of the oil leakage from the compressor. This is especially important in order to accurately quantify the heat transfer coefficient and pressure drop in the micro condenser. It is also convenient to set and adjust small mass flow rates of the refrigerant across a broad range.
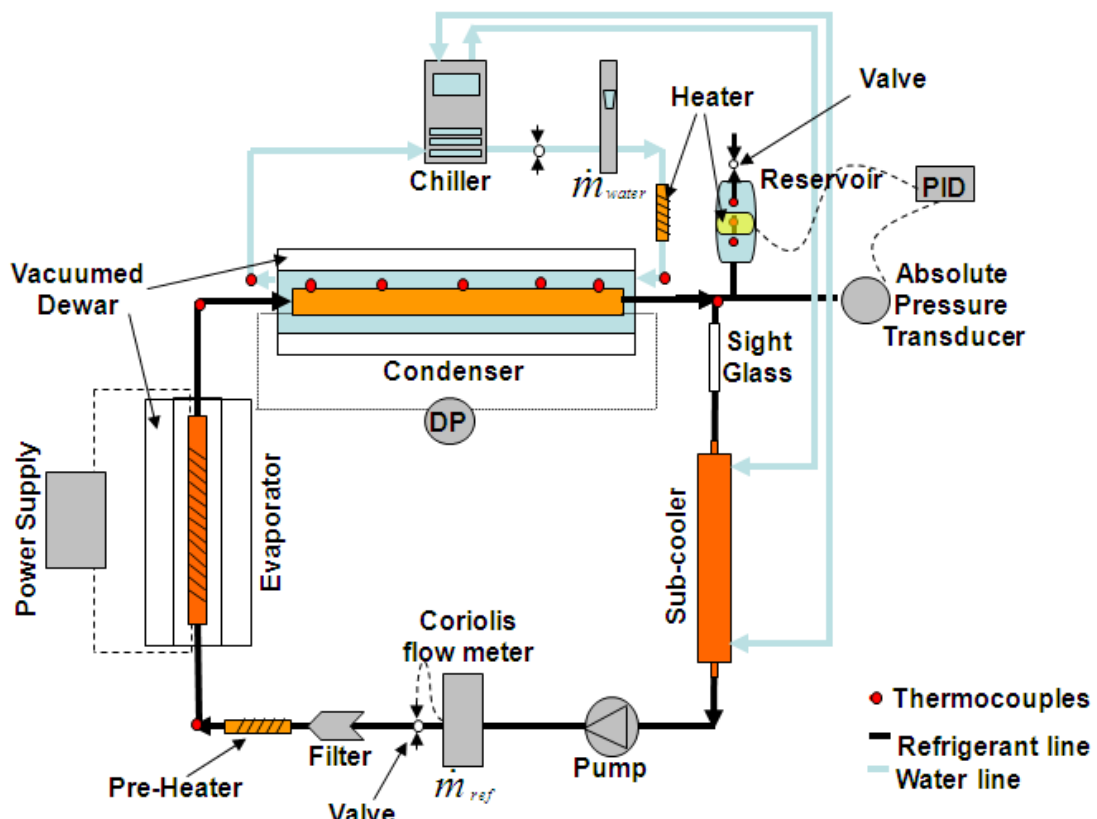
Figure 3-1 Schematic of experimental test setup

Figure 3-2 depicts segmental pictures of the experimental loop set-up before assembling. The insulation of Dewar cylinders shells consist of two concentric glass cylinders with diameters of 1 in. (25.4 mm) and 2 in (50.8 mm) with a high vacuum between the walls. The condenser and evaporator Dewars span to the length of the condenser channel and evaporator tube, respectively. In addition, the inner cylinder of the condenser Dewar acts as a water jacket. The vacuum is expected to provide good insulation from the heat loss or gain. Figure 3-3 shows the details of the Dewar insulations used. A copper elbow connects the Dewar cylinders; the elbow has Kapton ® heater patches controlled by a PID temperature controller, which maintains the surface temperature of the elbow equal to that of the inlet refrigerant, thus minimizing heat losses from the inlet T-connection acting as an adiabatic thermal shield.
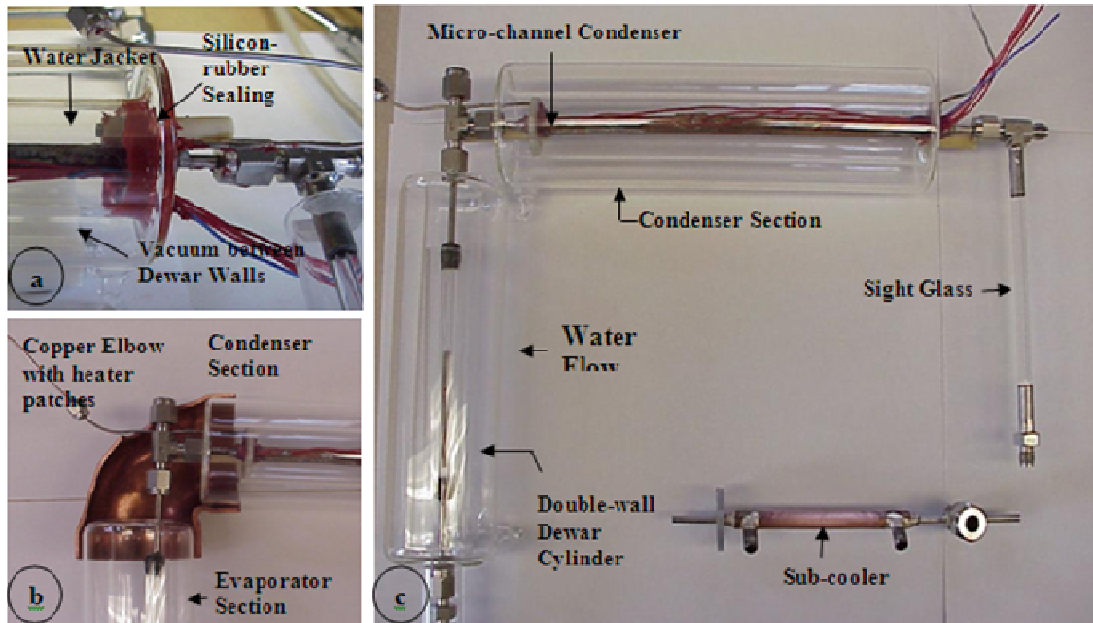
Figure 3-2 Details of test section: (a) details of the joint between condenser section and sight-glass (b) details of the joint between evaporator Dewar and condenser Dewar (c) view of the arrangement of various parts in the refrigeration loop.
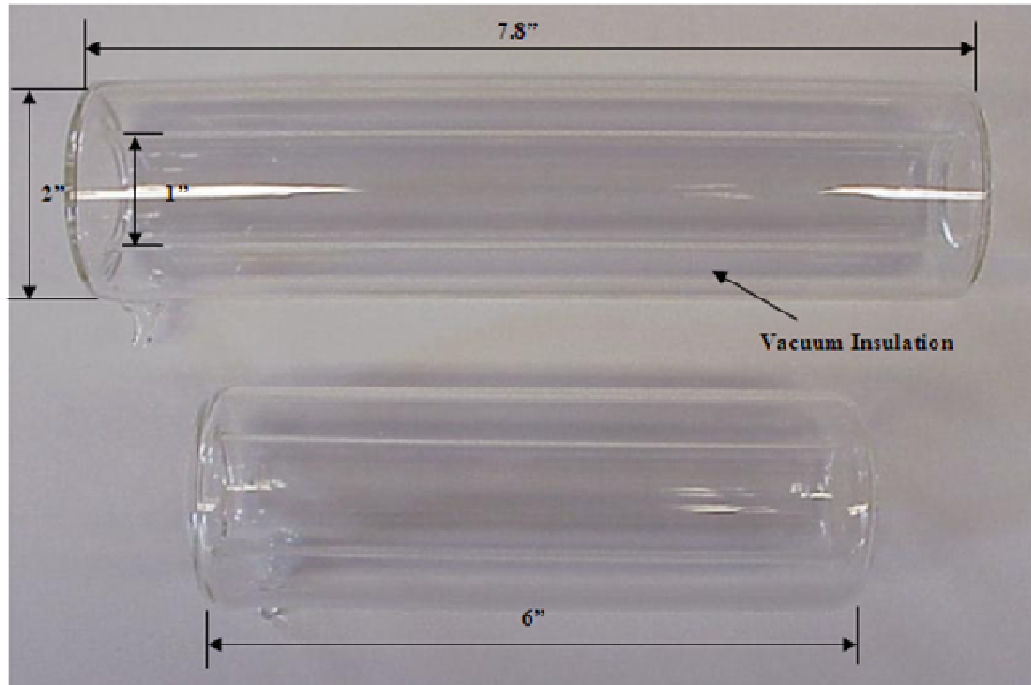
Figure 3-3 Details of test section: (a) details of the joint between condenser section and sight-glass (b) details of the joint between evaporator Dewar and condenser Dewar (c) view of the arrangement of various parts in the refrigeration loop.

Since the inlet temperature to the evaporator is very sensitive to room temperature, change is room temperature throughout the day causes the inlet temperature to change. To control the inlet temperature, a pre-heater was installed prior to the evaporator inlet. The pre-heater controls the evaporator inlet temperature from fluctuating, where the refrigerant coming from the gear pump is sub-cooled.

The evaporator consists of a copper tube with a resistance wire wound around the tube from the outside. By adding the desired amount of heat, the desired inlet quality can be achieved.

When vapor refrigerant enters the test section, the heat exchange between the refrigerant and the cooling water takes place resulting in condensation of the refrigerant. A Data Acquisition System (DAS) collects the experimental data. The

state of refrigerant at the outlet of the test section is controlled to achieve the thermodynamic zero quality state.

A reservoir is located between the condenser outlet and the sub-cooler. When the refrigerant enters the liquid reservoir/separator, vapor (if it exists) is collected and only liquid is allowed to leave the pump. Two electrical heaters are attached on the outer surface of the liquid reservoir. The heaters, along with proper setting of the water loop, help to set and adjust the operating pressure of the test loop. A Watlow ® PID controller is installed in the system as a means of pressure stabilization. The controller receives a 0-5 Volt output signal from the absolute pressure transducer, this determines the corresponding system pressure and controls the power input to the heaters on the reservoir, thereby controlling the system pressure by adjusting the reservoir temperature.

After saturated liquid refrigerant passes through the sub-cooler to become sub-cooled liquid, it is pumped by the gear pump and another round of circulation starts.

Pressure transducers and thermocouples were installed in the test loop to determine the conditions of the refrigerant at each section. The readings were then collected and stored by the DAS.

3.1.2 Water loop

The water loop was used to cool both the micro condenser and the sub-cooler. It consisted of a refrigerated bath/circulator with a pump that supplied flow to the condenser water jacket and the sub-cooler. The bath/circulator was used to provide constant water flow at the designated test conditions. For water flow rate measurements, a highly accurate capillary water flow meter was used to decrease the

overall error of the data. Two such flow meters—one for the low flow range and the other for the high flow range—were constructed and used in the system. Figure 3-7 and Figure 3-8 are the experimentally derived calibration charts for both the water flow meters. The low-flow water flow meter was calibrated using a calibrated gear-micro-pump, and the high-flow meter was calibrated by the timed mass-measurement technique. Accurate RTDs were installed at the beginning of this investigation to measure water temperatures at the inlet and outlet of each water jacket. However, some inconsistencies were found using the RTDs. (See Section 3.4.1.4)

3.2 *Micro-channel Design and Fabrication*

Three different micro-channels were designed and fabricated for this study one of which was used to conduct a study of heat transfer coefficient and pressure drop of a fully condensed flow, and also for a study of pressure drop of constant quality flow. The other two channels were used for visualization purposes.

The micro-channel test section that was used to study the heat transfer coefficient and pressure drop was fabricated from a pure, long copper block. Copper was chosen as the channel material because of its high thermal conductivity, k, which could minimize axel conduction. This was then verified by using the results collected in this study and found out that the axel conduction was less than 1% of the heat transferred from the four other surfaces of the micro-channel. In addition, the cross-sectional area of the micro-channel tube was very small compared to the heat transfer surface that was used to calculate the heat transfer coefficient.

A slitting hacksaw in a milling machine was used to construct a 190 mm long micro-channel, 2.8 mm height and 0.4 mm width on the long copper block. The

channel was constrained with 1.0 mm thick walls from all four sides, which created the cross-sectional area 11.52 mm^2 where as the heat transfer area was 1064 mm^2. This machining technique provided an accurate geometry and minimum surface roughness along the length of the channel. The channel roughness was measured and found to be less than 3 micron. For the inlet and outlet of the condenser, two 1/8" (3.2 mm) holes were drilled at each. Two short stainless steel tubes were inserted in the holes. In addition, a 1/16" (1.6 mm) holes was constructed at each end of the channel, for pressure drop measurements. Then, the channel was filled with jeweler's wax and the top surface was scraped flat and chemically cleaned as a preparation for electroplating the of channel. Next, the three inactive faces were painted with a nonconductive paint to resist deposition during electroplating. Then the top of the wax-filled portion was painted with a thin strip of silver solution to make it electrically conductive. The channel was then submerged into a copper-sulfate solution to be plated to the desired thickness on the remaining open surface of the channel. After electro-plating, the wax in the channel was melted and drained by heating the channel. The channel was then chemically cleaned to remove traces of wax or silver paint. On the outer surface of the channel, five single constantan wires and one copper wire were braised to act as T-type thermocouples. The fabricated copper micro-channel is shown Figure 3-4 below. For a more detailed description of the fabrication process of this micro-channel see Sourav et al. (2008).
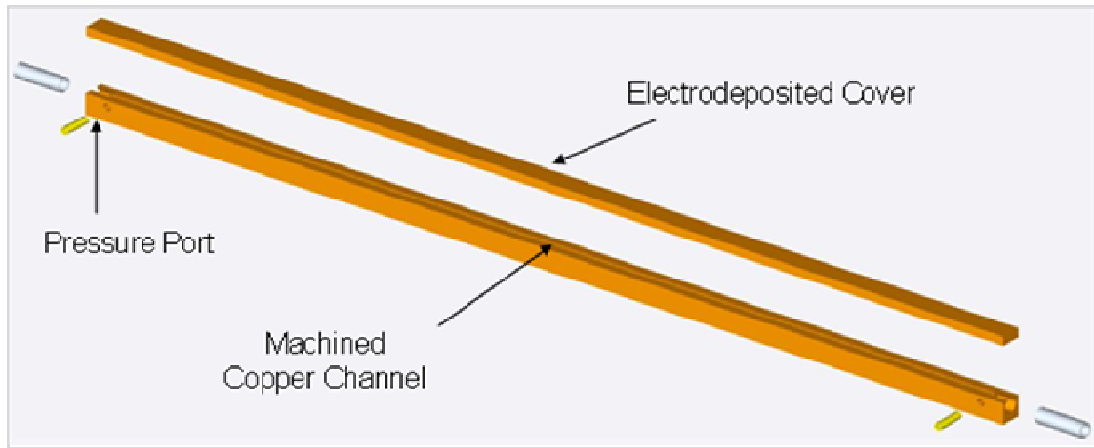
(a)
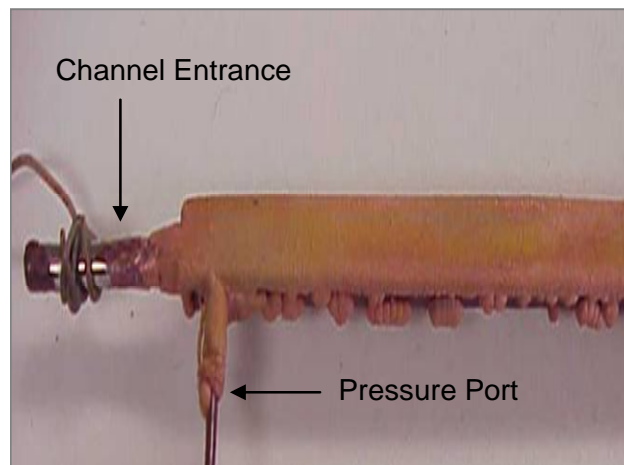
(b)

Figure 3-4 (a) A drawing of the fabricated micro-channel (b) Electroplated micro-channel

The other two micro-channels that were used in visualizations were also made from copper. These channels were relatively shorter than the channel shown above to allow the camera to view the entire length of the channel from a close distance. Since the channel had a high aspect ratio (7:1), it was interesting to view the two-phase flow from each side of the channel cross-sections. Therefore, the two channels had different viewing windows. One of the channels was fabricated on a copper plate by using a milling machine. With very precise measurements a channel with 25.4 mm length, 0.4 mm height and 2.8 mm width was constructed on the copper plate, Figure

3-5. The 2.8 mm width was the open side of the channel, which was used as the viewing window. Then 1/8" holes were drilled on the back side of the copper plate to provide the inlet and outlet ports. Also a grove was machined around the channel to house the gasket to seal the channel. A rubber gasket was then positioned in the grove where a glass plate was placed on top of the channel, which was followed by an aluminum plate that acted as a clamp to sandwich the parts together to form the channel. A 1/8" copper tube was then soldered on the back of the copper plate which acted as the coolant side
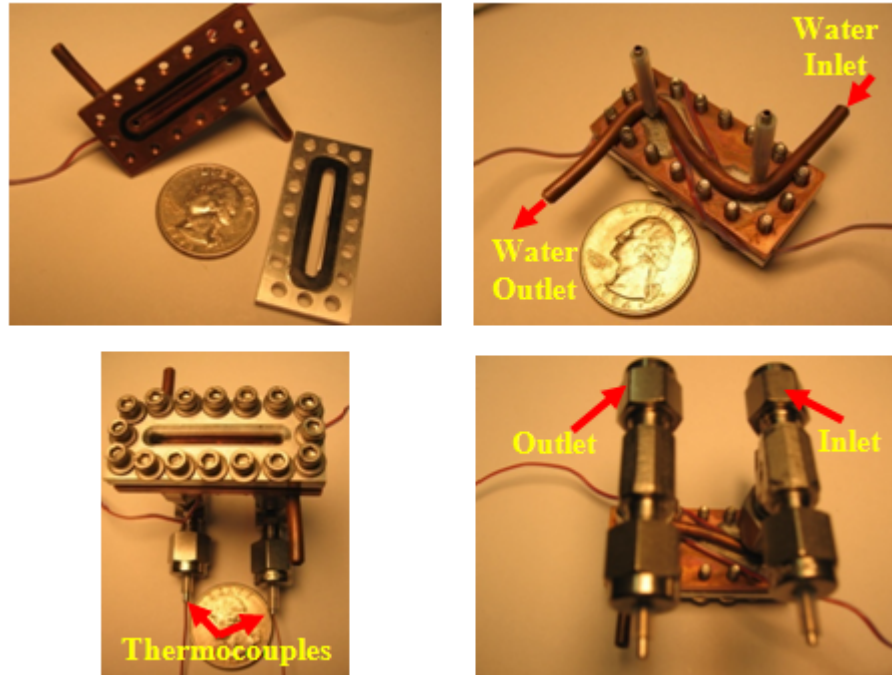
Figure 3-5 Visualization test section with viewing window of 2.8 mm

The second visualization channel was constructed on a copper-rod with 1/8" diameter using EDM (wire machining). First two parallel-flat-surfaces were machined on the outer surface of the copper-rod using a milling machine, shown in Figure 3-9. Then two holes at each end of the copper-rod were drilled to provide the inlet and outlet orifices of the channel. Next, two 1/8" diameter copper tubes were cut to the

desired length and bent into a U-shape form. The bottoms of the U-shaped tubes were flattened using a milling machine. Subsequently, the flattened surfaces of the U-shaped copper tubes were aligned with the flat-surfaces on the copper-rod one copper tube on each side of the copper-rod. In other words, the copper-rod was placed in the middle and the U-shaped copper tubes were placed one on each side of the rod. The U-shaped copper tubes and the copper-rod were then soldered to the condenser where the U-shaped tubes acted as the coolant sides. Then the top and bottom of the bundled U-shaped tubes and rod were flattened as well. A 1/32" hole was then drilled ¼" away from one of the copper-rod ends. The hole was constructed to allow the insertion of the EMD wire. Using the EMD wire machining, a channel with a length of 19.05 mm, a height of 2.8 mm and a width of 0.4 mm was constructed through the copper rod. The 0.4 mm width was the opening of the channel which was used as the viewing window. Then, two groves were made around the channel one on each side (top and bottom) to house the gasket. After the gaskets were put in place two glass plates were attached to the condenser from each side (top and bottom) and then using two aluminum clips the micro-channel, the two gaskets and the two plate glasses were sandwiched together to form the second visualization channel.
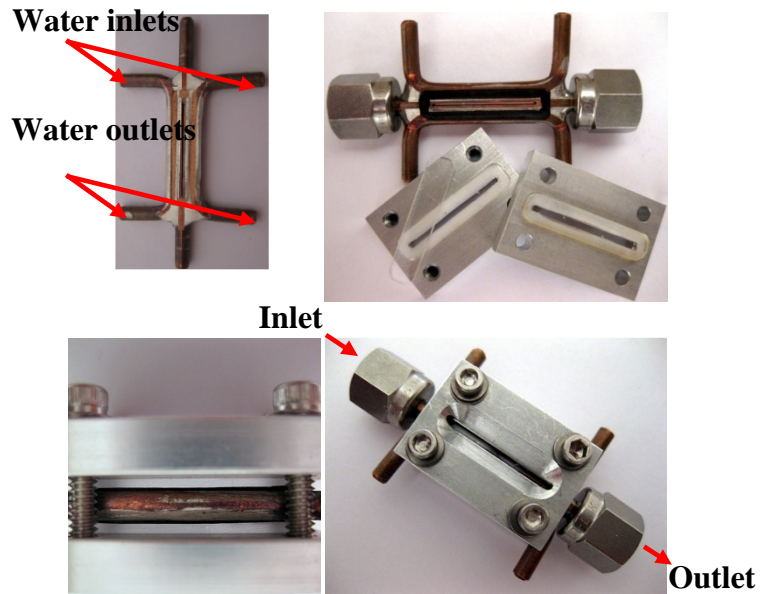
Figure 3-6 Visualization test section with viewing window of 0.4 mm

3.3 *Testing Refrigerants*

Initially, this work was supported by the American Society of Heating, Refrigeration and Air-Conditioning Engineering (ASHRAE). The work statement suggested to use two different refrigerants in this investigation where R134a was chosen by ASHRAE to be one of the refrigerants and the second refrigerant choice to be made was left for the Project Investigator. R245fa was chosen by our research group to be the second refrigerant. R245fa was chosen because it is a replacement of outdated refrigerants and because it has a slightly better heat transfer coefficient than R134a, as shown in Table 3-2. R245fa has a different density and surface tension than that of R134a, which provides a wide enough band of difference in parametric ranges explored in this investigation and their respective effects on both heat transfer and pressure drop coefficients.

Table 3-2 Comparison of refrigerants properties

	T_{sat} (^{o}C)	P_{sat} (kPa)	Conductivity (mW/m.K)		Viscosity (µPa.s)		Density (kg/m^3)		Enthalpy (kJ/kg)		Surface Tension (mN/m)
			liquid	vapor	liquid	vapor	liquid	vapor	liquid	vapor	
R134a	30	770	79.0	14.33	185.8	12.04	1187.5	37.53	241.7	414.8	7.42
	70	2116	61.7	20.45	106.4	14.65	996.2	115.6	304.3	428.7	2.61
R245fa	30	179	79.2	12.52	376.4	10.51	1325.1	10.11	239.6	427.5	13.41
	70	610	70.2	14.78	226.8	12.0	1204.7	33.43	295.7	456.6	8.35

3.4 *Measurements and Instrumentation*

To assure that the results are within a maximum error band of 15%, highly accurate instruments were purchased, such as a: gear pump with accurate flow rate reader, absolute and differential pressure transducers, highly accurate water flow meters, PID controllers, and other accessories that collectively could provide such accuracy. In addition, prior to installing all these instrumentations, each of them was carefully calibrated. Figure 3-7 through Figure 3-13 show the calibrations of all the instruments installed in the system. In addition, Table 3-3 provides the ranges and accuracies of various instruments used in the experimental apparatus.

Table 3-3 Range and accuracy of instruments

Measurement /Operation	Range(s)	Instrument	Accuracy
Refrigerant Flow Rate	0.06 – 0.6 gm/sec	Coriolis Flow Meter	3% of rate
Water Flow Measurement	0 – 1.0 l/min	Calibrated Capillary Flow Meter	<1% of FS
Absolute Pressure Transducer	40 – 320 psi & 0-100 psi	Setra 205 Transducer	0.11% of FS (FS: 0 – 500 psi)
Differential Pressure Transducer	0 – 14 kPa (0 – 2 psi)	Validyne DP15-32	0.25% FS
Temperature measurement	0 – 100 ^{o}C	T-type & K-Type Thermocouples	0.1^{o}C
Pressure Stabilization	0 – 5 V input	Watlow Series SD PID Controller	0.1% of FS
Water Cooling	0 – 300 Watts	Neslab Bath/Circulator	Stability: +/-0.01^{o}C

3.4.1   Instruments Calibrations

To assure the accuracy of the data collections, all the instruments,

measurement devices and thermocouples were carefully calibrated.

3.4.1.1 Water flow rate measurement

For measurement of water flow rate, which is critical to reduce error in the

energy balance, two graduated capillary flow meters with short, stainless-steel

capillaries were constructed and calibrated repeatedly by measuring the mass of

steadily flowing water with an accurate electronic balance. Two flow meters were

needed to cover the entire range of coolant water flow needed. Figure 3-7 and Figure

3-8 show the calibration curves for the low- and the high-flow water flow meter,

respectively. The nonlinear trends can be expected due to the entrance effects.
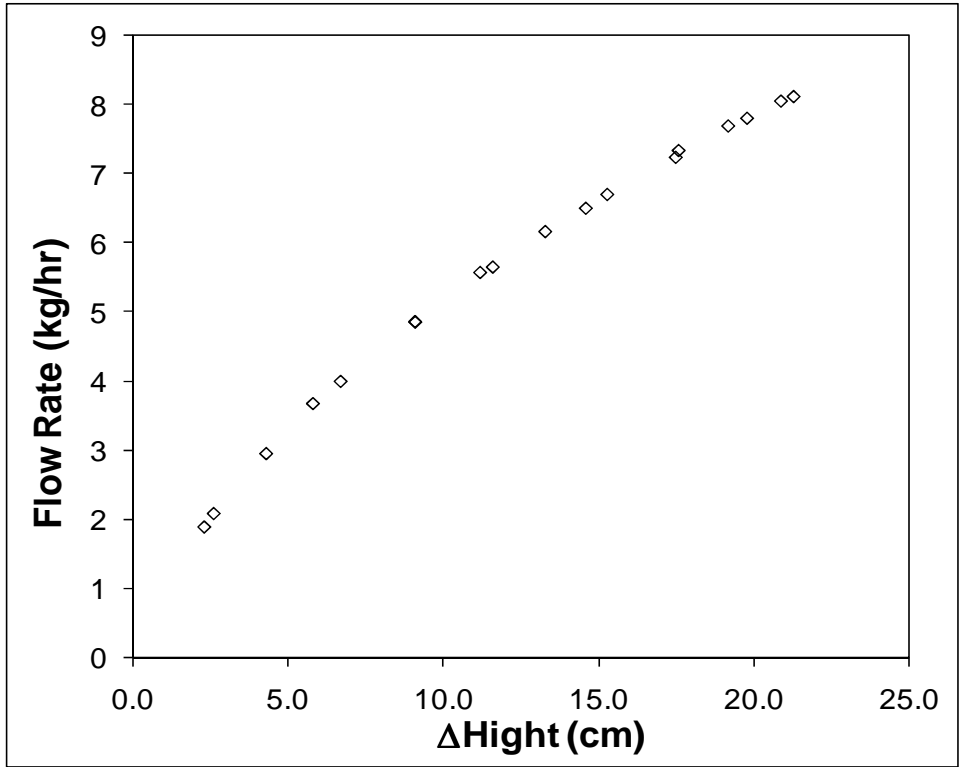
Figure 3-7 Calibration chart for low-flow meter
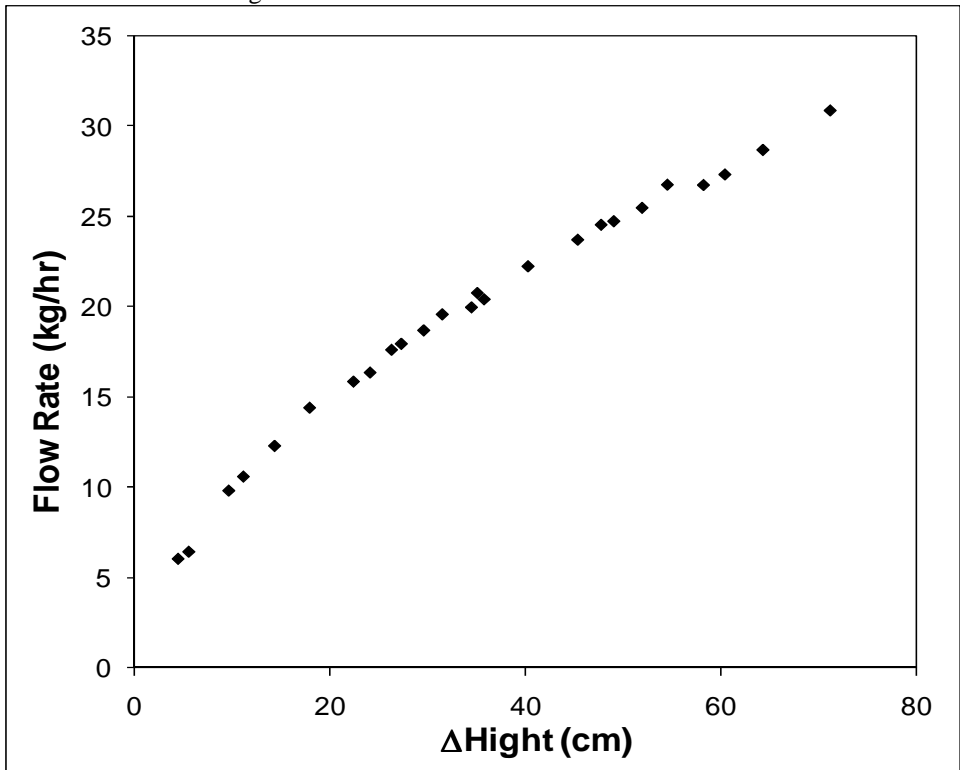
Figure 3-8 Calibration chart for high-flow meter

3.4.1.2 Refrigerant flow rate measurement

In the beginning of this investigation, a micro-pump with an accurate digital read out of flow rate values was used as a flow rate measurement device. However, after completing the full set of test of refrigerant R134a and part of R245fa test, we discovered that the gears of the pump were worn out. The reason for the wear-out and the time that the wear started are unknown. This issue affected the flow rate measurement and, thus, the data results, significantly. Therefore, an alternative pump was combined with a rotameter. The rotameter was calibrated with the pump by measuring the mass of water and time. Then the calibration was converted by a density correction factor relation (Wojtkowiak & Popiel, 1996) to accommodate for the testing fluids used in this study, Eq. (3.1)

$$F_{dens} = \left[\frac{\rho_{des}(\rho_{fl} - \rho_{th})}{\rho_{th}(\rho_{fl} - \rho_{des})} \right]^{0.5} \tag{3.1}$$

Flow rate measurement was still not as accurate as anticipated. Hence, a highly accurate measurement was needed to complete the study, a Coriolis flow meter was purchased from Bronkhorst. The device provided a very precise measurement and control of flow. To minimize the flow rate measurement error, the Coriolis flow meter was chosen to have a maximum flow rate close to our operating maximum flow rate, about 2 kg/hr. The Coriolis flow meter had a maximum flow rate of 5 kg/hr and an accuracy of 1.0% of the reading rate. The Coriolis flow meter was calibrated with water, R134a and R245fa as shown in, Figure 3-9, and then the set of experimental tests was repeated for both refrigerant (R134a and R245fa).
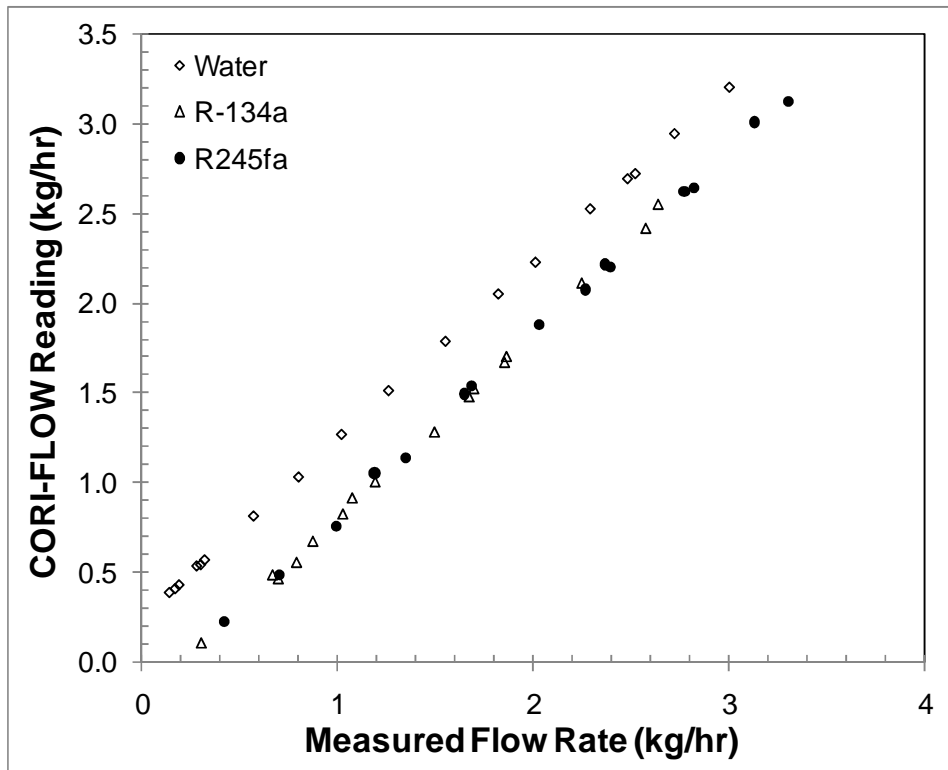
Figure 3-9 Calibration of the Coriolis flow meter with water, R134a and R245fa

3.4.1.3 Pressure measurement

The differential pressure transducer is a bi-directional membrane-type

transducer that was calibrated by a graduated U-tube manometer with water. The

transducer was attached to one end of the U-tube, and the other end was open to the

atmosphere. Water was poured into the U-tube to exert a stable static pressure and the

voltage output was measured by a multi-meter. The transducer port was also reversed

to calibrate for negative pressure. The calibration chart is shown in Figure 3-10.
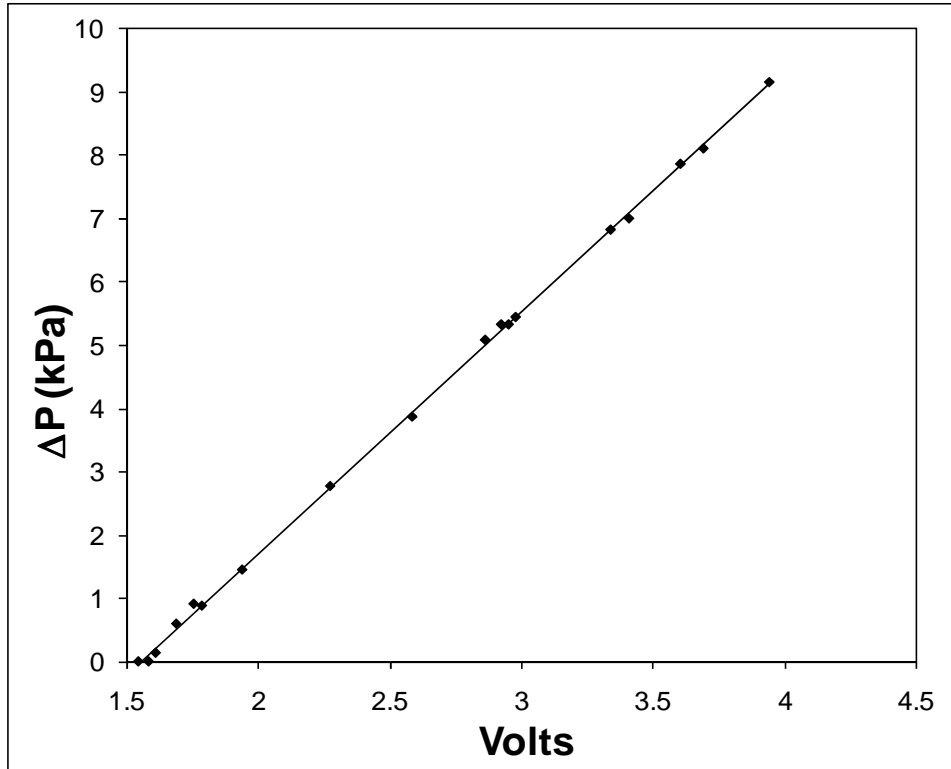
Figure 3-10 Calibration of the differential pressure transducer used for pressure drop measurements

To calibrate the absolute pressure transducer, it was connected to a pressurized air tank and the pressure was slightly increased at each reading of voltage and pressure. Figure 3-11 shows the calibration curve for the absolute pressure transducer.

38
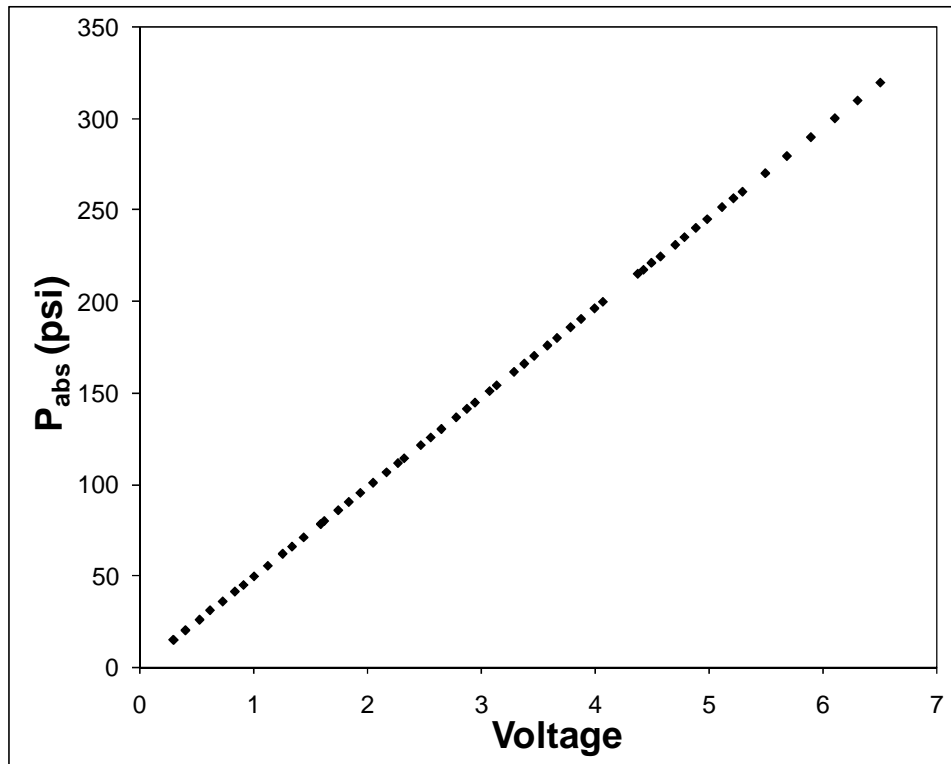
Figure 3-11 Calibration of absolute pressure transducer

3.4.1.4 Temperature measurement

Normally for all temperature measurements, T-type thermocouples are fabricated and calibrated using a high accuracy RTD device (reported accuracy $\pm$ 0.003$^{\rm o}$C) and are believed to be within $\pm$ 0.1$^{\rm o}$C accurate. The energy balance was found to be highly sensitive to the accuracy of temperature measurements, especially the water-side. Therefore, four platinum RTDs each with $\pm$ 0.08$^{\rm o}$C accuracy were tested for cooling water temperature measurement. However the actual error of temperature measurement by RTD was significantly higher than listed and also varied with the fluid temperature, shown is Figure 3-12. Therefore carefully calibrated K-Type thermocouples, shown in Figure 3-13, were finally selected for temperature measurements.

39
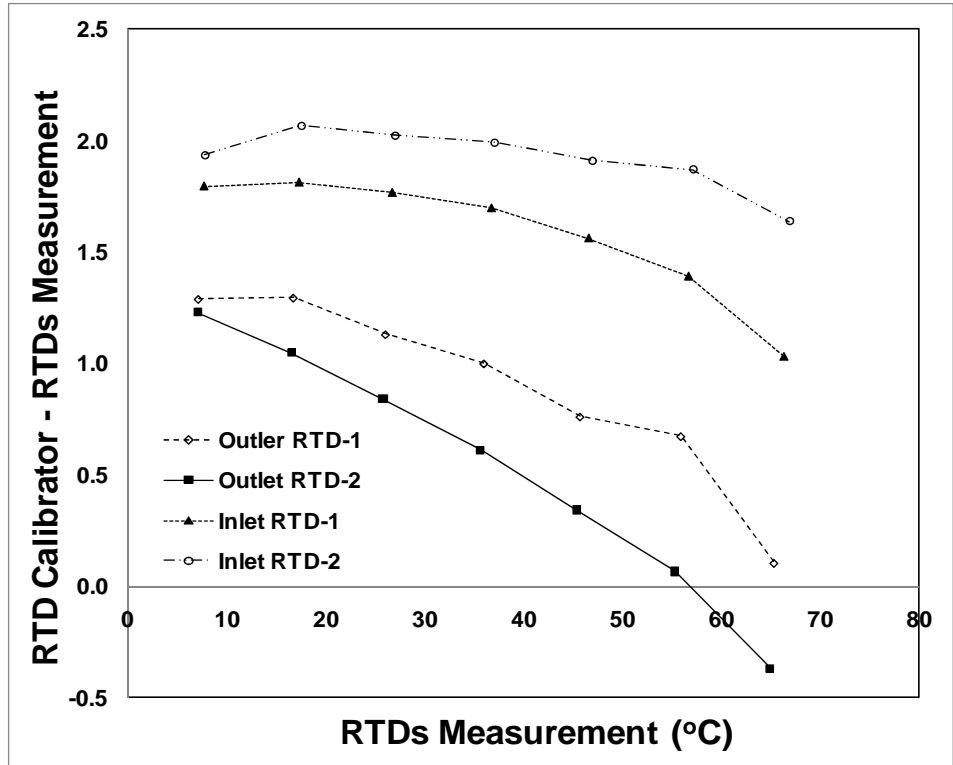
Figure 3-12 Water side RTDs temperature measurements calibration
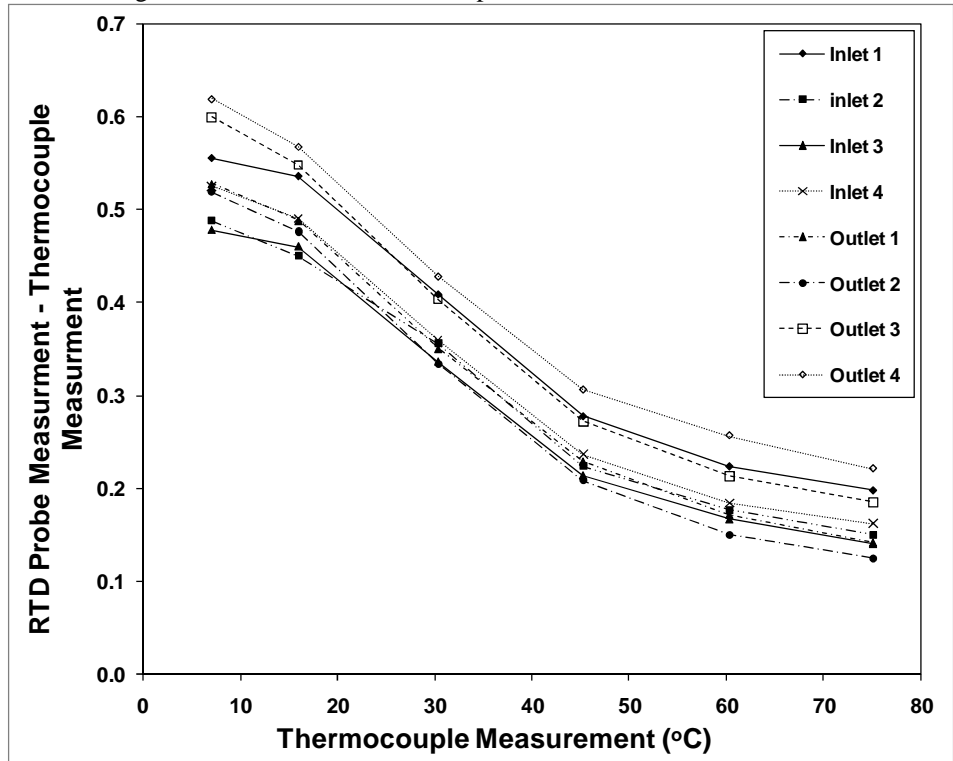
Figure 3-13 Water side thermocouple temperature measurements calibration

3.4.2 Data Reduction

Normally, the process described above took about ½ ~ 1 for atypical experiment. Once the steady state conditions were reached, the DAS began recording signals of temperatures, pressure drops, heating powers, and flow rates. Then the data were taken through the following data deduction process to correct some of the measured values.

The heat transfer coefficient of condensation was calculated by:

$$h_{avg} = \frac{Q_{water}}{A_{channel\ surface}\left(T_{sat,avg} - T_{wall,avg}^{corrected}\right)} \qquad (3.2)$$

Where, $A_{channel\ surface}$ is the total heat transfer surface area of refrigerant side. The water-chilled length was chosen to be the nominal length for the micro condenser to calculate the area, $A_{channel\ surface}$. Therefore, a length of 190 mm was used instead of total micro-channel length of 200 mm. The difference between using these two different lengths is within 2%. $T_{sat,avg}$ refers to the saturation temperature of the refrigerant corresponding to a predetermined system pressure. Considering that the saturation temperature may change slightly due to the possible high pressure drop in the micro channel, this factor was also taken into account by correcting $T_{sat,avg}$ based on the practical pressure drop of refrigerant during the tests. $T_{wall,avg}$ represents the average temperature of the micro-channel walls. The average wall temperature was calculated based on the readings of five single-wires, calibrated, T-type thermocouples, embedded in the outer wall of the micro-channel condenser. Since the $T_{wall,avg}$ is the measurement of average temperature of the outer surface of the channel, then it is corrected as:

41

$$T_{wall,avg}^{corrected} = T_{wall,avg} + \frac{Q_{water}^{''}\tau}{k_{Cu}A_{channelsurface}'} \qquad (3.3)$$

Q is the total heat transfer from the refrigerant to the cold water. This was

determined from an energy balance on the waterside:

$$Q_{water} = \dot{m}_{water}\left(h_{@T=T_{out}}^{out} - h_{@T=T_{in}}^{in}\right) \qquad (3.4)$$

where

$$\Delta h = C_p \Delta T + v\Delta P \qquad (3.5)$$

The pressure drop on the water side was not measured during experiments;

however, when calculated the result was in fractions of Pascal. In addition, the

specific volume of water was relatively small, 0.001 m³/kg, which makes the second

term in the right side of equation (3.5) negligible. This reduces the Q_{water} to:

$$Q = Q_{water} = \dot{m}_{water}C_p(T_{water-out} - T_{water-in}) \qquad (3.6)$$

$\dot{m}_{water}$ refers to the mass flow rate of water entering the test section.

$T_{water-out}$ and $T_{water-in}$ represent temperatures of water at the outlet and inlet of the

water jacket, respectively.

The heat transfer coefficient was calculated based on average refrigerant

saturation temperature, average wall temperature and water-side extracted heat.

3.4.3 Uncertainty Analysis

Based on all the possible measurements and instrumentation errors, an error

propagation scheme was adopted to estimate the uncertainties in the energy balance

e, average heat transfer coefficient h_{avg}, and total pressure drop ΔP. A numerical

program, Engineering Equation Solver (EES®) was used to perform error

propagation, the results of which are summarized below, in Table 3-4:

Table 3-4 Summary of uncertainty

Parameter	Uncertainty/Error
e	± 12 %
h (W/m^{2}K)	± 11 %
ΔP (kPa)	± 5 %

The main sources contributing to the ± 12% uncertainty in energy balance and

± 11% uncertainty in heat transfer coefficient were the flow rate measurements of

water and refrigerant sides, and the thermocouples errors of measurement. In the case

of differential pressure measurement, the uncertainty of ± 5% is essentially the

instrumental error and is a direct measurement of pressure fluctuation.

3.5 *Experimental Procedure*

3.5.1 *Fully Condensed Flow Tests*

Thermodynamic state of condensation – The calculated vapor quality at the

condenser outlet was 0% i.e. the calculated enthalpy at the condenser outlet was equal

to enthalpy of saturated liquid. In this case, at the condenser outlet, vapor bubbles

existed along with sub-cooled liquid, and, if an adiabatic section was provided after

the condenser, eventually the bubbles collapsed to form complete liquid, without

further heat extraction. However, the refrigerant leaving the condenser was sub-

cooled due to pressure drop in the channel. The amount of sub-cooling depended on

the pressure drop on the refrigerant used and flow rate. For example, when R134a is

used as the refrigerant and if mass flux is varied from 300 to 500 kg/m^{2}s, the sub-

cooling ranges from 0.2 to 1.0 ^{o}C. On the other hand, using R245fa as the refrigerant

sub-cooling could reach up to 8 ^{o}C at 500 kg/m^{2}s mass flux. This is mainly due to the surface tension of the refrigerants.

The inlet conditions for all the tests presented in this study were conducted with 100% saturated vapor and based on heat extracted from the water-side: the outlet quality was kept at a calculated value of 0%. Although the vapor quality at the outlet was 0%, bubbles still passed with the flow through the sight section of the test setup.

To start the experimental tests, the refrigerated bath/circulator and the reservoir heaters were first turned on while the cold water was passed through the test section and the sub-cooler cooled down the refrigerant to a desired sub-cooling temperature. The reservoir heaters heated the liquid in the reservoir to reach the desired saturation temperature/pressure of the system. Once the predetermined temperature and system pressure were reached, the gear pump was switched on and the refrigerant was circulated in the test loop. Subsequently, the pre-heater and the evaporator heater were turned on. By adjusting the heaters and the bath-circulator, the system conditions could be set to predetermined values.

The experimental parameters that were controlled during a test were: refrigerant flow rate, water flow rate, refrigerant-side heat input, and water inlet temperature. Each test began with determining the desired inlet conditions such as: the saturation temperature and mass flux. Subsequently the following procedures were followed for an adequate final result:

1. Determine the desired inlet condition to the condenser (i.e. vapor quality or degree of superheat, as may be the case) and desired refrigerant mass flux.

2. Determine prevailing refrigerant saturation temperature (T_{sat}) and sub-cooled evaporator inlet temperature ($T_{evap,in}$).

3. Based on 1 and 2 (above), determine the electrical heat input in the evaporator.

4. In order to achieve condensation, the amount of heat that needs to be extracted and also the corresponding flow rate of water required are calculated, keeping a fixed inlet-outlet water temperature difference at 2.5 °C for all test cases. Keeping a fixed water temperature difference ensures uniformity of data or the error thereof.

5. Apply the heat input and water flow rate obtained from steps 3 and 4 respectively. The only remaining parameter to control thereafter is the water inlet temperature.

6. Increase or decrease the chiller water temperature to achieve condensation (i.e. when water-inlet-outlet temperature difference is monitored to be very close to 2.5 °C).

7. At steady state, monitor T_{sat} and $T_{evap,in}$, go to step 2 and revise the inputs as necessary. By this iterative approach conditions close to desired values can be achieved. Then, at steady state, data is recorded for approximately 20 minutes.

The reason for keeping water-side ΔT at 2.5 °C is that there is a possibility of alteration in the heat transfer behavior due to variation of water-temperature along the flow direction. Any ΔT below 2 °C would adversely affect the uncertainty in calculations.

The average heat transfer coefficient was calculated based on the average refrigerant saturation temperature, average wall temperature and the water-side extracted heat. It was found that the calculated values of the heat transfer coefficient for repeated tests were within ± 5% variation. The energy balance analysis (which includes consideration for instrumental uncertainty) indicates a value of ±11% for low heat-flux cases which are especially vulnerable to heat losses. The uncertainty analysis taking into consideration all errors in individual instrumental and channel dimensions, results in an error of ±12% on the heat transfer coefficient. The main contributing sources to the ±12% uncertainty in heat transfer coefficient were water and refrigerant side flow rate measurements. The measurement of pressure drop was measured by a Validyne DP-15 transducer with 0-34 kPa diaphragm having an accuracy of ± 0.25% of full scale. However, pressure drop was dependent on the existing flow conditions, the regulation of which has an uncertainty. Hence the observed fluctuation in pressures, which was ± 5%, typical in two-phase flows could in turn introduce variation in pressure drop.

3.5.2 Constant Quality Tests

The procedures for the tests that studied the constant quality pressure drop were similar to the test procedures explained above; however, the tests for this study were run under adiabatic conditions. Once heat was applied to the evaporator to obtain the desired quality, the system was kept to run until steady state was reached. Then the data were collected for 20 minutes by the DAS. The data were then

averaged to obtain a single pressure drop point. The tests conditions for this study are characterized in Table 3-5.

Table 3-5 Local pressure drop test matrix

Test Set	Mass flux (kg/m^{2}s)	Saturation Temp (^{o}C)	Quality	Study
1		30	0.1	*Effect of Saturation Temperature*
2		30	0.2	
3			0.3	
4	300	40	0.4	
5			0.5	
6			0.6	
7		50	0.7	
8			0.8	
9			0.9	
10	200		0.1	*Effect of Mass Flux*
11			0.2	
12			0.3	
13	300	50	0.4	
14			0.5	
15			0.6	
16	400		0.7	
17			0.8	
18			0.9	

3.5.3 Visualization Tests

The tests for this part of the study were carried out in a similar fashion to the tests described in section 3.5.2 and for the same testing conditions. However, two different channels were used in the flow visualization study, see sections 6.1.1 and 6.1.2 for detailed description .High-resolutions, high-quality videos were captured for each of the testing conditions shown in Table.

3.5.4 Summary

This chapter presents the design and fabrication of the test sections and the testing facility as well as the calibration curves for all the instruments used in the

testing facility. The chapter also includes a step by step methodology of testing that was use to obtain the data. Data reduction results are also present in this chapter.

CHAPTER 4: RESULTS AND DISCUSSION

4.1 *Heat Transfer and Pressure Drop Results for Fully Condensed Flows*

Experimental tests were conducted in accordance with the parametric ranges listed in Table 3-1. This chapter presents the effects of mass flux, saturation temperature, and inlet superheat on average heat transfer coefficient and overall pressure drop coefficients for the two refrigerants selected as the test refrigerants in this study, R143a and R245fa.

In addition, to assess the impact of various parameters studied on heat transfer and pressure drop coefficients a statistical analysis of the collected data was carried out. An ANOVA[®] regression analysis was used for the statistical study. Regression analysis illustrates the relationship between a single variable for example Y (dependent variable) and one or more independent variables, $X_1,\ldots,X_p$. When p =1, it is called simple regression but when p >1 it is called multiple regression. In this investigation a multiple linear regression model was applied to the data. The general form of this model is:

$$Y = f(X_1, X_2 \ldots X_P) + \epsilon$$

(4.1)

where *f* is some unknown function and ϵ is the error in this representation which is stabilizer in this instance, Faraway J. (2002). $X_1, X_2 \ldots X_P$ are the independent parameters, such that.

$$Y = \beta_0 + \beta_1 X_1 + \beta_2 X_2 + \cdots + \beta_P X_P + \epsilon$$

(4.2)

Where β_0 is called the intercept term. $\beta_1, \beta_2, \ldots \beta_p$ are unknown parameters. The sign (plus or minus) of the regression or β coefficients interpret the direction of

the relationship between the dependent and independent variables. If a β coefficient is positive, then the relationship of this independent variable with the dependent variable is positive; if the β coefficient is negative then the relationship is negative. Of course, if the β coefficient is equal to 0 then there is no relationship between the variables.

Another valuable coefficient to observe when performing such a statistical analysis is R, which is called the correlation coefficient, where R is a way to express the degree to which two or more predictors (independent variables X) are related to the dependent (Y) variable.

In this chapter, it is presented how heat transfer coefficient and pressure drop are affected by several operating parameters and fluid properties. Therefore, the statistical analysis presented in this section will show the magnitude of each of those effects. Then, a general statistical linear equation that represents the relationship between the independent variables (parameters and fluid properties) versus the dependent variables (heat transfer coefficient and the pressure drop) will be presented.

4.1.1 Heat Transfer

4.1.1.1 Effect of Superheat

Figure 4-1 and Figure 4-2 illustrate that as the inlet superheat increases; the average heat transfer for refrigerants R134a and R245fa modestly increases, respectively. This could be because at high degree superheat the length of the annular flow region increases, which would cause more heat to be transferred than the heat transferred at the lower inlet superheat. The heat transfer difference between 0 and 15

^{o}C superheat is insignificant (10-15% of total heat transfer in the channel); and the local heat transfer coefficient at the inlet is significantly high; hence, the "extra" heat due to inlet superheat is quickly absorbed in the initial part of the channel. Since the figure shows average heat transfer, the inlet superheat is not obvious.
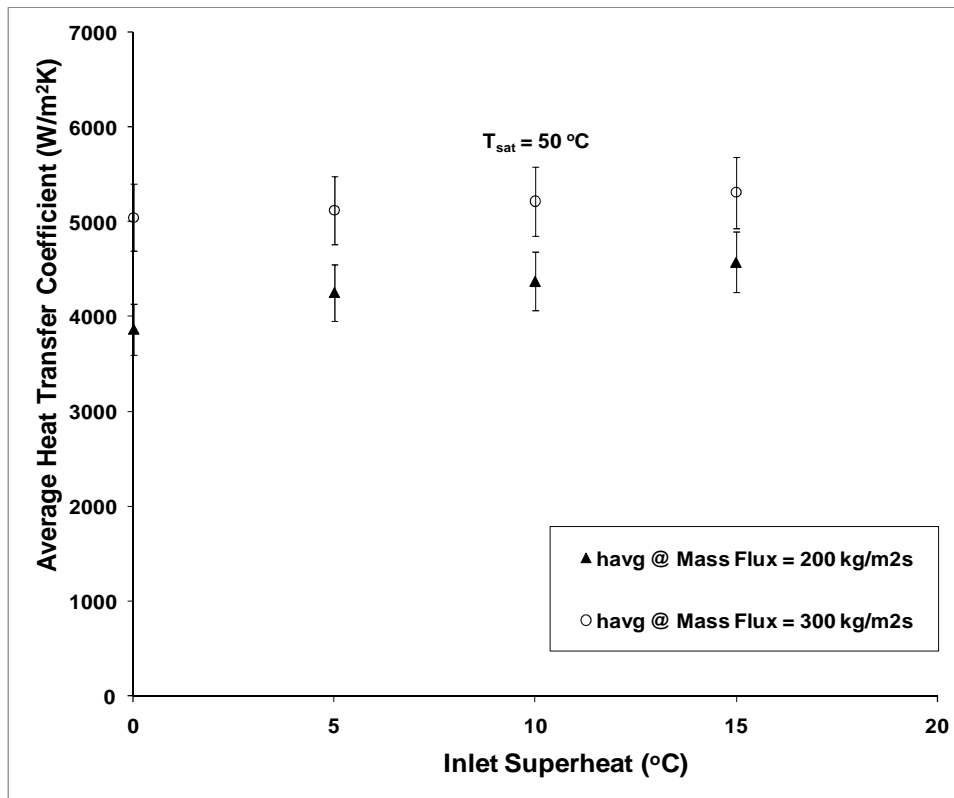
Figure 4-1 Effect of inlet superheat on average heat transfer coefficient at $T_{sat} = 50\ ^{o}$C for R134a
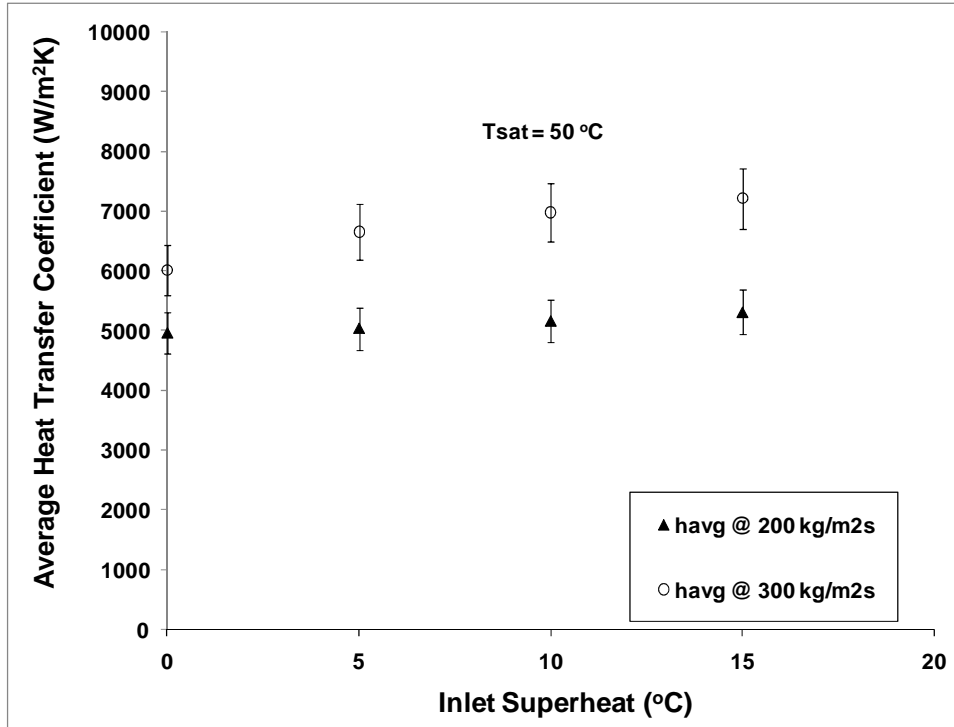
Figure 4-2 Effect inlet superheat on average heat transfer coefficient at $T_{sat} = 50\ ^{o}C$ for R245fa

To verify the above analogy, a simple calculation to find the effective length of the super heated region was preformed. This was achieved by first finding $Q_{superheat}$, which is the amount of heat due to super heat, is defined as follow:

$$Q_{superheat} = \dot{m}_{refrigerant}\left(h_{superheat} - h_{sat\ vapor}\right) \tag{4.3}$$

`The remaining amount of heat after the superheated region can be calculated using the enthalpy of saturated vapor and saturated liquid as follow:

$$Q_{after\ superheat} = \dot{m}_{refrigerant}\left(h_{sat\ vapor} - h_{sat\ liquid}\right) \tag{4.4}$$

Then the total amount of heat equals the amount of heat transferred to the water (equation (3.4)).

$$Q_{total} = Q_{after\ superheat} + Q_{superheat} = Q_{water} \tag{4.5}$$

Then the heat transfer coefficient due to $Q_{superheat}$, $Q_{after\ superheat}$ and Q_{water} can be obtained from the following equations, respectively.

$$h_{superheat} = \frac{Q_{superheat}}{A_{superheat\ surface}\left(T_{superheat} - T_{wall,avg}^{corrected}\right)} \tag{4.6}$$

$$h_{after\ superheat} = \frac{Q_{after\ superheat}}{A_{surface\ after\ superheat}\left(T_{sat} - T_{wall,avg}^{corrected}\right)} \tag{4.7}$$

$$h_{water} = \frac{Q_{water}}{A_{channel\ surface}\left(T_{sat} - T_{wall,avg}^{corrected}\right)} \tag{4.8}$$

By iteration, the surface areas of the superheated region and the remaining region after superheat can be obtained and then the length of the superheated region can be calculated.

As an example, at mass flux of 300 kg/m^{2}s, saturation temperature 50 ^{o}C and superheated temperature of 15 ^{o}C the longest superheated region occurs and equals 10 mm only, where the total length of the channel is 190 mm. This means that at the highest inlet superheat investigated in the present work only 5% of the length of the inter channel length is used for heat transfer that is due to superheat. This confirms that the effect of superheat is insignificant as the data presents.

4.1.1.2 Effect of Mass Flux

Figure 4-3 and Figure 4-4 show the effect of mass flux on average heat transfer for the two refrigerants at a fixed saturation temperature of 50 ^{o}C. This saturation temperature is chosen as the midpoint of the experimental range (30 – 70 ^{o}C). As seen in the figures, the heat transfer coefficient is positively affected by the mass flux for the range of mass flux studied 50 – 500 kg/m^{2}s. This is because as the velocity is increased, the convection effects are enhanced, thus higher heat transfer coefficient. Moreover, the heat transfer coefficient is dominated by the thin-film

condensation process, and when the velocity is increased, the annular flow regime becomes longer, therefore contributing a thinner liquid film which then causes an increase in heat transfer.

When comparing the performance of the two refrigerants in terms of average heat transfer coefficient, it is clear that R245fa has on average 15% better heat transfer than that of R134a. For example, at mass flux of 300 kg/m^{2}s the average heat transfer coefficient of R134a is 5051 W/m^{2}K, compared with 6018 W/m^{2}K, for R245fa.
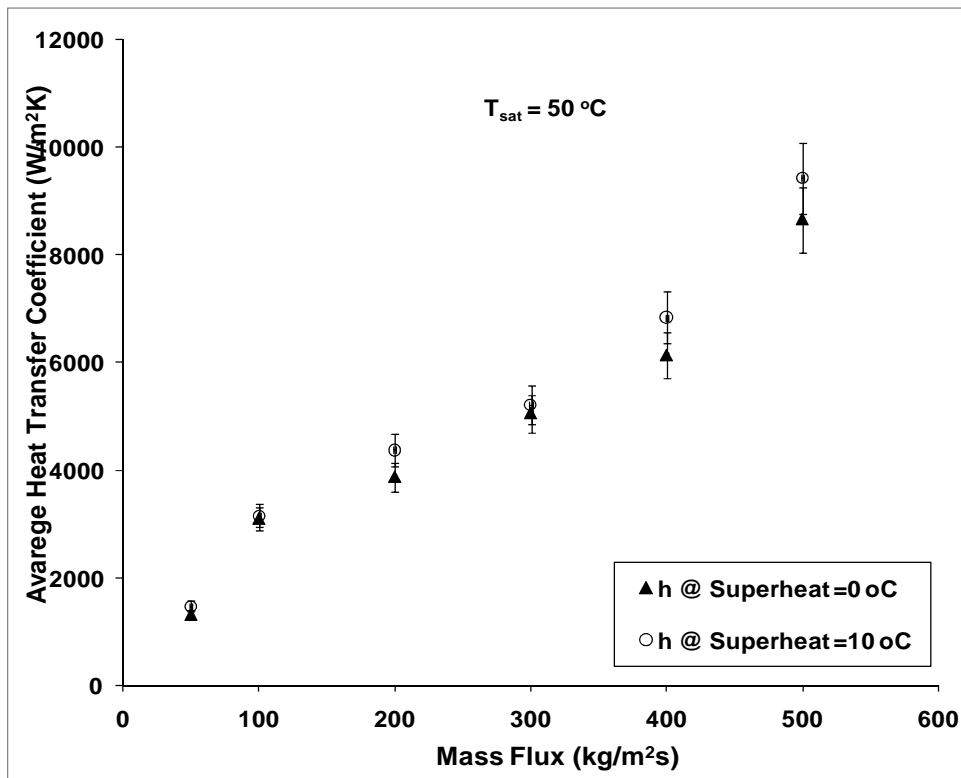
Figure 4-3 Effect of mass flux on average heat transfer coefficient for R134a at T_{sat} = 50 ^{o}C
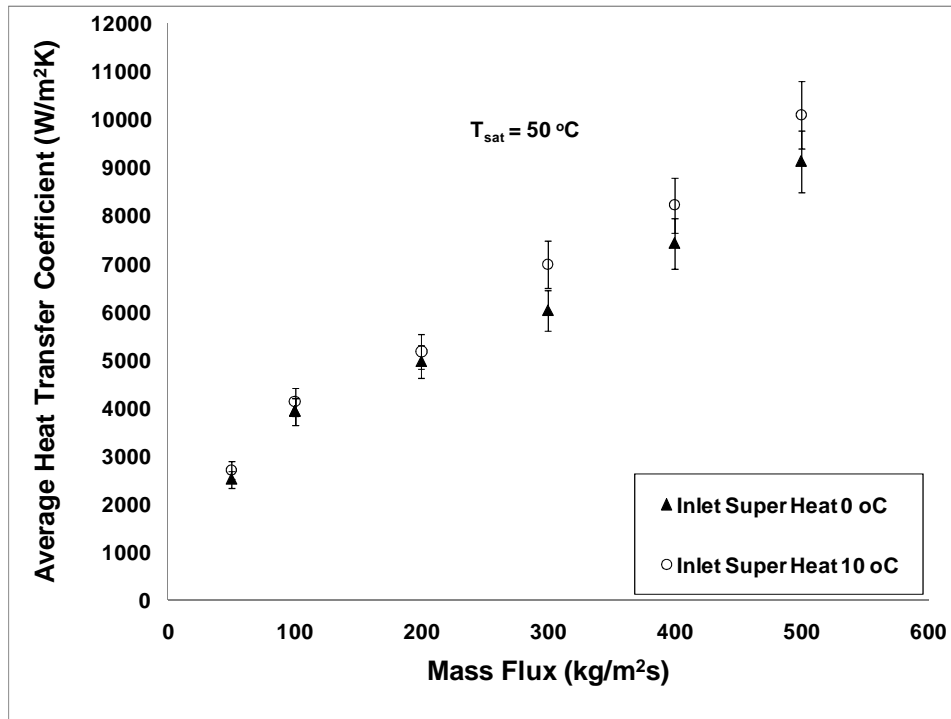
Figure 4-4 Effect of mass flux on average heat transfer coefficient for R245fa at $T_{sat} = 50\ ^oC$

4.1.1.3 Effect of Saturation Temperature

The average heat transfer coefficient is negatively affected by increasing the saturation temperature, as shown in Figure 4-5 and Figure 4-6. This is mainly due to the fact that increase in system pressure when increasing the saturation temperature, leads to reduced specific volume, thus higher vapor density. A higher vapor density in turns results in reduced vapor velocity, this lower hear transfer coefficients.

55
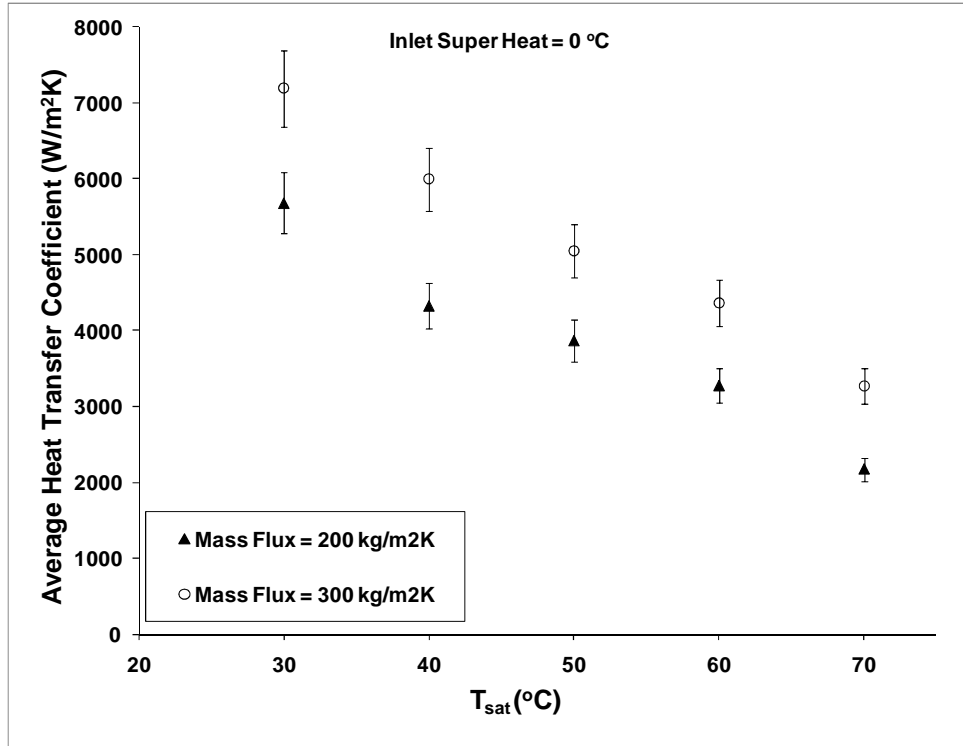
Figure 4-5 Effect of saturation temperature on average heat transfer coefficient for R134a
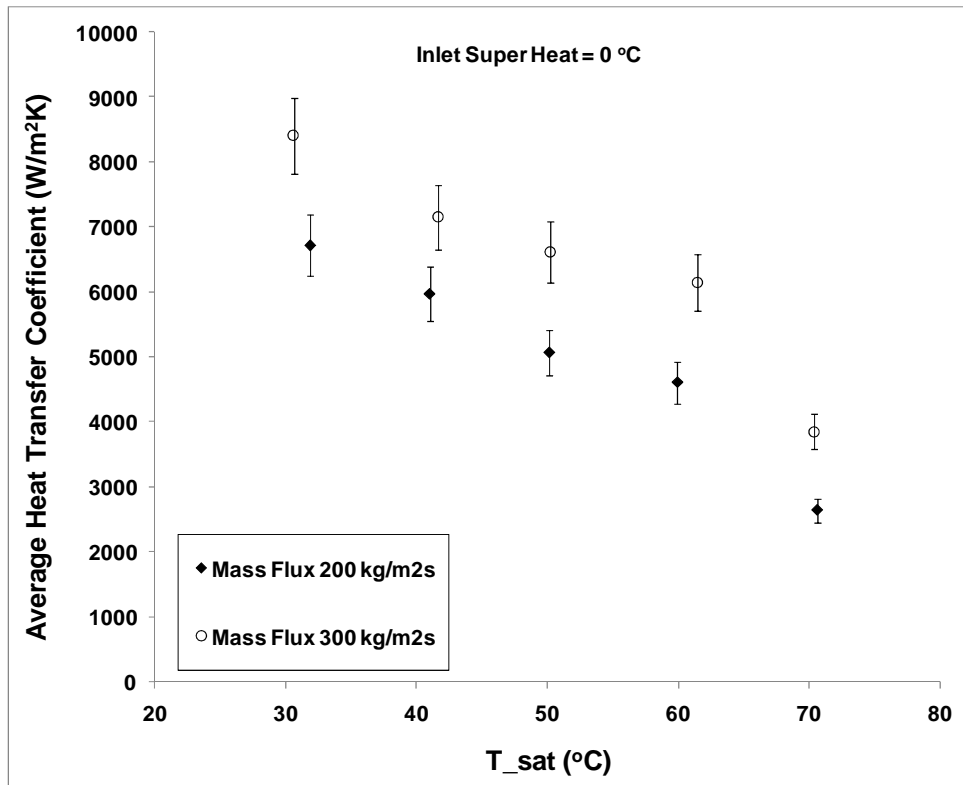
Figure 4-6 Effect of saturation temperature on average heat transfer coefficient for R245fa

4.1.1.4 Statistical Analysis

Considering the average heat transfer coefficient (h_{avg}) as the dependent variable and $\rho_l, \rho_v, \mu_l, \mu_v$, mass flux, saturation temperature, and super heat as the independent variables, we obtained the results tabulated in Table 4-1 from the ANOVA® linear regression analysis tool. The table shows the statistical results of each refrigerant evaluated separately. Consisted with the results presented earlier, the analysis confirms that the effects of degree spear heat and vapor viscosity are minimum when compared to the effect of other parameters involved.

Table 4-1 Regression statistics for heat transfer coefficient of R134a & R245fa separately

	R134a	*R245fa*
Multiple R	0.986	0.984
R Square	0.972	0.968
Adjusted R Square	0.859	0.852
Standard Error (ϵ)	382.05	533.11
	Coefficients β	*Coefficients β*
Intercept	247390.69	582455.19
Super Heat (SH) °C	0	0
Mass Flux (G) (kg/m²s)	14.20	19.09
T$_{sat}$ °C	487.32	1755.01
ρ_v (kg/m³)	-448.74	-2952.65
ρ_l (kg/m³)	-293.80	-597.56
μ_v (mPa.s)	0	0
μ_l (mPa.s)	584.28	500.66

From the statistical results general linear equations can be obtained for both R134a and R245fa and presented as follows, respectively:

$$h_{avg_{R134a}} = 247390.69 + 14.2G + 487.32\,\text{T}_{sat} - 448.74\rho_v - 293.8\rho_l$$
$$+ 584.28\mu_l \pm 382.05 \tag{4.9}$$

$$h_{avg_{R245fa}} = 582455.19 + 19.09G + 1755.01\,\text{T}_{\text{sat}} - 2952.65\rho_v - 597.56\rho_l \qquad (4.10)$$

$$+\ 500.66\mu_l \pm 533.11$$

Equations (4.3) and (4.4) give the values of average heat transfer coefficient of R134a and R245fa, respectively, within the standard error given from the regression analysis results in the table above. The R value for both refrigerants evaluated individually shows how well equations (4.3) and (4.4) relate the heat transfer coefficient with to the parameters and fluid properties. This relationship is graphically presented in Figure 4-7 and Figure 4-8 for R134a and R245fa, respectively. The ±error band in the figures represents the standard error calculated by the regression analysis.
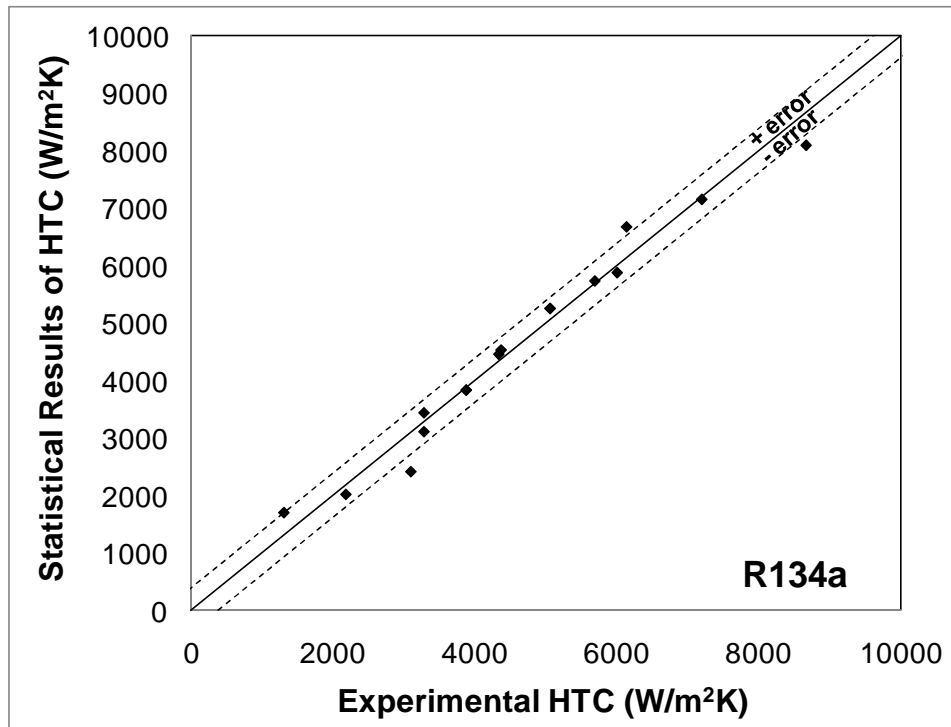
Figure 4-7 Comparison of experimental HTC vs HTC obtained from equation (4.3) for R134a
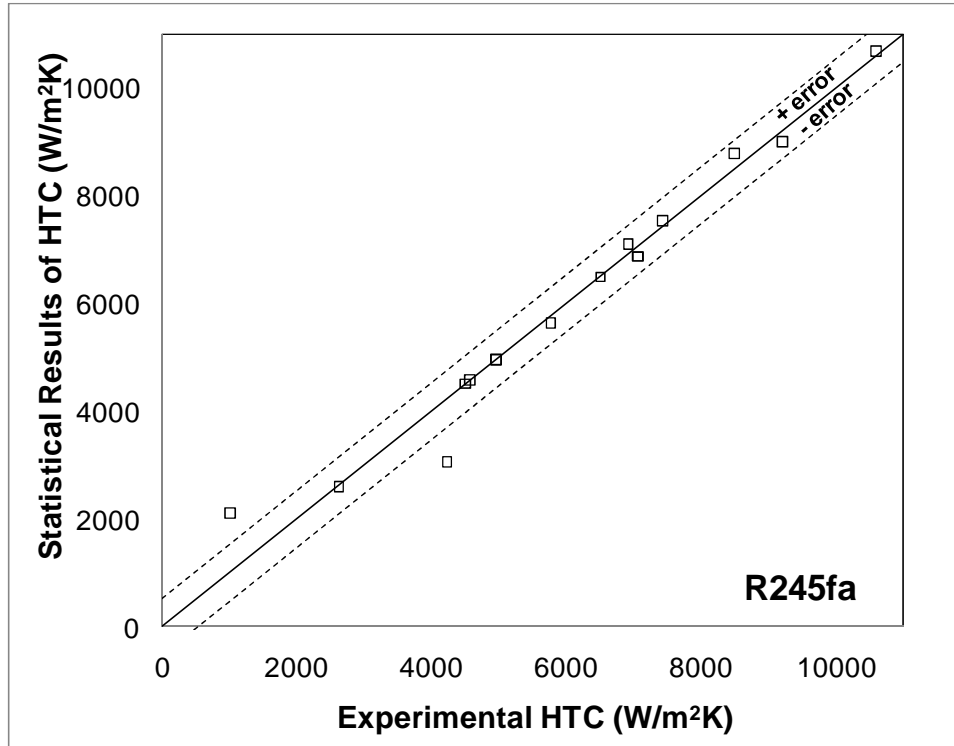
Figure 4-8 Comparison of experimental HTC vs HTC obtained from equation (4.4) for R245fa

To obtain a general equation that takes into account both refrigerants, a

regression analysis was performed on both refrigerants at once, which then generated

the results in Table 4-2.

Table 4-2 Regression statistics for heat transfer coefficient for all the data of both refriegerants

	R134a & R245fa
Multiple R	0.975
R Square	0.950
Adjusted R Square	0.938
Standard Error (ϵ)	501.86
	Coefficients β
Intercept	37257.84
Super Heat (SH) ^{o}C	1.63
Mass Flux (G) (kg/m^{2}s)	-6.11
T$_{sat}$ ^{o}C	16.64
ρ_v (kg/m^3)	124.11
ρ_l (kg/m^3)	14.71
μ_v (mPa.s)	-4433.13
μ_l (mPa.s)	-16.53

Then the general heat transfer coefficient for both refrigerants combined in one regression analysis can be presented as follow:

$$h_{avg} = 37257.84 + 1.63 SH - 6.11G + 16.64\, T_{sat} + 124.11\rho_v +$$

$$14.71\rho_l - 4433.13\mu_v - 16.53\mu_l \pm 382.05 \tag{4.11}$$

A comparison of equation (4.5) and heat transfer coefficient data obtained from experiments for both refrigerants is shown in Figure 4-9.
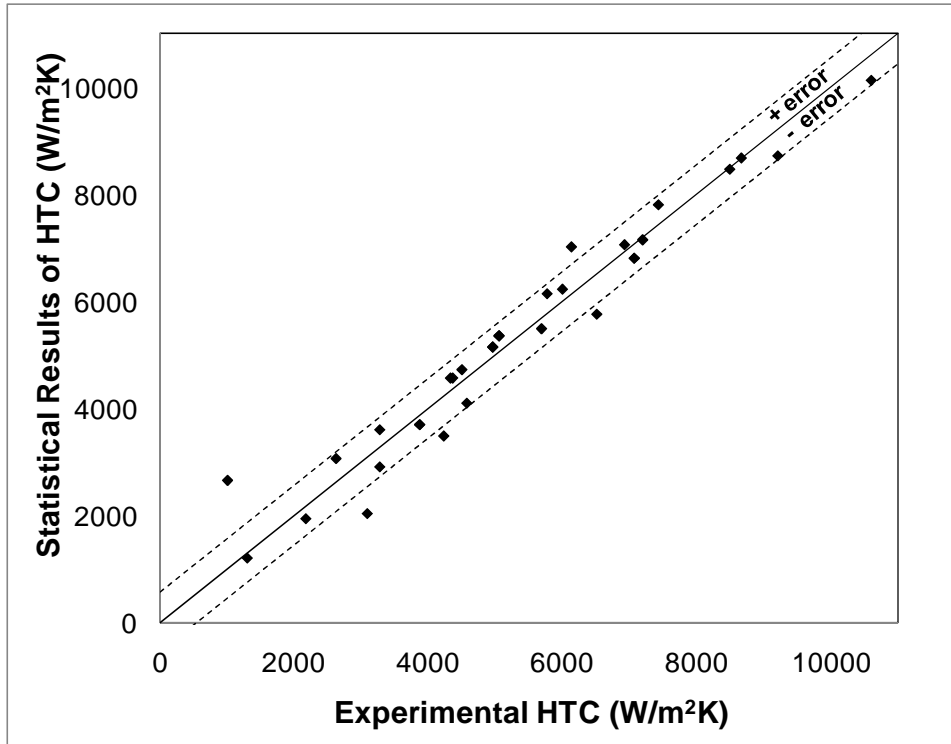
Figure 4-9 Comparison of experimental HTC for R134a & R245fa vs HTC obtained from equation (4.5)

4.1.2 Pressure Drop

4.1.2.1 Effect of Superheat

The variation of pressure drop as a function of degree superheat at a given mass flux (200 & 300 kg/m^{2}sec) and at 50 ^{o}C saturation temperature is shown in Figure 4-10 and Figure 4-11. As seen in the figures, the effect of degree super heat on pressure drop is negligible. Moreover, they are within the uncertainty of the

experimental results. It is known that pressure drop of two-phase flows differs from

one flow regime to another which mean that pressure drop is very much dependant on

flow regime. Thus, it is believed that the flow pattern in the significant remaining

length of the channel (after the annular flow zone that may be created due to the

degree super heat) is more or less the same in higher superheats as in the zero-

superheat case.
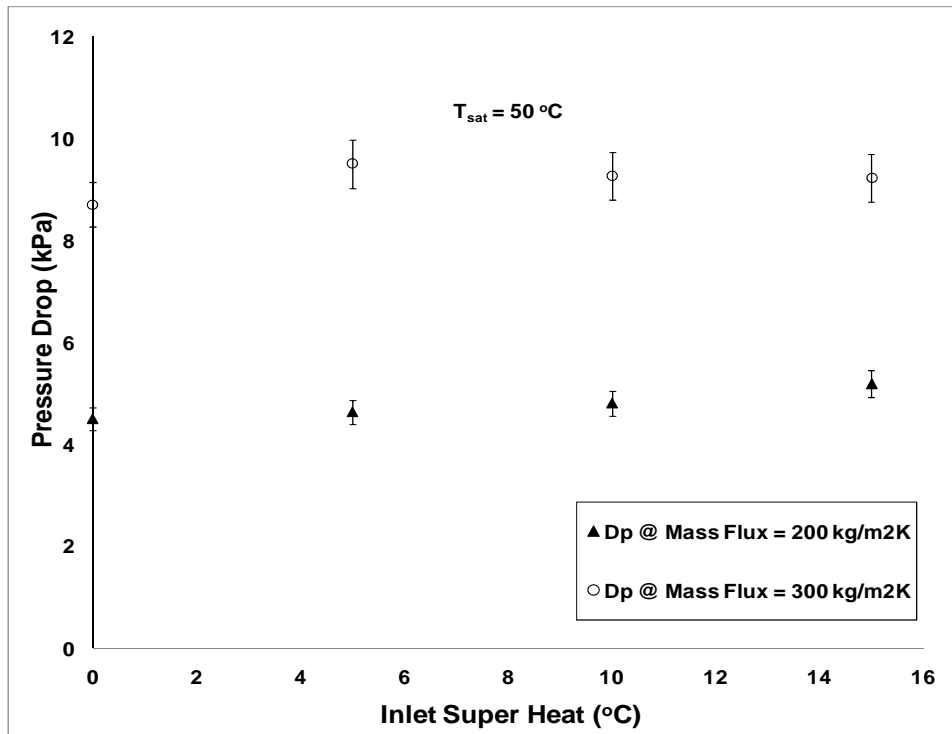
Figure 4-10 Effect of inlet superheat on pressure drop at $T_{sat} = 50\ ^{o}C$ for R134a
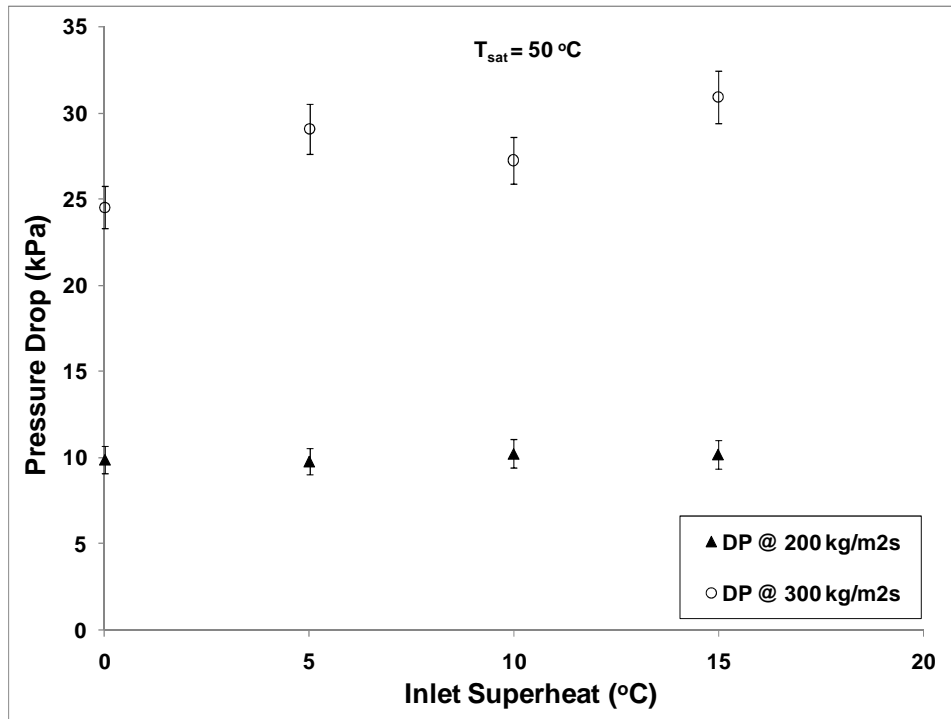
Figure 4-11 Effect of inlet superheat on pressure drop at $T_{sat} = 50\ ^{o}C$ for R245fa

4.1.2.2 Effect of Mass Flux

Figure 4-12 and Figure 4-13, show that pressure drop is significantly affected by increase in the mass flux. This is due to the increase in vapor and liquid velocities at higher mass flow rates. Figure 4-14, shows how vapor and liquid velocities change with changing mass flux and vapor quality. There is an average 30% increase in vapor and liquid velocities as mass flux is increased from 300 to 400 kg/m^{2}s. It is obvious from Figure 4-14 that the vapor velocity, for a constant mass flux and saturation temperature, increases more than six times when vapor quality is increased from 10% to 90% whereas liquid velocity increases three times for the same conditions. This analogy was verified by the visualization test results as it was clear that vapor bubbles at low vapor qualities, 10 % and lower, traveled at velocities close to the liquid velocity but a bit higher. Whereas at high vapor qualities, it was clear

that the vapor core traveled at much higher velocity than that of the liquid. The vapor and liquid velocities are calculated using a void fraction, which represents the amount of vapor and liquid at each vapor quality, x. The void fraction used in the calculations is similar to that used by El Hajal (2003) which is expressed as follow:

$$\varepsilon = \frac{\varepsilon_h - \varepsilon_{ra}}{\ln\left(\frac{\varepsilon_h}{\varepsilon_{ra}}\right)} \tag{4.12}$$

Where ε_h is the homogenous void fraction and ε_{ra} is the Rouhani and Axelsson (1970) void fraction and are defined as, respectively.

$$\varepsilon_h = \left(1 + \left(\frac{1+x}{x}\right)\left(\frac{\rho_v}{\rho_l}\right)\right)^{-1} \tag{4.13}$$

$$\varepsilon_{ra} = \left(\frac{x}{\rho_v}\right)\left([1 + 0.12(1 - x)]\left(\frac{x}{\rho_v} + \frac{1-x}{\rho_l}\right) + \frac{1.18(1-x)[g_g\sigma(\rho_l-\rho_v)]^{-0.25}}{G\rho_l^{0.5}}\right)^{-1} \tag{4.14}$$

The vapor and liquid velocities are defied as follow, respectively.

$$U_l = \frac{G\,(1-x)}{\rho_l\,(1-\varepsilon)} \tag{4.15}$$

$$U_v = \frac{G\,x}{\rho_v\,\varepsilon} \tag{4.16}$$

In addition, it is noteworthy that R245fa has almost three times the pressure drop as R134a. This is mainly due to the higher surface tension, liquid viscosity and vapor density values of R245fa (refer to Table 3-2). However, from these properties vapor density contributes the most to the increase in pressure drop because vapor is dominant in the channel. This can be sensed when comparing the vapor density of the two testing refrigerants, where the vapor density of R245fa is more than three times lower than that of R134a (Table 3-2); therefore, the magnitude of pressure drop R245fa compared with R134a at the same mass flux is three times higher.
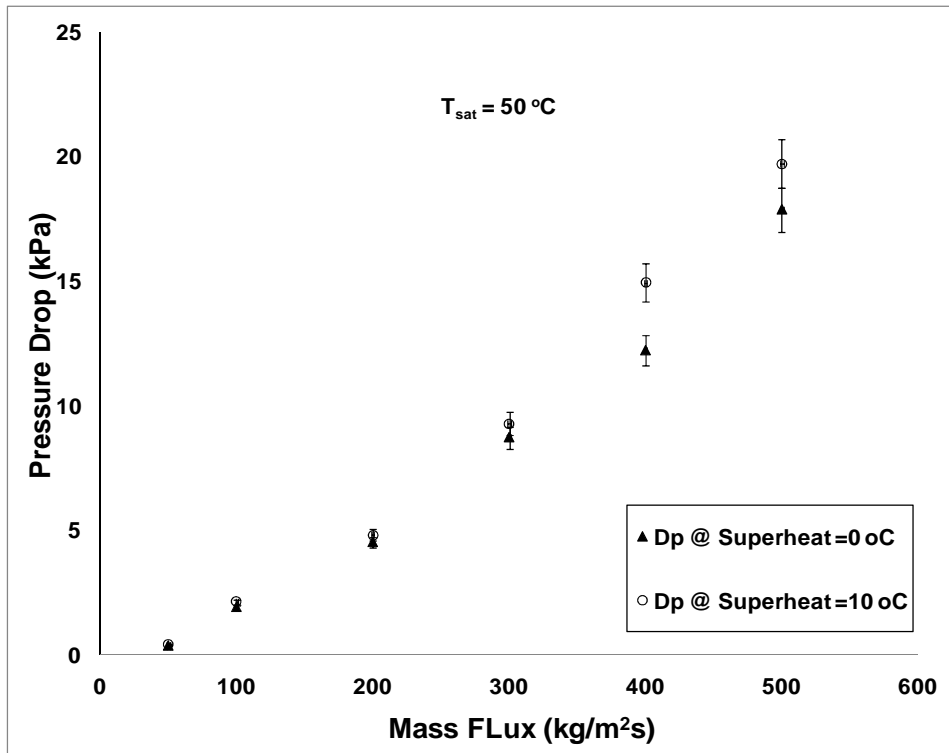
Figure 4-12 Effect of mass flux on pressure drop for R134a at T_{sat} = 50 ^{o}C
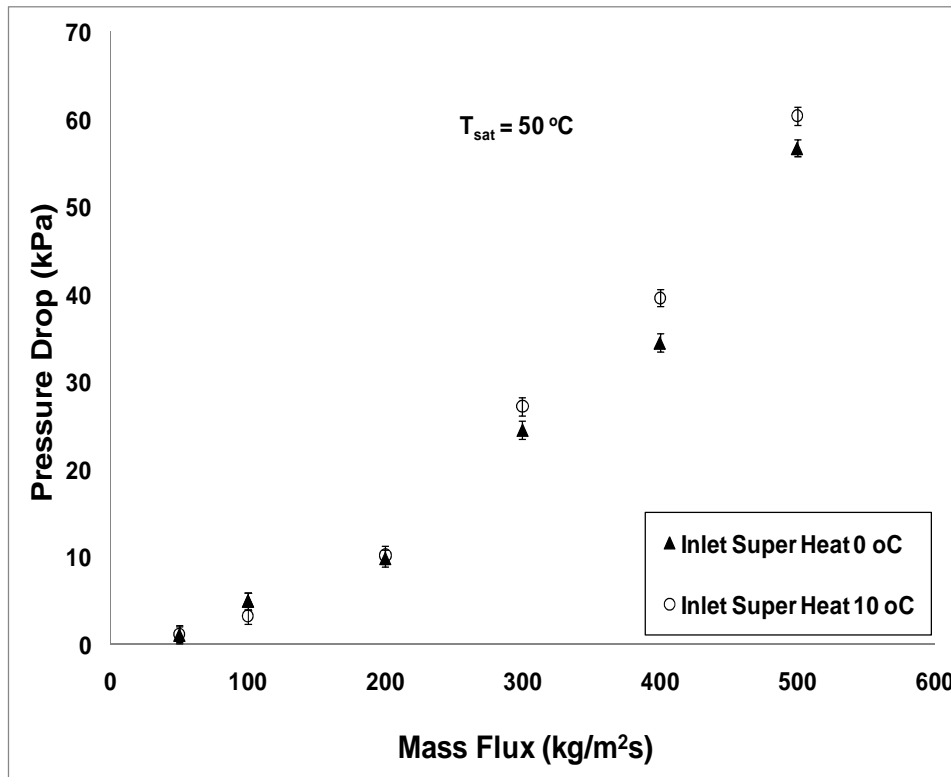
Figure 4-13 Effect of mass flux on pressure drop for R245fa at T_{sat} = 50 ^{o}C
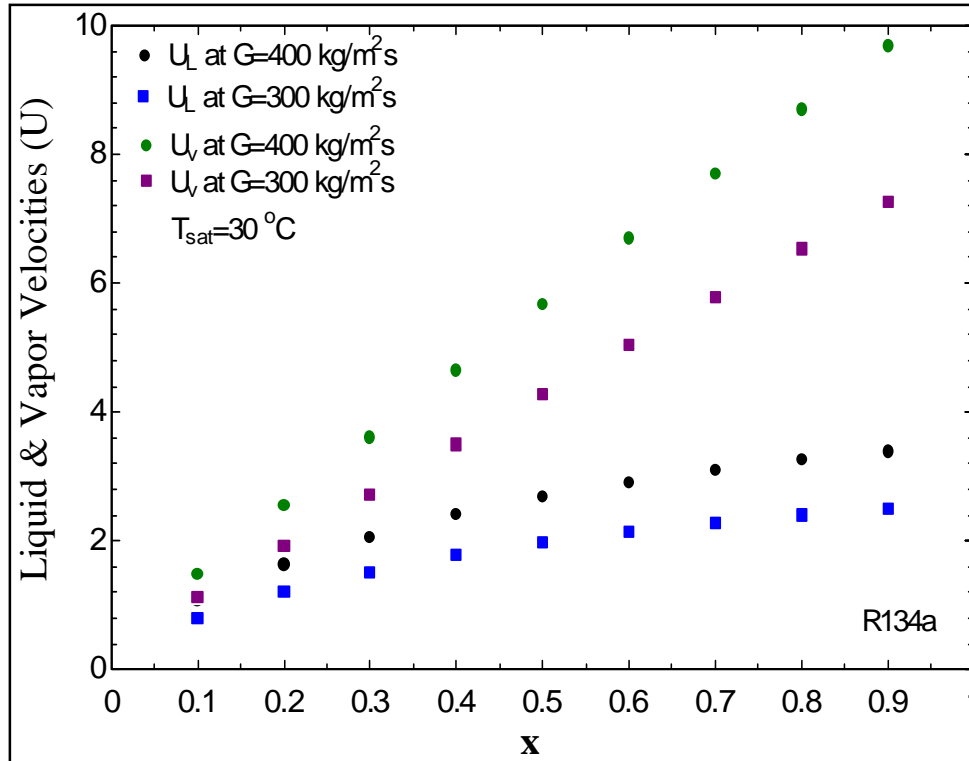
Figure 4-14 Vapor & liquid velocities of R134a at T_{sat} of 30 ^{o}C at different vapor qualities

4.1.2.3 Effect of Saturation Temperature

As for the pressure drop, increasing the saturation temperature has a significant effect on decreasing the pressure drop, as seen in Figure 4-15 and Figure 4-16. This is due to the sensitivity of pressure drop to liquid viscosity and vapor density; because liquid viscosity is higher and vapor density is lower at 30 ^{o}C than at 70 ^{o}C, as can be seen in Table 3-2, when the saturation temperature increases, the volumetric flow rate decreases therefore the velocity is lower. In other words, vapor is dominant in the channel and as saturation temperature increases, vapor density increases; thus decreasing the velocity and as a result, decreasing the pressure drop. The magnitudes of the effect of each of these properties are illustrated in Figure 4-17 and Figure 4-18. It is obvious that more than one fluid property is affected by changing saturation temperature, and then these properties have an effect on pressure

65

drop. However, only the two properties that most significantly affect the pressure drop may be: liquid viscosity and vapor density. On average the liquid viscosity of R245fa is twice that of R134a and decreases about 40% when the saturation temperature is changed from 30 to 70 ^{o}C. On the other hand, vapor density of R134a on average is three times higher than that of R245fa and the lower vapor density, the higher volumetric flow, thus the higher the pressure drop. In addition, it is believed that vapor is dominant in the channel; therefore, the effect of liquid viscosity is small compared to the effect of vapor density on pressure drop. This should explain why the pressure drop of R245fa is three times larger than that of R134a.
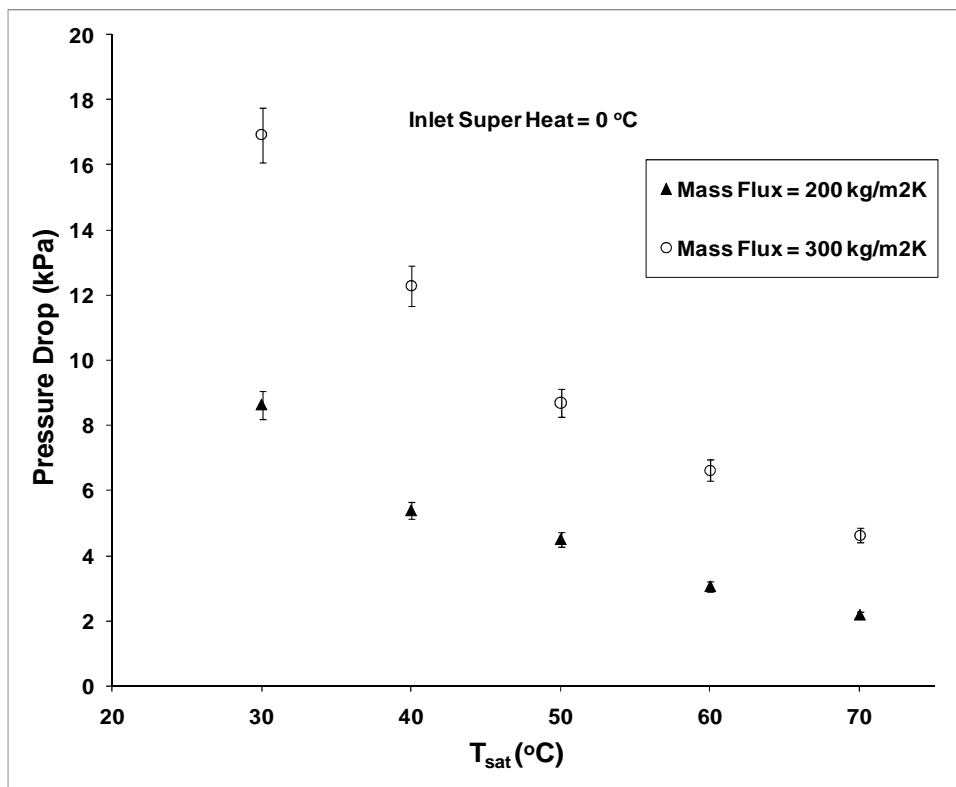
Figure 4-15 Effect of saturation temperature on average heat transfer coefficient for R134a
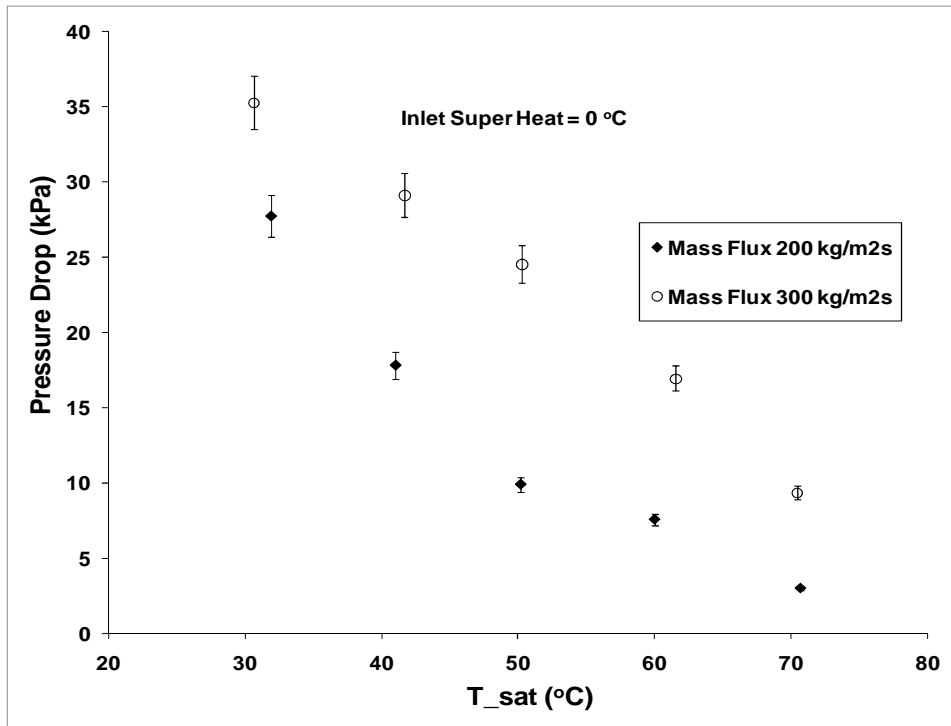
Figure 4-16 Effect of saturation temperature on average heat transfer coefficient for R245fa
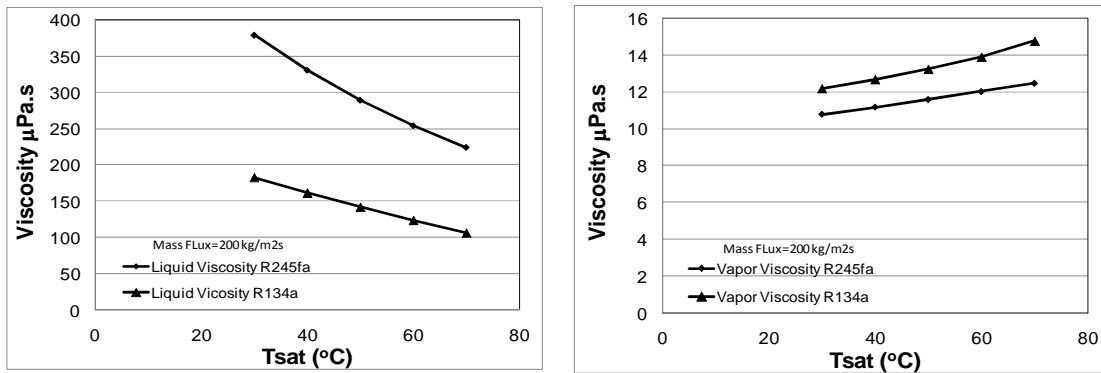
Figure 4-17 The change of liquid and vapor viscosity with saturation temperature for R134a & R245fa
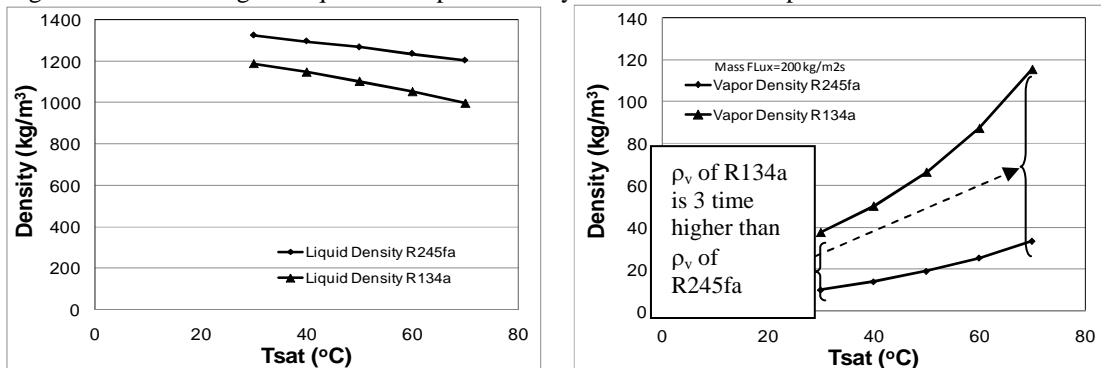
Figure 4-18 Change of liquid and vapor density with saturation temperature for R134a & R245fa

4.1.2.4 Statistical Analysis

A similar analysis to that of heat transfer coefficient is applied here. Where the pressure drop ΔP is considered the dependent variable and $\rho_l, \rho_v, \mu_l, \mu_v$, mass flux, saturation temperature and super heat as the independent variables. The generated results from the statistical analysis for refrigerants R134a and R245fa are shown in Table 4-3.

Table 4-3 Regression statistics for pressure drop of R134a & R245fa separately

	R134a	*R245fa*
Multiple R	0.976	0.962
R Square	0.953	0.925
Adjusted R Square	0.829	0.788
Standard Error (ϵ)	1.389	3.764
	Coefficients β	*Coefficients β*
Intercept	1827.43	-5324.18
Super Heat (SH) ^{o}C	0	0
Mass Flux (G) (kg/m^{2}s)	0.04	0.09
T$_{sat}$ ^{o}C	-2.11	10.7
ρ_v (kg/m^3)	-1.81	2.26
ρ_l (kg/m^3)	-1.61	3.65
μ_v (mPa.s)	0	0
μ_l (mPa.s)	1.22	0.36

From Table 4-3 a linear equation of the pressure drop value for R134a and R245fa can be generated in the following form:

$$\Delta P_{R134a} = 1827.43 + 0.04G - 2.11\,\text{T}_{\text{sat}} - 1.81\rho_v - 1.61\rho_l + 1.22\mu_l \pm 1.389 \qquad (4.17)$$

$$\Delta P_{R245fa} = -5324.18 + 0.09G + 10.7\,\text{T}_{\text{sat}} + 2.26\rho_v + 3.65\rho_l + 0.36\mu_l \pm 3.764 \qquad (4.18)$$

Figure 4-19 and Figure 4-20 show the comparison of the experimentally obtained pressure drop for R134a and R245fa versus the pressure drop obtained from Equations (4.11) and (4.12), respectively. From the figures Figure 4-11 and Figure

4-12 the R value in Table 4-3 for both refrigerants evaluated individually how well

Equations (4.11) and (4.12) relate the pressure drop with the parameters and fluid

properties.
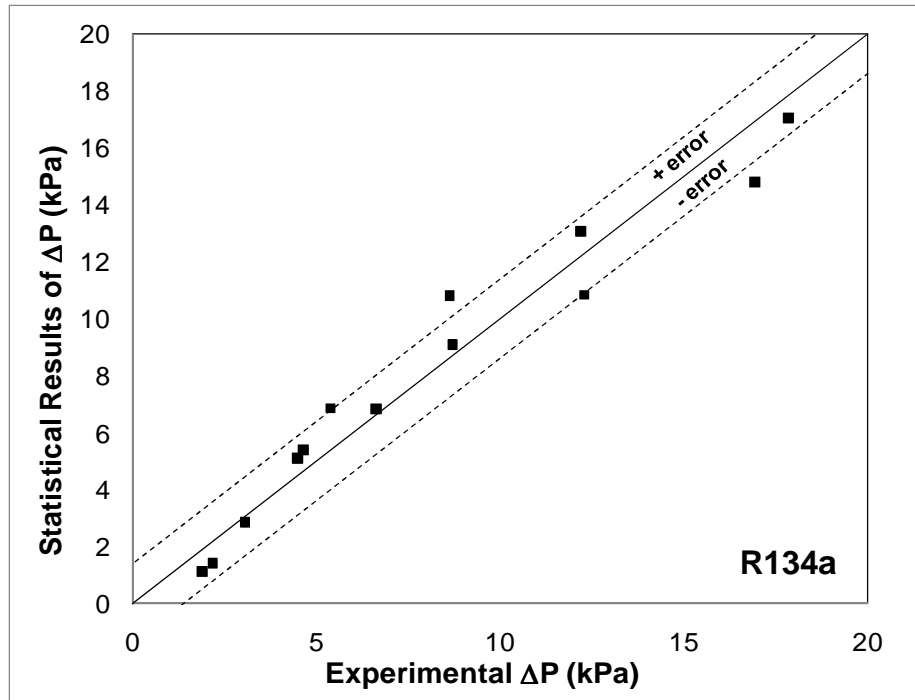
Figure 4-19 Comparison of experimental ΔP vs ΔP obtained from equation (4.6) for R134a
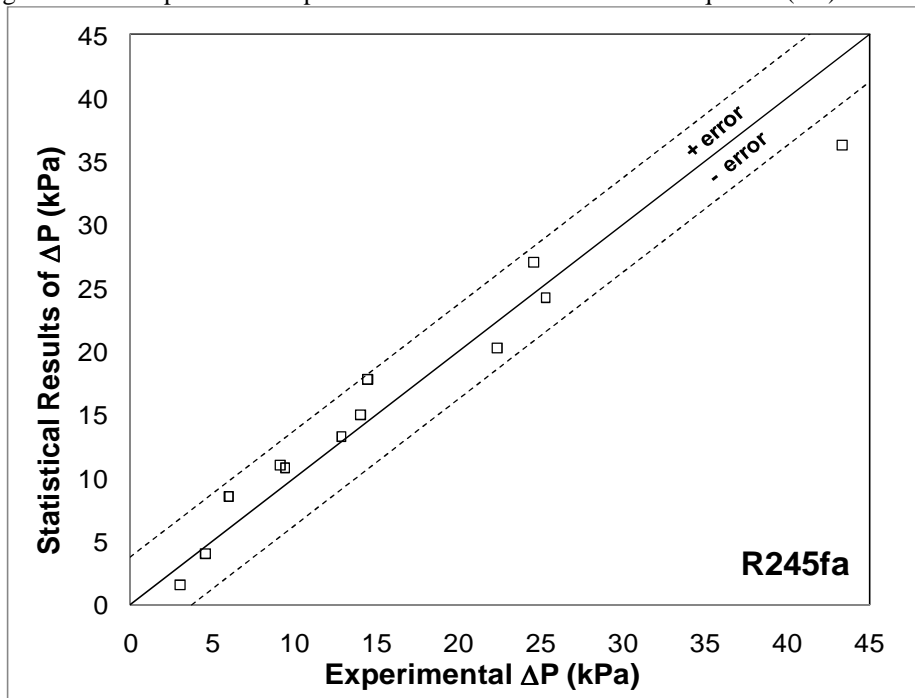
Figure 4-20 Comparison of experimental ΔP vs ΔP obtained from equation (4.7) for R245a

A regression analysis for all the pressure drop data collected for both R134a and R245fa was also preformed, which generated the results in Table 4-4.

Table 4-4 Regression statistics for pressure drop for all the data of both refriegerants

	R134a & R245fa
Multiple R	0.916
R Square	0.840
Adjusted R Square	0.801
Standard Error (ϵ)	4.052
	Coefficients β
Intercept	9.77
Super Heat (SH) ^{o}C	0
Mass Flux (G) (kg/m^{2}s)	0.04
T$_{sat}$ ^{o}C	0.066
ρ_v **(kg/m^3)**	0.646
ρ_l **(kg/m^3)**	0.142
μ_v **(mPa.s)**	-15.74
μ_l **(mPa.s)**	-0.086

Equation (4.13) represents the pressure drop of both refrigerants.

$$\Delta P = 9.77 + 0.04G + 0.066\text{T}_{sat} + 0.646\rho_v + 0.142\rho_l - 15.74\mu_l - \qquad (4.19)$$

$$0.086\mu_l \pm 4.052$$

The goodness of the fit of the pressure drop data and the pressure drop obtained from equation (4.13) are graphically shown in Figure 4-21.

70
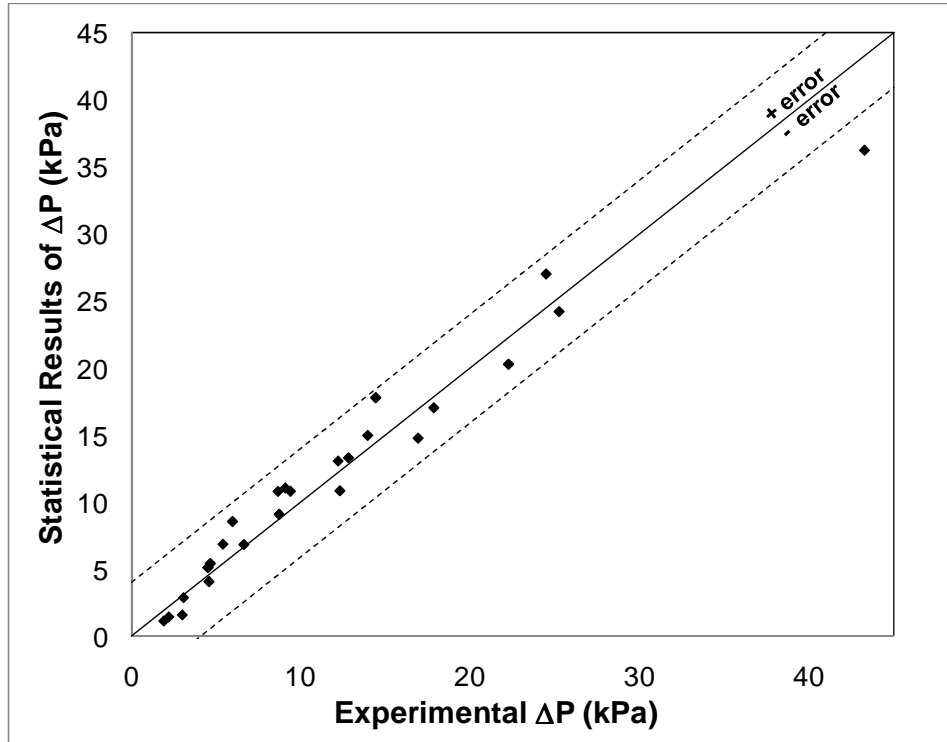
Figure 4-21 Comparison of experimental ΔP for R134a & R245fa vs. ΔP obtained from equation (4.8)

4.2 *Pressure Drop Results for Constant Quality Flows*

This section provides a detailed description of experimental results of pressure drop for phase change flows for the conditions shown in Table 3-5. The results are also compared with the literature and existing models.

4.2.1 *Effect of Mass Flux*

Figure 4-22 and Figure 4-23 show the variation of pressure drop for three different mass fluxes (200, 300 and 400 kg/m^{2}s) and the same saturation temperature (50 ^{o}C). The pressure drop results show similar trends as the results shown in the previous section. That is, the mass flux increases, pressure drop increases at a given quality and saturation temperature.

71

In addition, the pressure drop increases as the quality increases at a given mass flux. This is due to the change in volumetric flow rate. As the liquid evaporates, the vapor/liquid density ratio increases, therefore, the volumetric flow rate increases which then cause an increase in the pressure drops. Moreover, as the vapor/liquid ratio increases the interfacial sheer between the vapor and the liquid increases which also has an effect on increasing the pressure drop. It should be noted when comparing between pressure drop results due to mass flux or quality changes of the two refrigerants (R134a and R245fa) that the pressure drop of R245fa is three times that of R134a for the same operation conditions.
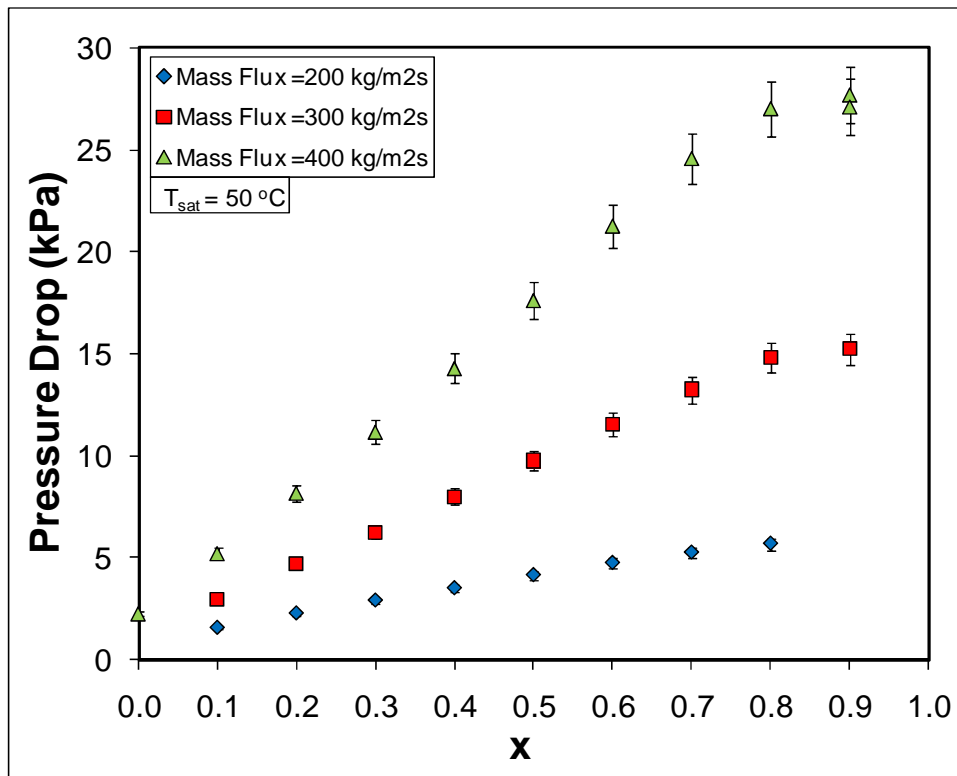
Figure 4-22 Effect of mass flux on local pressure drop for R134a
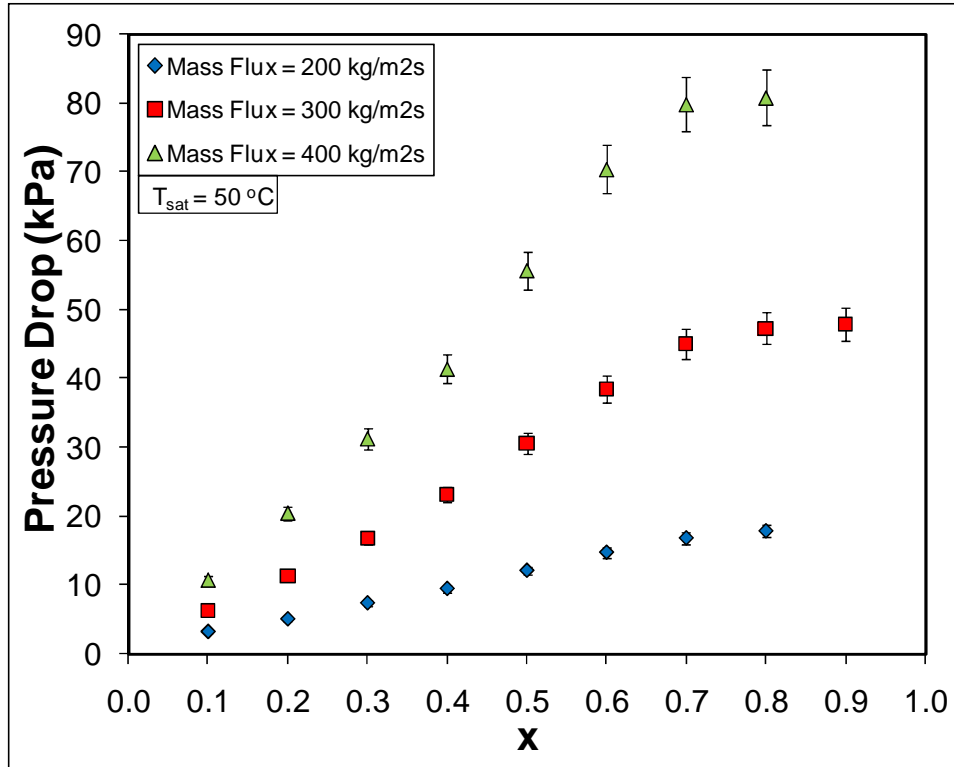
Figure 4-23 Effect of mass flux on local pressure drop for R245fa

4.2.2 Effect of Saturation Temperature

Figure 4-24 and Figure 4-25 illustrate the effect of saturation temperature (30, 40, and 50 $^{\circ}$C) on pressure drop for a given mass flux (300 kg/m^{2}s). As in the figures, with an increase in the saturation temperature, pressure drop decreases for the same mass flux and the same quality. This is due to the decrease in vapor density as saturation temperature decreases. For instance, the density of vapor R134a at 30 $^{\circ}$C saturation temperature is 37.53 kg/m^3 and when the saturation temperature is increased to 70 $^{\circ}$C the density of vapor increases three times to be 115.6 kg/m^3. It is worth mentioning that liquid viscosity decreases 40% from its value at 30 $^{\circ}$C when the saturation temperature is increased from 30 to 70 $^{\circ}$C, thus decrease the velocity of the liquid which in turn should reduce the pressure drop. However, the effect of

increasing vapor density is more dominant than the effect of decreasing liquid

viscosity on pressure drop as saturation temperature is increased.
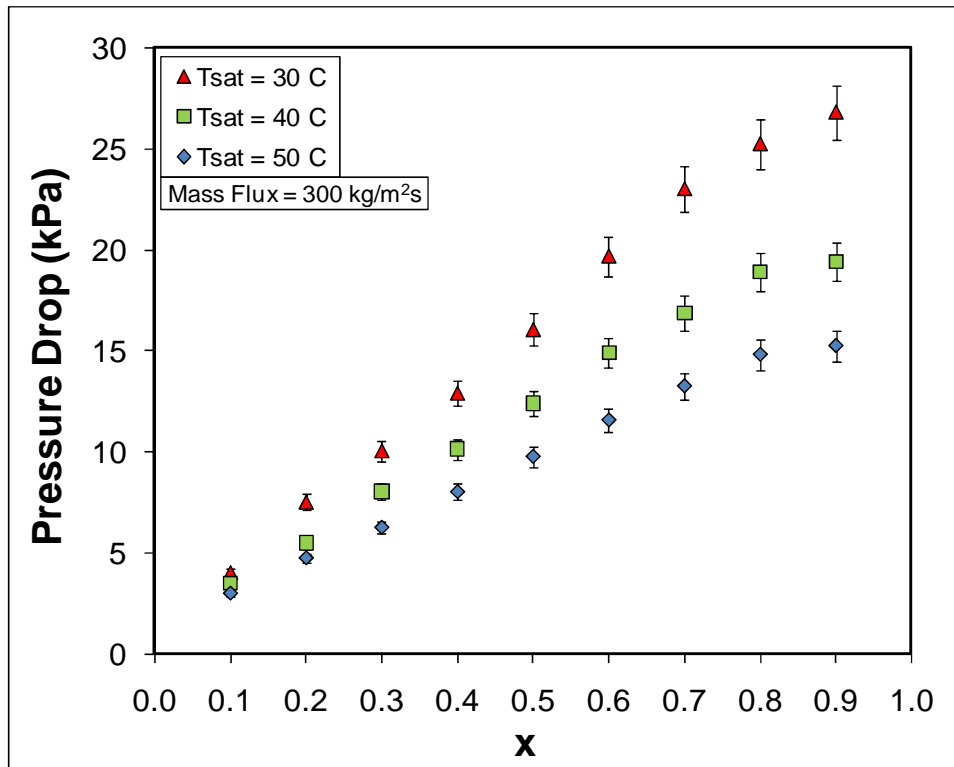
Figure 4-24 Effect of saturation temperature on local pressure drop for R134a
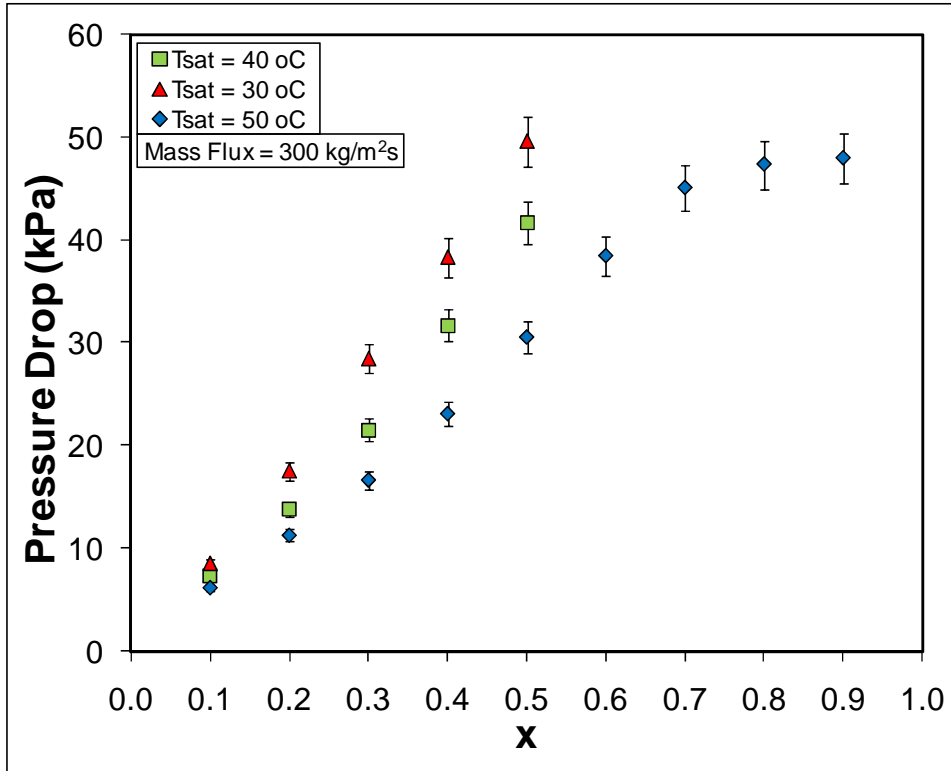
Figure 4-25 Effect of saturation temperature on local pressure drop for R245fa

Figure 4-26 and Figure 4-27 depict all the test condition shown in Table 3-5 for R134a and R245fa, respectively. When comparing between the tests results at 50 ^{o}C and 400 kg/m^{2}s mass flux versus the test results at 30 ^{o}C and 300 kg/m^{2}s, it is obvious from the figures that the results are very comparable.
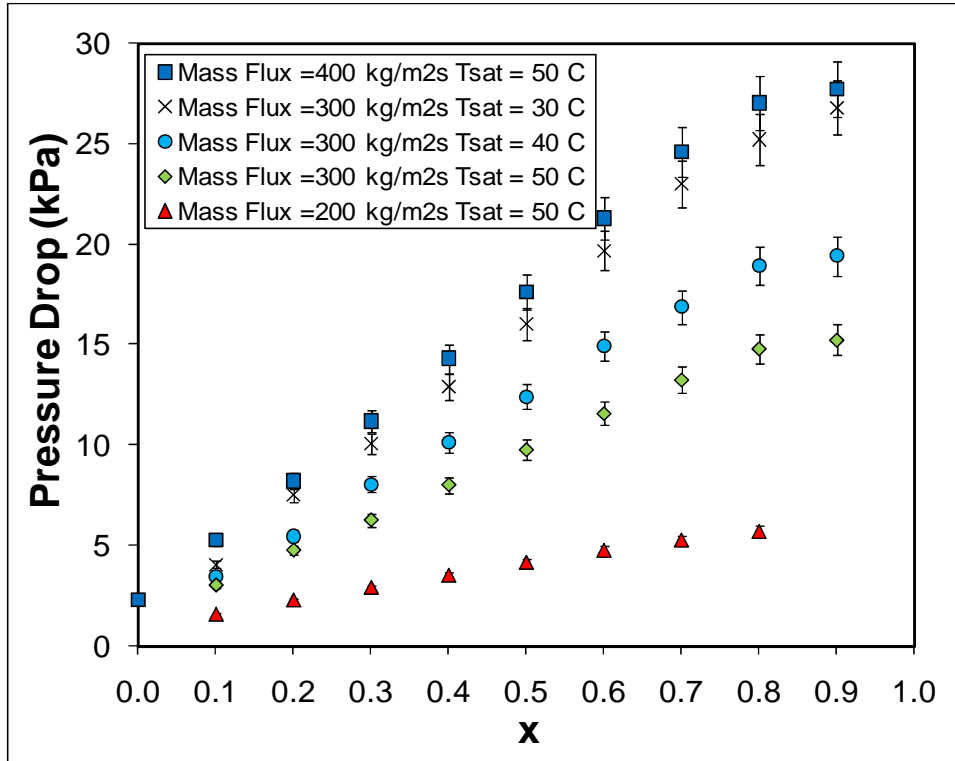
Figure 4-26 All the test results of local pressure drop for R134a
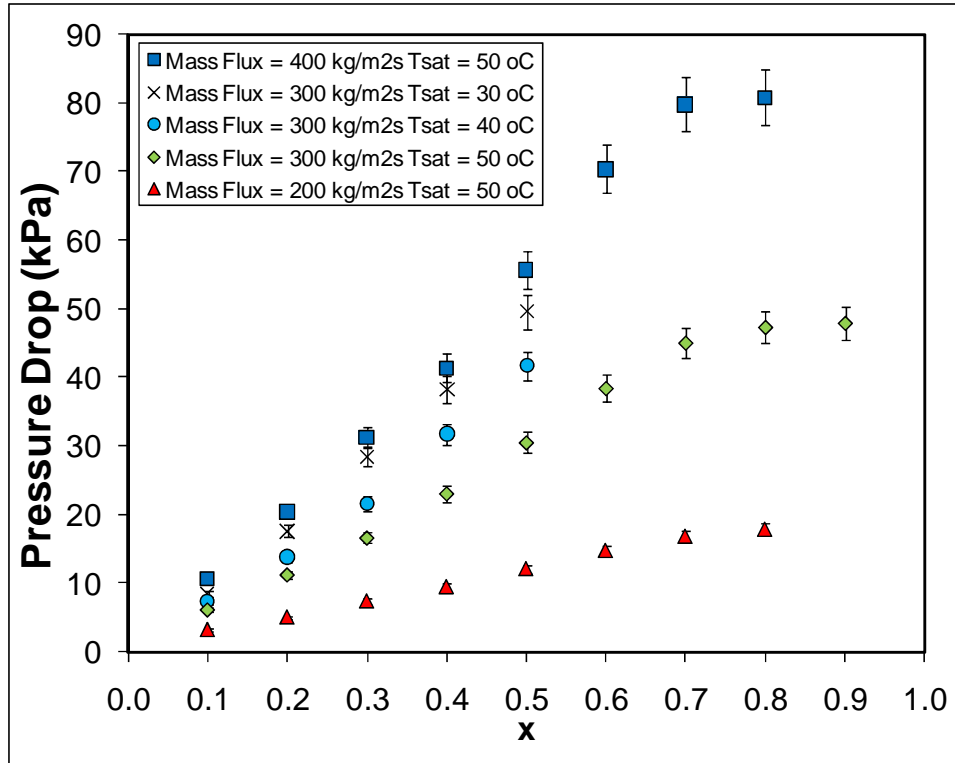
Figure 4-27 All the test results of local pressure drop for R245fa

76

4.3 *Comparison with the Literature*

This section presents a comparison of the present work results with some of the results available in the open literature. Most of the results in the open literature are for local values of heat transfer and pressure drop. For the present work, results of heat transfer coefficients are presented as averaged values, whereas the pressure drop results are presented as both averaged values, as well as local values. Therefore, in order to compare the results of this study with the results in the literature, both results must be in the same arrangements. Thus, local heat transfer coefficients values of the results of the current study were back calculated then compared with the results in the literature.

As an example, Garimella et al. (2004) has evaluated a square multi-channel (17 channels) condenser with a channel hydraulic diameter of 0.76 mm using R134a as the working fluid. The testing conditions of his study that is to be compared with one of the current study results are presented in Table 4-5. The local values of heat transfer coefficient obtained from Garimella et al. (2004) are compared with the back calculated local heat transfer coefficients in the present work. Figure 4-28 shows the comparison.

Table 4-5 Comparison of average heat transfer coefficients with data from Garimella et al. (2004)

	D_h (mm)	T_{sat} (^{o}C)	G (kg/m^{2}s)
Measured	0.70	50	300
S. Garimella	0.76	52	300
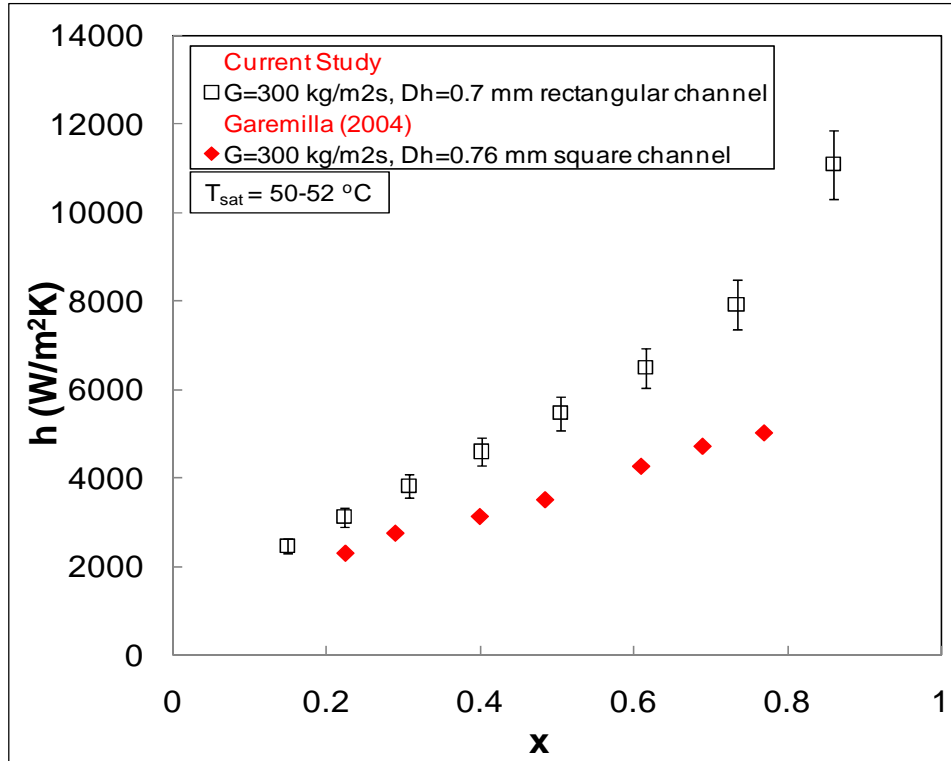
Figure 4-28 Average condensation heat transfer coefficients as a function of mass flux and quality for a square channel with $D_h = 0.76$ mm.

As seen in the figure, the back calculated local heat transfer coefficients on average are about 30% higher than the local heat transfer coefficient obtained from Garimella et al. (2004). This comparison reveals a very important fact of high aspect ratio channels that is micro-channels with high aspect ratios outperform square channels in terms of heat transfer. Figure 4-28 also shows that as quality increases the difference between the two compared results somewhat increases. This is mainly due to the channel shape effect. In a rectangular channel with high aspect ratio, when vapor volume increases, liquid is bushed to the sides of the channel. Since one side of the rectangular channel is 7 times larger than the other side (in this case) the liquid has more room to distribute in the two longer side of the channel, thus, causing the liquid to form a very thin layer, which leads to improving the heat transfer coefficient.

In the contrary, the liquid layer is evenly formed in the four sides of the square

channel, which is assumed to be relatively thicker than that of a high aspect ratio

rectangular channel for similar test conditions.

Shin and Kim (2004) have studied condensation in single rectangular micro-

channels with hydraulic diameters of 0.494, 0.658 and 0.972 mm. the tests were

conducted at 40 $^{\circ}$C saturation temperature, mass fluxes ranged from 100 – 600

kg/m^{2}s, heat fluxes between 5 – 20 kW/m^2 and qualities varying from 0.15 to 0.85.

Figure 4-29 shows a comparison of some of Shins' and Kims' results of heat transfer

coefficient with results from the current study. It is obvious from the figure below

that there is some agreement in the results especially at low range qualities. However,

at middle range and high range qualities, the difference in the results tends to

increase. This confirms the reasoning mentioned earlier, that at high qualities (more

than 70% quality) rectangular micro-channel with high aspect ratio has better heat

transfer performance than rectangular and square micro-channels.
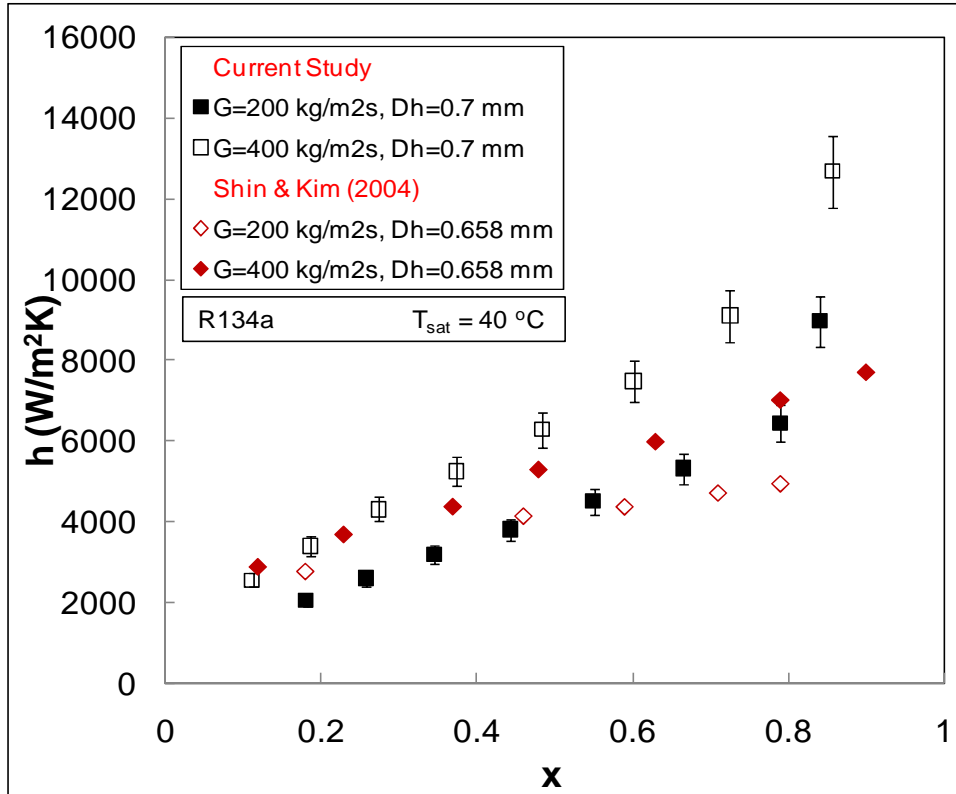
Figure 4-29 Comparison of heat transfer data from the current study and results from Shin and Kim (2004)

Shin and Kims' (2004) collected pressure drop results of the tests they conducted in all the micro-channels that they have tested in their investigation. In addition, Shin and Kim (2004) also investigated the pressure drop using a micro-channel with a hydraulic diameter of 0.691 mm at the same testing conditions presented above. Their results are compared with the current study of pressure drop results, Figure 4-30. Although the mass flux of the tests results shown in the figure from this study is 100 kg/m^2s less than what was used in Shin and Kims' tests, the pressure drop values are relatively similar. Since the hydraulic diameters of the micro-channels compared here are quite similar, it was expected that the pressure drop gradient at 300 kg/m^2s to be lower than the pressure drop gradient at 400 kg/m^2s, whereas, in the figure below the results for Kim (2003) seem a bit lower that the

results of the present study, confirming that the pressure drop in higher aspect ratio

channels are higher than those of square channels.
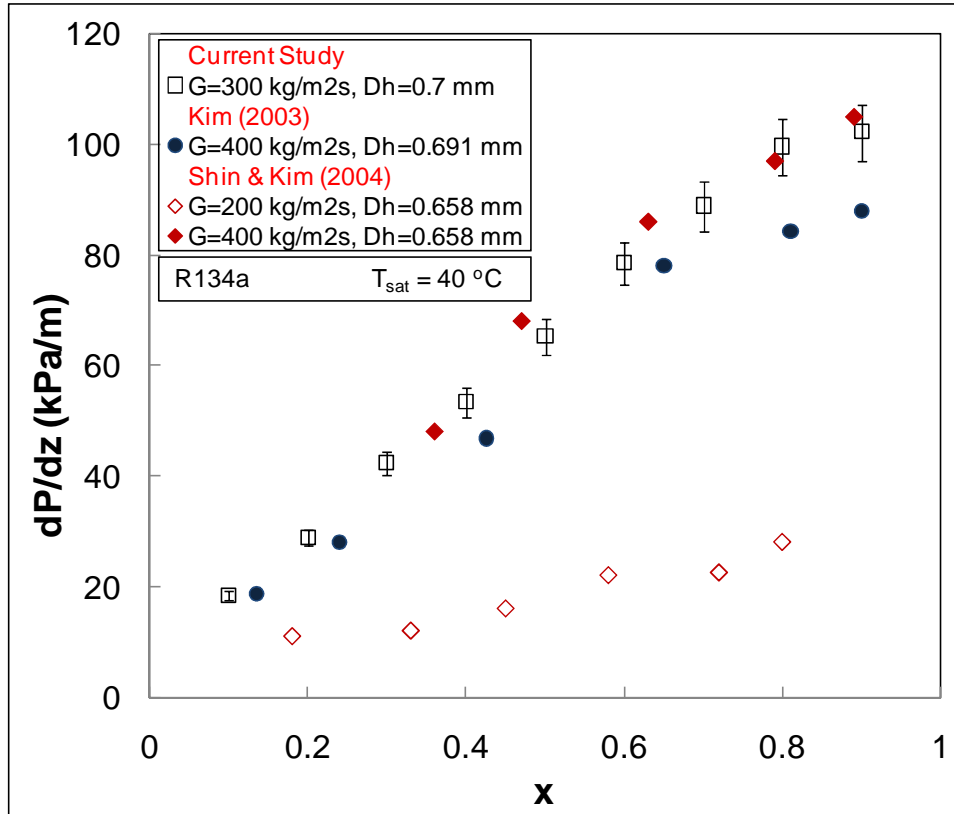
Figure 4-30 Comparison of pressured drop data from the current study and results from Kim (2003)
Shin and Kim (2004)

4.3.1 Summary

In this chapter, averaged heat transfer coefficient and the overall pressure drop

data were presented in terms of the effect of inlet superheat, mass flux and saturation

temperature. The results of this study show that the effect of inlet superheat can be

neglected when compared with the effect of mass flux and saturation temperature. As

for the effect of mass flux, there is an increase in both heat transfer coefficient and

pressure drop with increase in mass flux. Whereas for the effect of saturation

temperature, there is a decrease in heat transfer coefficient and pressure drop as

saturation temperature is increased. The remains of these results were also explained.

A regression analysis study on both heat transfer coefficient and the overall pressure

drop data of both fluids were also presented in this chapter. Results of local pressure

drop study were shown and compared with results available in the open literature.

CHAPTER 5: EMPIRICAL CORRELATIONS

5.1 *Heat Transfer Correlations*

One of the main objectives of this study was to develop correlations for heat transfer and pressure drop coefficients of condensation in micro-channels to be used in designing micro-channel heat exchangers. As a starting point, several widely used and well-defined correlations for both heat transfer and pressure drop coefficients were obtained from the literature. The vast majority of the correlations is for local heat transfer and pressure drop; however, the data collected in this investigation were average values of heat transfer coefficient and the overall pressure drop of the channel.

Since the data collected in this study for heat transfer coefficient were average values, a comparison between the data and correlation of local heat transfer coefficients would not be useful. Therefore, a technique was developed to compare the average local values obtained from experiments with the average values calculated from the correlations. To achieve these averages from the local value correlations, the channel was divided into nine segments as shown in Figure 5-1. Both the pressure and the temperature of the condenser inlet were measured using an absolute pressure transducer and T-type thermocouple, respectively. Also, the temperature of the condenser outlet, five temperature measurements along the channel wall, and the differential pressure were obtained experimentally. On the water side, inlet and outlet water temperatures and the water flow rate were also obtained from the experiments. All this information was then used in the correlations

to calculate by iterative means the local heat transfer coefficient. Once the local HTCs were attained from the calculations, the mean average of the local HTCs was compared with the average heat transfer coefficient obtained from the experiments.
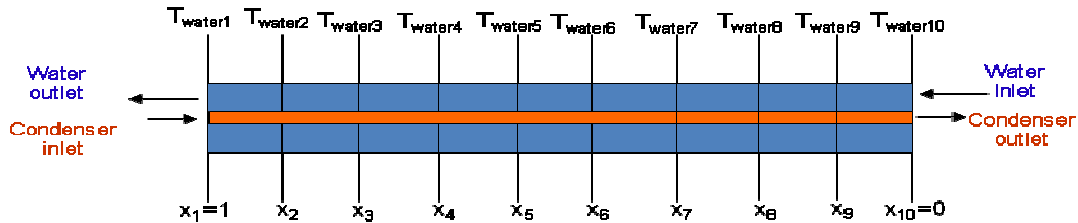
Figure 5-1 Schematic of the micro-channel divided to nine segments

The correlations presented in this investigation are of macro- and micro scale-channels, such as those developed by Dobson and Chato (1998), Shah (1978), and the void fraction model correlation by El Hajal et al. (2003). The Dobson-Chato correlation is a recent correlation based on R12 and R134a as the working fluids; it uses the Martinelli parameter (Dobson & Chato, 1998). D. Jung, Song, Cho, and Kim (2003) modified the Dobson-Chato correlation, and their modified correlation was also compared to the experimental data of this investigation. Shah's (1978) correlation used nine different fluids, three different orientations, and a wide variety of tube diameter sizes. It was useful to compare Shah's macro-channel correlation with our micro-channel results to quantify any difference between the macro- and micro-channel results. The void fraction model correlation was also evaluated in this study due to the physics that this model employs and the different approach that this model takes from the previous two models.

5.1.1 Dobson-Chato Correlation

The Dobson-Chato correlation takes into account Martinelli's parameter, which is the ratio of the two-phase heat transfer coefficient to the liquid-phase heat transfer coefficient and it expresses the liquid fraction of a flowing fluid:

$$\chi_{tt} = \left(\frac{1-x}{x}\right)^{0.9} \left(\frac{\rho_v}{\rho_l}\right)^{0.5} \left(\frac{\mu_l}{\mu_v}\right)^{0.125} \tag{5.1}$$

This parameter is also used in convective evaporation in boiling, (Chen, 1966). The heat transfer coefficient is defined as the liquid heat transfer coefficient,

$$h_l = 0.023 Re_l^{0.8} \, Pr_l^{0.4} \frac{k_l}{D_h} \tag{5.2}$$

multiplied by the inverse of the Martinelli's parameter, as shown in Equation (5.3):

$$h_{Dobson-Chato} = h_l \left(1 + \frac{2.22}{\chi_{tt}^{0.89}}\right) \tag{5.3}$$

D. Jung, Song, Cho, and Kim (2003) have also evaluated this correlation using Martinelli's data. They found that Dobson and Chato's correlation under-predicted his data in the low quality and mass flux regimes, while it over-predicted the high mass flux data. Therefore, they modified the correlation to fit Dobson and Chato's data. The following heat transfer coefficient is Dobson-Chato correlation modified by Jung, et al (2003):

$$h_{Modified\ Dobson-Chato} = h_l \left(1 + \frac{2.65}{\chi_{tt}^{0.79}}\right) \tag{5.4}$$

A comparison of the data with both the Dobson-Chato and the modified correlations is shown in Figure 5-2 and Figure 5-3 for R134a and R245fa, respectively. Both correlations were able to capture the majority of the data points;

however, they failed to accurately predict the low mass flux, and low and high

saturation temperature regimes, as shown for the cases of 30 °C and 70 °C saturation

temperatures. In Jung et al.'s findings, there is a slight difference between the

Dobson-Chato correlation and the modified correlation. This was evident after

applying the correlations to our data, especially when using R134a, as shown in

Figure 5-2. Both correlations were able to predict the R134a data. However, the

Dobson-Chato and the modified Dobson-Chato correlations were not quite similar for

the R245fa data (Figure 5-3), especially at high flow rates, for which they mainly

under-predicted the data.
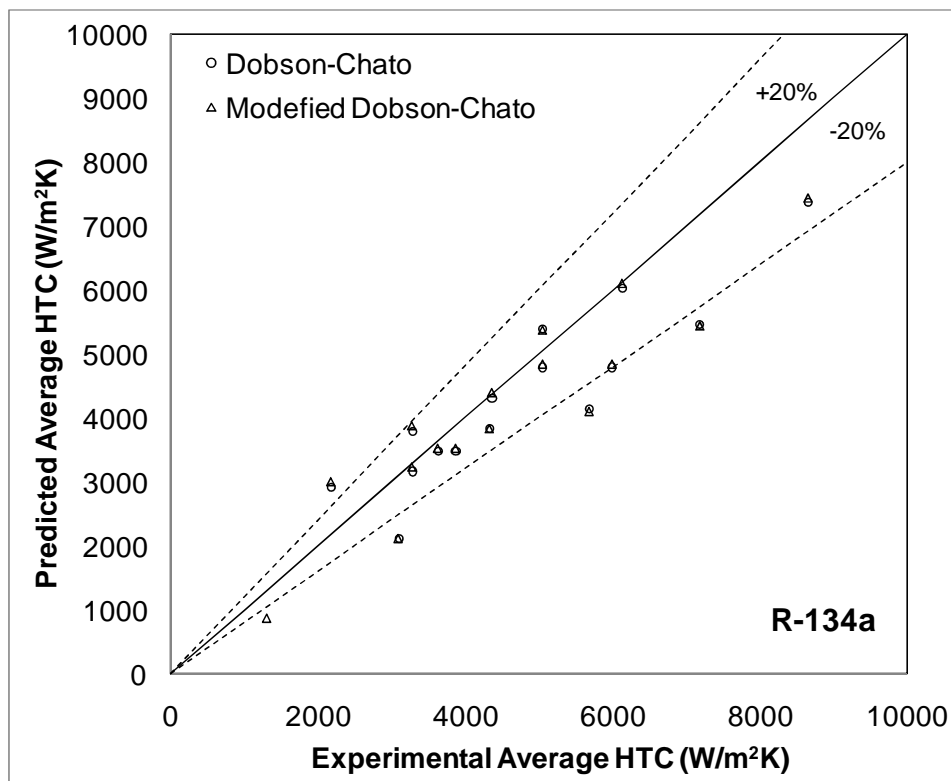
Figure 5-2 Comparison of the Dobson & Chato HTC correlation against the present data of R134a
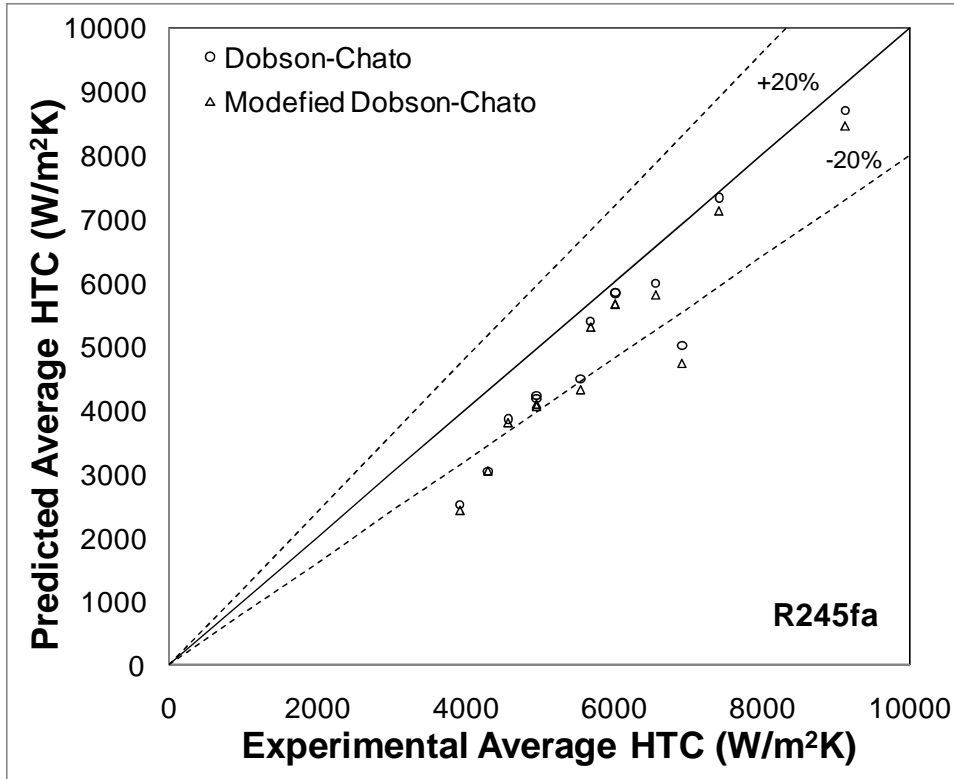
Figure 5-3 Comparison of the Dobson & Chato HTC correlation against the present data of R245fa

In order to fit the data, Dobson and Chato's approach was modified by changing the power of the Martinelli parameter as follows:

$$h_{Newly\ Modified\ Dobson-Chato} = h_l \left(1 + \frac{2.22}{\chi_{tt}^{0.97}} \right) \qquad (5.5)$$

Since the two refrigerants, R134a and R245fa, gave different outcomes when compared with the correlation, it was evident that fluid properties were a cause. Given the fact that the Martinelli parameter is a relation of fluid properties in liquid and vapor states, we assumed a modification to this parameter would give a better fit to our data. Thus, the Martinelli parameter was modified to fit the data of both refrigerants well. This simple modification resulted in a better fit of the data for both refrigerants, as illustrated in Figure 5-4.

87

It is obvious from equation (5.1) that at a certain saturation temperature, the second term and the third term in the right hand side remain constant and only the first term in the right hand side changes when quality of vapor is changed. As quality of vapor is increased, the Martinelli parameter decreases as shown in Figure 5-5. From the figure, it is obvious that the Martinelli parameter becomes smaller than 1 after 20% vapor quality; therefore, mathematically by increasing the power of the Martinelli parameter (χ), the parameter becomes even smaller. Moreover, the denominator in equation (5.5) becomes smaller than what it is in equation (5.3) which causes an increase in heat transfer coefficient. What happens physically in the channel was verified by visualization tests. In section 6.1.2 it is clear from Table 6-3 that after 20% vapor quality, the regime changes to annular flow regime and since the channel width is 0.4 mm, then the average liquid layer thickness is less than 0.2 mm; therefore, an increase in heat transfer is depicted at that stage. In addition, since the Martinelli parameter expresses the liquid fraction of a flowing fluid, then increasing or decreasing the power of the Martinelli parameter adjusts the amount of liquid flowing inside the channel.
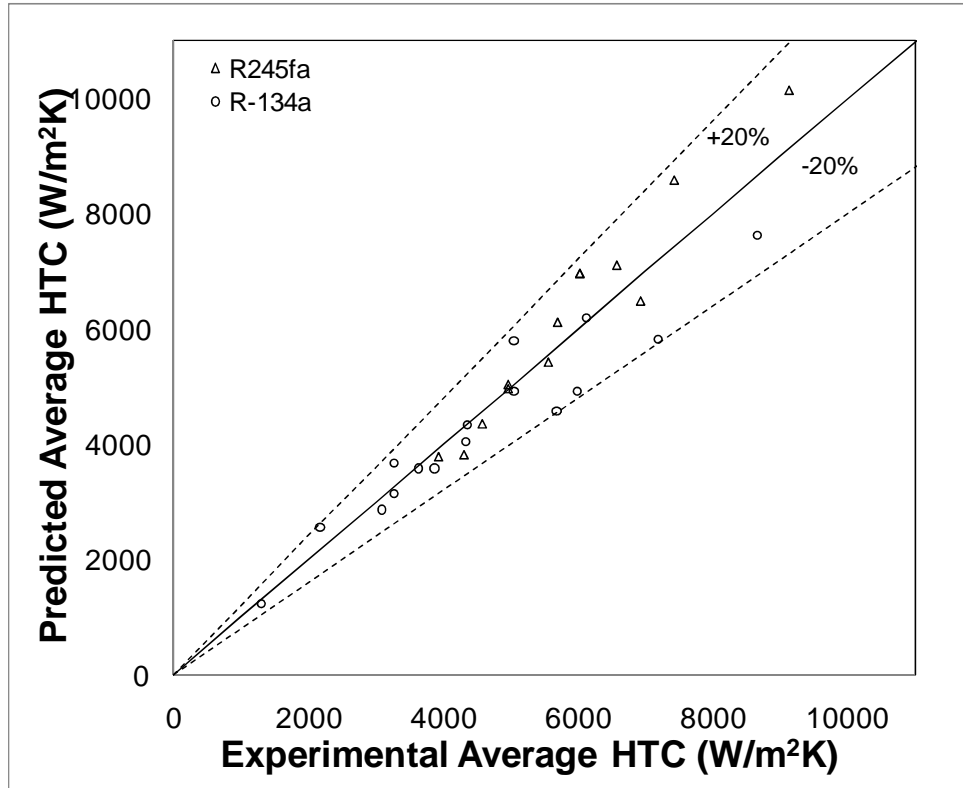
Figure 5-4 Comparison of the newly modified Dobson-Chato HTC correlation against the present data of R134a & R245fa
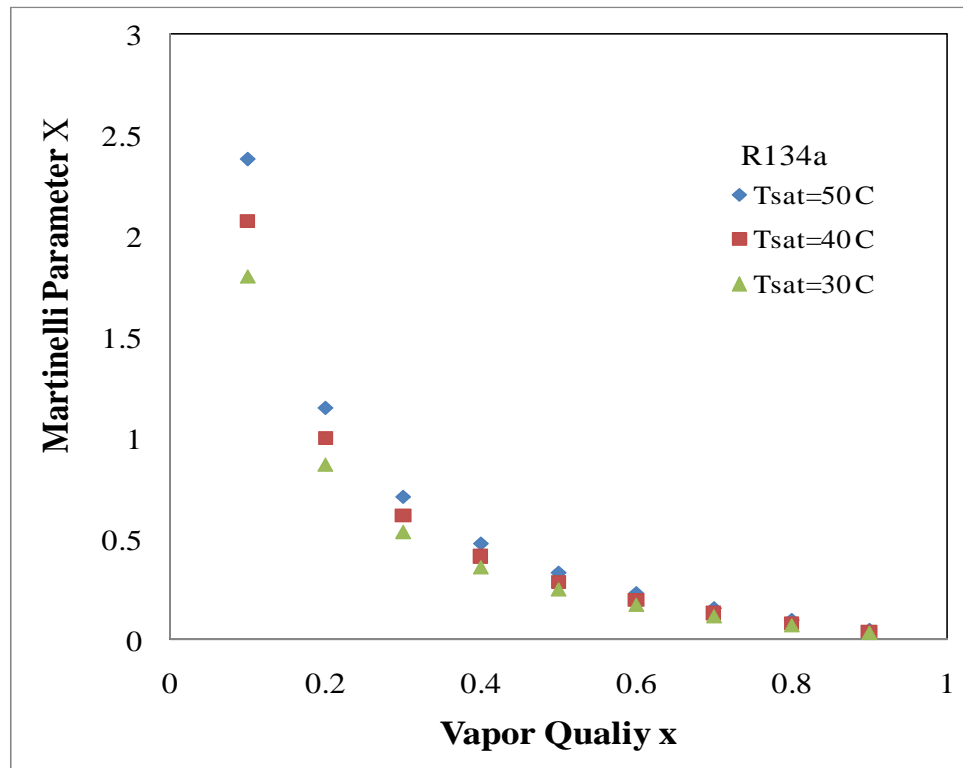
Figure 5-5 Martinelli parameter vs. vapor quality

5.1.2 Shah's Correlation

Shah generated his correlation (1978) by eliminating bubble nucleation from his former correlation for saturated boiling (Shah, 1976). To find the heat transfer coefficient for condensation, Shah adopted two approaches to reach the best-fitting correlation for his data. In the first approach, a vapor-liquid density ratio was used, Equation (5.6):

$$C_o = \left(\frac{1}{x} - 1\right)^{0.8} \left(\frac{\rho_v}{\rho_l}\right)^{0.5} \tag{5.6}$$

Then the two-phase heat transfer coefficient was defined as the superficial heat transfer coefficient of the liquid-phase divided by the constant C_o, Equation (5.7):

$$h_{tp} = \frac{1.8 \, h_l (1 - x)^{0.8}}{C_o^{0.8}} \tag{5.7}$$

where h_l is the heat transfer coefficient, assuming all the flowing mass is liquid:

$$h_l = 0.023 Re_l^{0.8} \, \Pr_l^{0.4} \frac{k_l}{D_h} \tag{5.8}$$

Shah developed the second approach to replace the vapor-to-liquid density ratio $\frac{\rho_v}{\rho_l}$ by the reduced pressure, which is the ratio of saturation pressure to critical pressure,

$$p_{red} = P_{sat}/p_c \tag{5.9}$$

A new parameter was also defined to fit his data to the correlation, which is defined as:

$$Z = \left(\frac{1}{x} - 1\right)^{0.8} p_{red}^{0.4} \qquad (5.10)$$

Then the two-phase heat transfer coefficient yields:

$$h_{tp} = \frac{1 + 3.8}{Z^{0.95}} h_l (1 - x)^{0.8}$$

$$= h_l \left((1 - x)^{0.8} + \left(\frac{3.8 \, x^{0.76}(1 - x)^{0.04}}{p_{red}^{0.38}} \right) \right) \qquad (5.11)$$

Shah (1978) also defined a mean heat transfer coefficient, assuming negligible change in transport properties of the liquid phase and pressure drop along the channel. He did this first by finding the relation of the vapor quality distribution to length, and then, integrating the later two-phase heat transfer coefficient, defined above, over the length of the channel. This led to Equation (5.12) for the case of x =1 to x = 0:

$$h_{tp-Mean} = h_l \left(0.55 + \left(\frac{2.09}{p_{red}^{0.38}} \right) \right) \qquad (5.12)$$

All three of the above heat transfer coefficient correlations that Shah (1978) developed for two-phase heat transfer coefficient were compared with the data collected in the present study. The comparisons are shown in Figure 5-6 and Figure 5-7.

The reduced pressure and the mean methods were able to predict the R134a data fairly well; however, the density method under-predicted all the data, as shown in Figure 5-6.
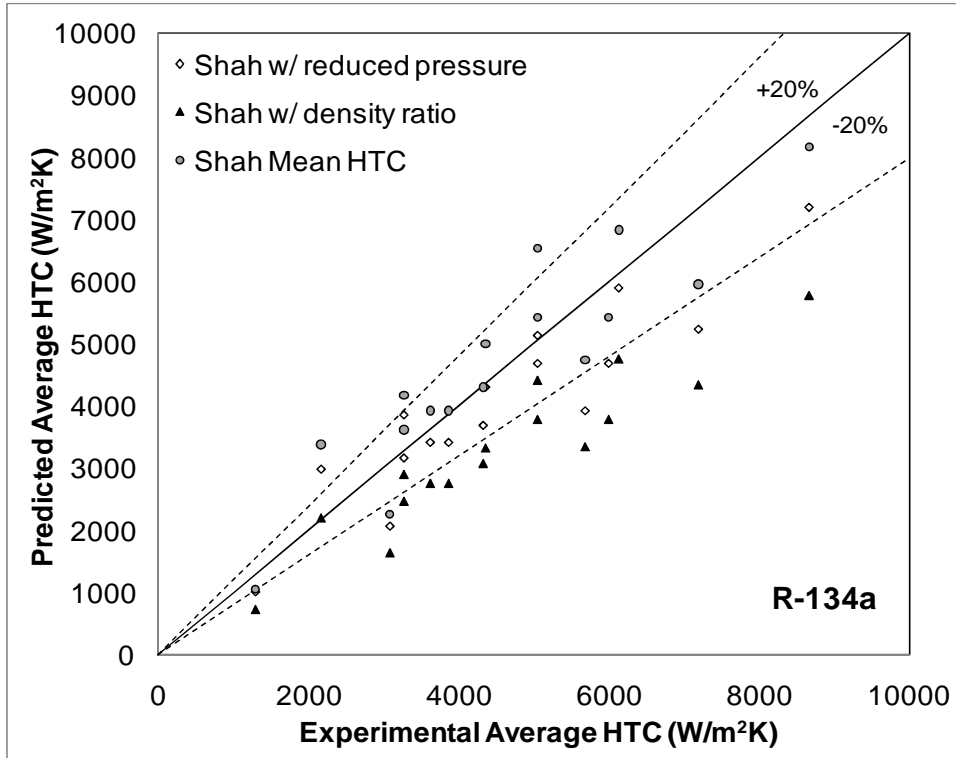
Figure 5-6 Comparison of Shah HTC correlation versus the current data of R134a

Figure 5-7 shows the comparison between the R245fa data and the correlation. It is obvious from the figure that the correlation under-estimated the majority of the data.
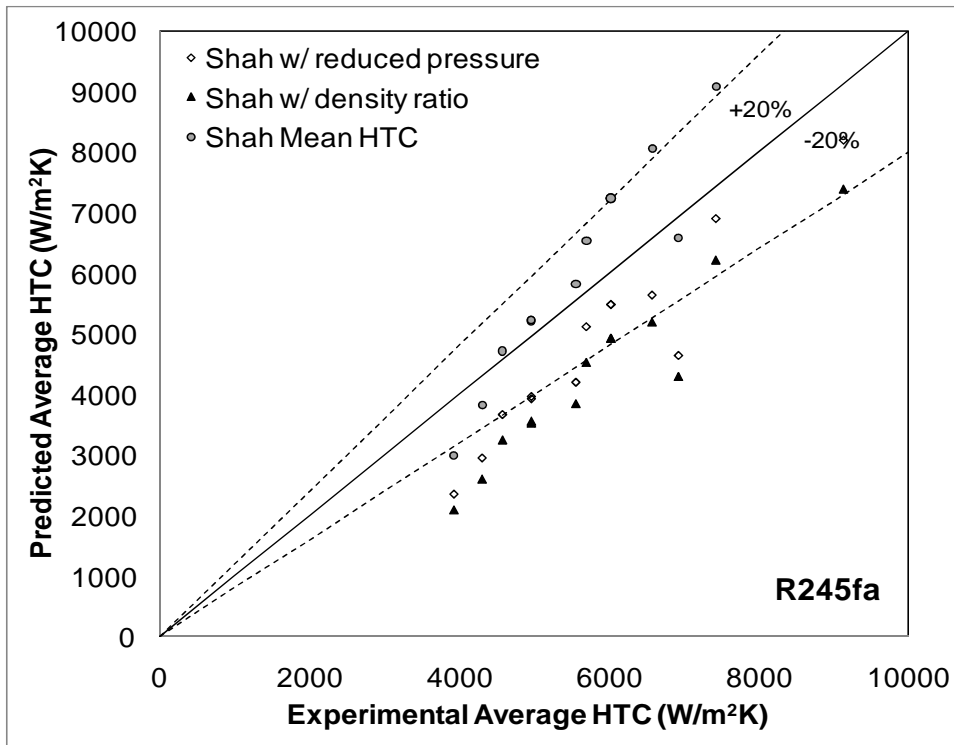
Figure 5-7 Comparison of Shah HTC correlation against the current data of R245fa

To fit the data from the current study to this correlation, since the reduced

pressure model predicted the R134a data well, Shah's model was modified. In

addition, since the refrigerants have different critical pressures, it was clear that the

disagreement between the R245fa results and the correlation was most likely due to

its fluid properties. It has been shown previously that vapor density has a dominant

effect when saturation temperature is changed and that reduced pressure is

proportional to the saturation pressure; thus increasing saturation pressure, increases

the vapor density, which then decreases the velocity and therefore decrease the heat

transfer. This can also be seen from Equation 5.11, where increasing the saturation

temperature increases the reduced pressure, and since the reduced pressure has an

inverse relationship with heat transfer coefficient in the Shah correlation, the heat

transfer coefficient decreases. Consequently, when modifying the power of the

reduced pressure in the Shah two-phase heat transfer coefficient correlation from 0.38 to 0.53, the data for both refrigerants were in good agreement with the correlation, as seen in Figure 5-8.

The reduced pressure factor (P_{red}) for both of the testing fluids are always positive numbers that are lower than 1, because the critical pressure (p_c) is always larger than the saturated pressure (P_{sat}). Therefore, increasing the power of P_{red} produces a smaller value of P_{red}, mathematically, and since P_{red} is in the denominator; therefore, increasing the power of P_{red} causes h_{tp} increase in equation (5.11).
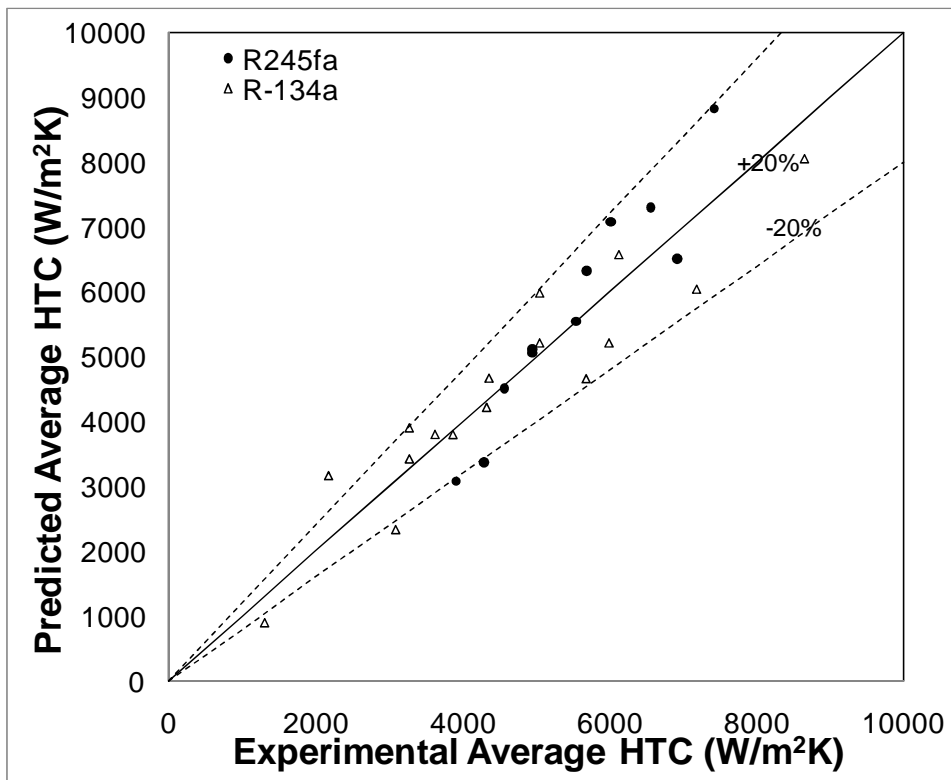
Figure 5-8 Comparison of the newly modified Shah's HTC correlation against the present data of R134a & R245fa

94

5.1.3 Void Fraction Model

The void fraction is defined as the cross-sectional area occupied by the vapor with respect to the total cross-sectional area of the channel. El Hajal et al. (2003) have reported several prediction methods of void fractions. Amongst those methods is the homogenous model, which assumes that the two phases travel at same velocity, ε_h, and the drift flux model, which takes into account the effect of surface tension and the mass velocity, ε_{ra}. The drift flux model was developed by Rouhani and Axelsson (1970) for flow boiling. These models are defined as

$$\varepsilon_h = \left(1 + \left(\frac{1+x}{x} \right) \left(\frac{\rho_v}{\rho_l} \right) \right)^{-1} \tag{5.13}$$

and

$$\varepsilon_{ra} = \left(\frac{x}{\rho_v} \right) \left([1 + 0.12(1-x)] \left(\frac{x}{\rho_v} + \frac{1-x}{\rho_l} \right) \right.$$
$$\left. + \frac{1.18(1-x)[g_g \sigma(\rho_l - \rho_v)]^{-0.25}}{G \rho_l^{0.5}} \right)^{-1} \tag{5.14}$$

The homogenous model is mostly applicable at very high reduced pressures because the density of the vapor approaches that of the liquid (El Hajal et al. 2003), whereas the drift flux model is mainly effective at low to medium pressures. As pressure approaches the critical point, the drift flux model does not work towards the homogenous void fraction limit (El Hajal et al. 2003). Both models are sensitive to saturation pressures; however, they produce reversed trends, as the investigators found. Therefore, a more general void fraction model was developed by Al Hajal et al. to correct the effect of pressure on the models, which involved interpolation between the values of the models, the homogenous and the drift flux. The model was

95

developed by taking the logarithmic mean void fraction between the values of ε_h and $\varepsilon_{ra,}$ which is defined as

$$\varepsilon = \frac{\varepsilon_h - \varepsilon_{ra}}{\ln\left(\frac{\varepsilon_h}{\varepsilon_{ra}}\right)} \qquad (5.15)$$

This method gave the best fit to the data used in their investigation (El Hajal et al. 2003). Since this correlation comprises different physics from the previous two correlations by Dobson-Chato and Shah, it was considered in this study.

The heat transfer coefficient (Equation 5.16) that was used in El Hajal et al. (2003) is for the convective evaporation of Kattan, Thome, and Favrat (1998) that includes two empirical constants c and n:

$$h_{tp} = c \, Re_l^n \, Pr_l^{0.5} \frac{k_l}{\delta_t} \qquad (5.16)$$

where c and n are the empirical constants and are 0.0039 and 0.734, respectively. Re_l and δ_t are the liquid film Reynolds number and the liquid film thickness for annular flow, respectively, and they are defined as, (assuming $\delta_t \ll D_h$),

$$Re_l = \frac{G(1-x)D_h}{\mu_l} \qquad (5.17)$$

and

$$\delta_t = D_h \frac{(1-\varepsilon)}{4} \qquad (5.18)$$

Figure 5-9 and Figure 5-10 show how the data from this investigation fit the correlation. In the case of R134a, it is obvious from the figure that the majority of the data points falls into the $\pm 20\%$ error lines and that the correlation under-predicts the data results. As for R245fa, it seems like the correlation was very poor in predicting

the data. The correlation did not generate as much discrepancy as the other two

correlations when compared with the current data of R134a, which motivated us to

modify the correlation to fit these data as well.
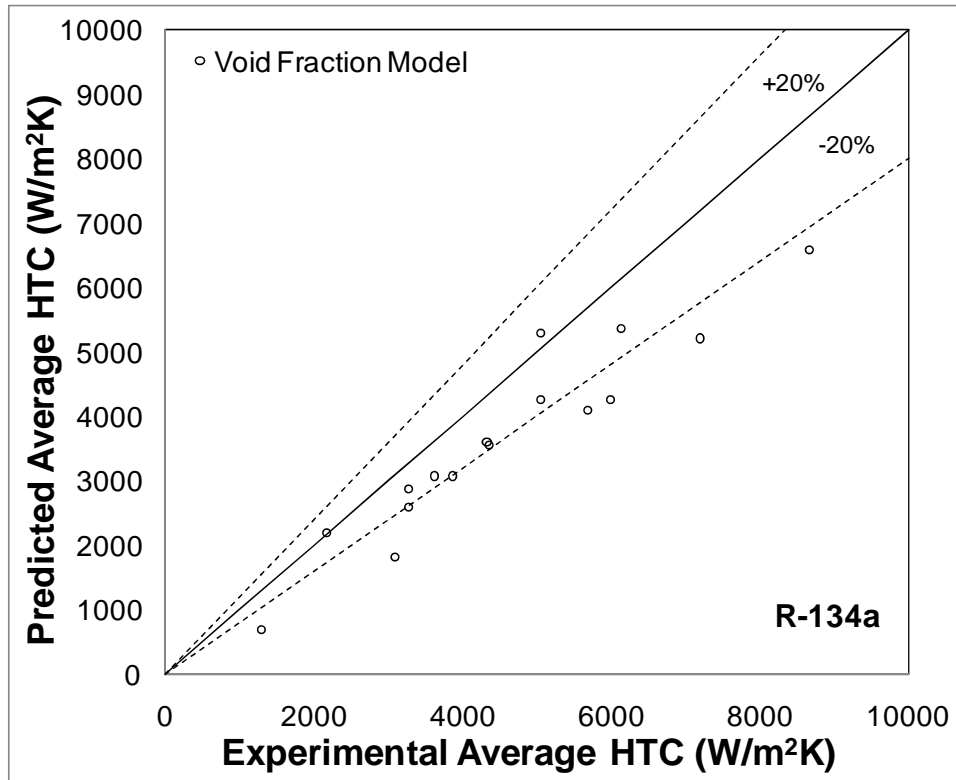
Figure 5-9 Comparison of the void fraction model against the current data of R134a
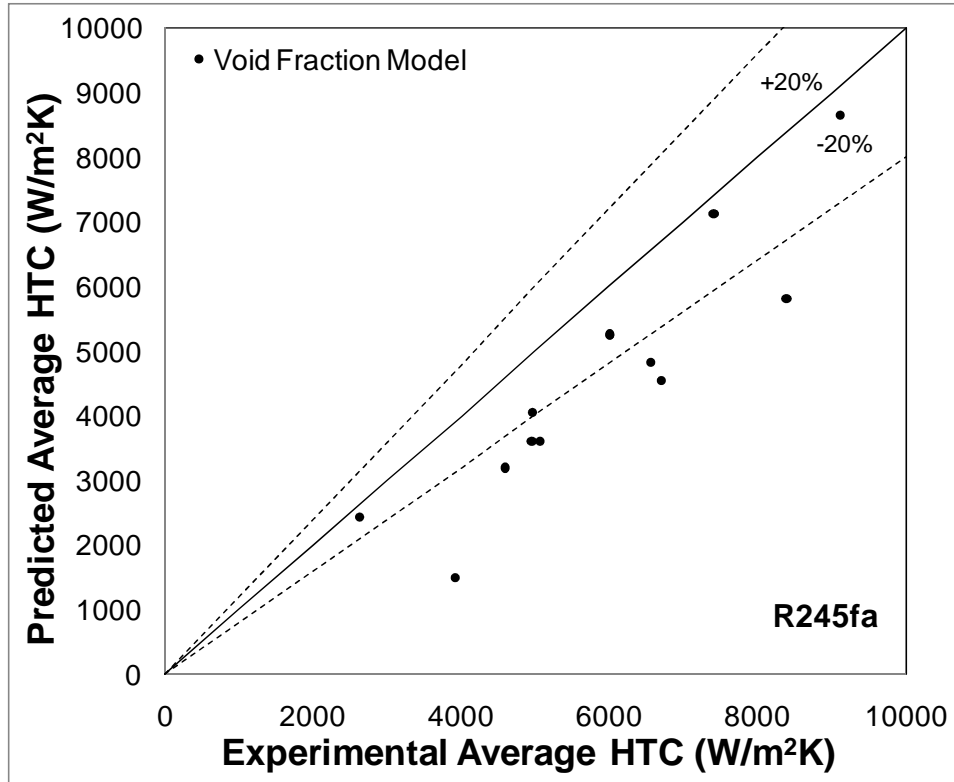
Figure 5-10 Comparison of the void fraction model against the current data of R245fa

In order to improve the correlation to fit the data, the constants *c* and *n* were

changed to 0.0045 and 0.75, respectively; thereafter, the modified correlation was

compared with the data to generate Figure 5-11. It is apparent from the figure that the

modification to the empirical constant has improved the correlation to fit the current

data well. Increasing *c* mathematically means that the interception of the data curve

with the h_{tp} axis is shifted up and the increase of *n* adjusts the Reynolds number of the

liquid film which then increases the heat transfer coefficient of equation (5.16).
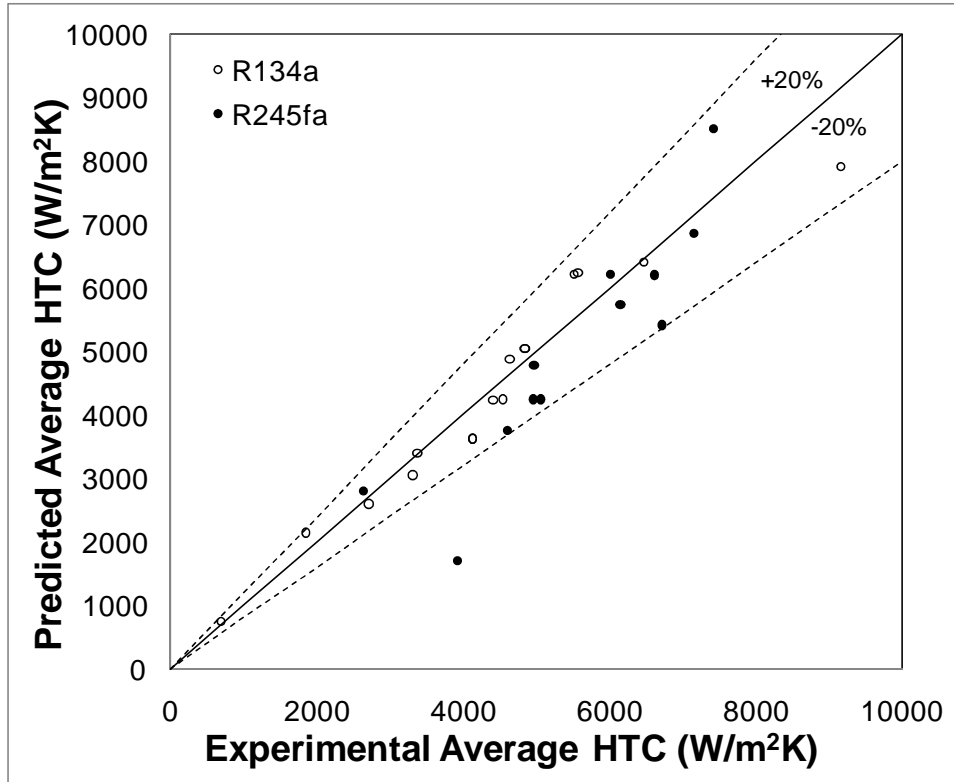
Figure 5-11 Comparison of the newly modified void fraction model against the current data of R134a

5.2 *Pressure Drop Correlations*

Similar to the heat transfer coefficient case, the overall pressure drop value

was obtained from experiments. As explained earlier in the experimental setup

section, an accurate differential pressure transducer was used to measure the pressure

difference from the inlet and the outlet of the micro-channel. It is acknowledged that

in two-phase flows different regimes have different pressure drops, and, in this study

only the overall pressure drop was measured as required by the project work

statement.

The correlations introduced in this section are for local pressure drops. Again,

using these correlations directly to correlate our data was not adequate unless local

information was obtained using the same technique used to obtain the local heat

transfer coefficient in Section 5.1. Given the saturation pressure at the inlet of the condenser, the temperatures of the condenser walls, and the pressure drop across the condenser, local pressure drops were obtained where the channel was divided into nine segments by using the correlations. The local pressure drops were averaged and compared with the overall pressure drop acquired from experimentation.

Most of the descriptive two-phase pressure drop correlations that take into account the effect of different flow regimes make use of flow mapping information. It is important to obtain and study the flow regime pattern to develop an accurate two-phase flow model (Thome et al. 2003), (El Hajal et al. 2003), (Garimella et al. 2003), (Baker, 1954) and (Coleman and Garimella, 2003). This investigation did not develop a flow map due to the work statement requirements and also to the fact that this work only considered the condensation case where 100% quality enters the condenser and 0% quality leaves from the condenser. One data point (T_{sat}=50 ^{o}C, mass flux = 300 kg/m^{2}s and a rectangular channel shape with D_h= 0.7 mm) of the current study was compared with one data point of Garimella, Agarwell, & Killion (2005) that was obtained at similar testing conditions and channel size, (T_{sat}=50 ^{o}C, mass flux = 300 kg/m^{2}s and a square channel shape with D_h= 0.76 mm). The comparison was done in order to determine whether Garimella, Agarwell, and Killion's (2005) flow map could be used in the current work to find a more accurate pressure drop model. However, the heat transfer of the current study was 25% higher than that of Garimella, et al. Thus, no flow map was used in this study to develop pressure drop correlation. However, the pressure drop correlations presented in this section are derived from physical and classical approaches.

5.2.1 Lockhart-Martinelli Model

This model considers different velocities for each phase and assumes that the velocity of each phase is uniform at any axial cross section. For one-dimensional, adiabatic flow in a constant cross sectional area channel, the total pressure drop is defined as

$$\frac{dP}{dz} = \left[\Phi_l^2 \left(\frac{dP}{dz}\right) - ((1-\varepsilon)\rho_l + \varepsilon\rho_v)g_g\right] \tag{5.19}$$

where $(dP/dz)_l$ indicates the pressure gradient of only liquid flowing in the channel, and Φ_l^2 is the Lockhart and Martinelli key multiplier, which was defined by Martinelli and Nelson (1948) and Lockhart and Martinelli (1949), and which compares the two-phase frictional pressure gradient $(dP/dz)_{tp}$ with a single-phase frictional pressure gradient $(dP/dz)_l$ assuming only one phase in the tube:

$$\Phi_l^2 = \frac{\left(\frac{dP}{dz}\right)_{tp}}{\left(\frac{dP}{dz}\right)_l} = \left[1 + \frac{20}{\chi_{tt}} + \frac{1}{\chi_{tt}^2}\right] \tag{5.20}$$

where χ_{tt} is a parameter that Lockhart and Martinelli (1949) developed and is the square root of the ratio of liquid frictional pressure drop to the vapor frictional pressure drop:

$$\chi_{tt} = \left[\frac{\left(\frac{dP}{dz}\right)_l}{\left(\frac{dP}{dz}\right)_v}\right]^{1/2} = \left(\frac{1-x}{x}\right)^{0.875} \left(\frac{\rho_v}{\rho_l}\right)^{0.5} \left(\frac{\mu_l}{\mu_v}\right)^{0.125} \tag{5.21}$$

where the frictional gradient for a separated two-phase flow model can be defined as

$$\left(\frac{dP}{dz}\right)_l = -\frac{1}{2}f_l \frac{G^2(1-x)^2}{\rho_l D_h} \tag{5.22}$$

$$\left(\frac{dP}{dz}\right)_v = -\frac{1}{2}f_v \frac{G^2(1-x)^2}{\rho_v D_h} \tag{5.23}$$

where f_l and f_v are the fanning friction factor, assuming that only liquid or only vapor is flowing alone at the same superficial velocity of the phase. They are presented as

$$f_l = 0.316\left(\frac{G(1-x)D_h}{\mu_l}\right)^{-0.25} \tag{5.24}$$

$$f_v = 0.316\left(\frac{GxD_h}{\mu_v}\right)^{-0.25} \tag{5.25}$$

Although this model assumes adiabatic condition, the physics of each flow regime in condensation is captured using the proper quality and void fraction to find the corresponding local pressure drop. The void fraction is obtained from the quality and the density of both liquid and vapor, which is defined as

$$x = \frac{\rho_v \varepsilon}{(1-\varepsilon)\rho_l + \varepsilon\rho_v} \tag{5.26}$$

A comparison of the correlation and the experimental results is shown in Figure 5-12 and Figure 5-13. As seen in these graphs, it is obvious that the Lockhart and Martinelli model was very poor in predicting the pressure drop for the micro-channel condensation for both refrigerants.
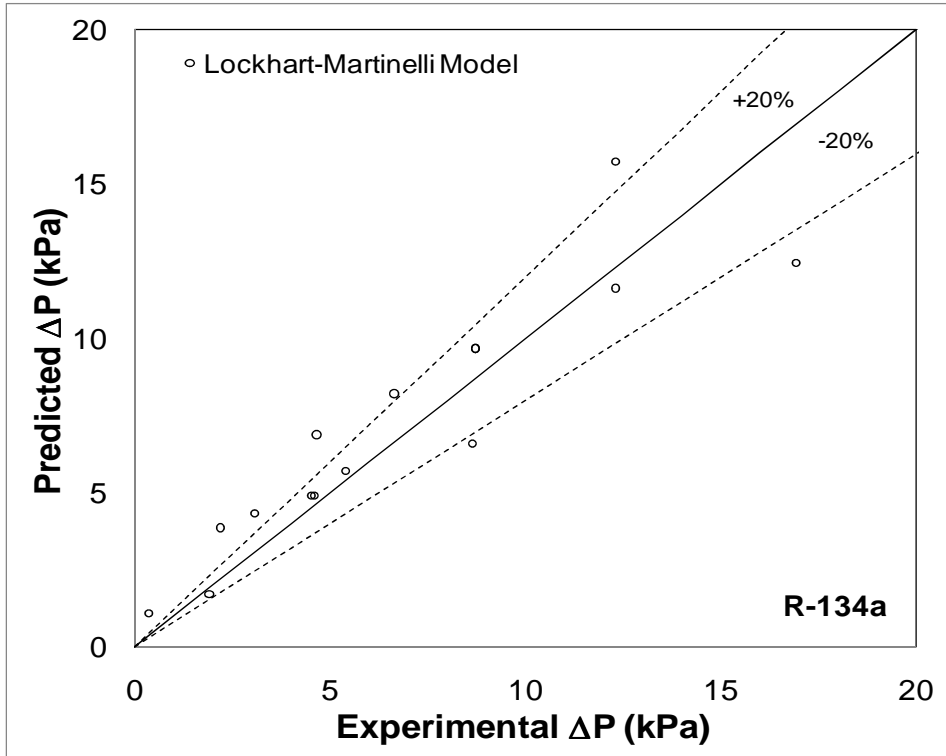
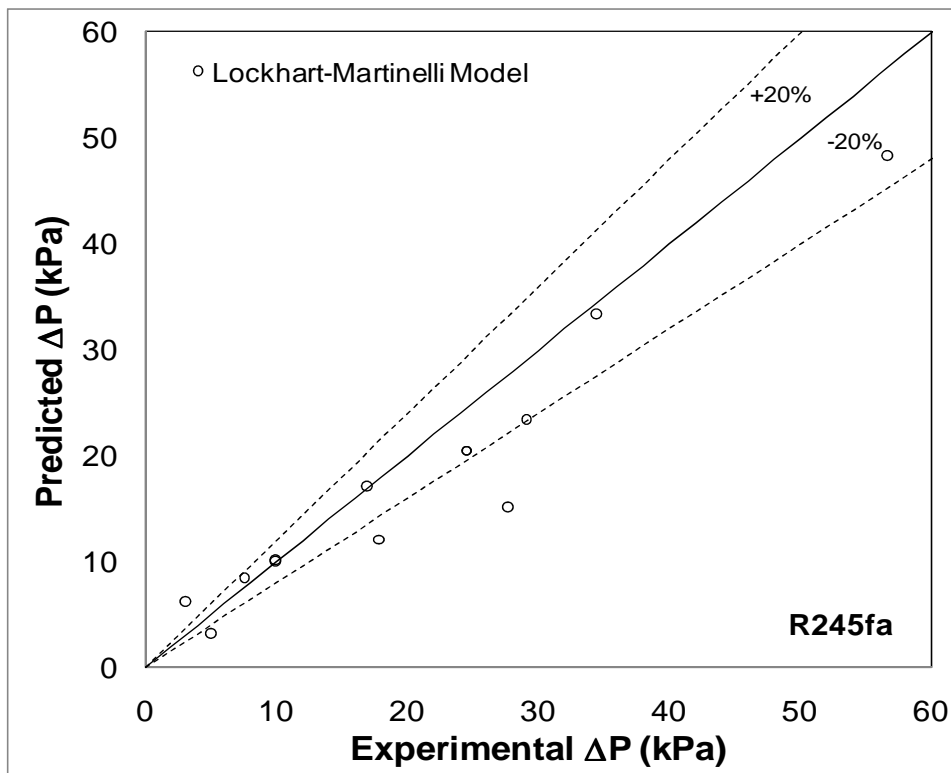Figure 5-12 Comparison of Lockhart-Martinelli pressure drop model against the current data of R134a

Figure 5-13 Comparison of Lockhart-Martinelli pressure drop model against the current data of R245fa

5.2.2 *Classical Pressure Drop Model*

This model consists of several effects, such as friction, acceleration or deceleration due to momentum changes, and gravitational components (Shao & Granryd, 2000). The total pressure drop for two-phase flow is presented as follows:

$$\left(\frac{dP}{dz}\right) = \left(\frac{dP}{dz}\right)_f + \left(\frac{dP}{dz}\right)_m + \left(\frac{dP}{dz}\right)_g \qquad (5.27)$$

Since the experiments were conducted on a horizontal plane, the gravitational component can be neglected. Thus the total pressure drop is reduced to

$$\left(\frac{dP}{dz}\right) = \left(\frac{dP}{dz}\right)_f + \left(\frac{dP}{dz}\right)_m \qquad (5.28)$$

The subscripts *f* and *m* indicate the pressure drop due to friction and momentum, respectively.

The friction term uses the Lockhart-Martinelli correlation to find the two-phase pressure gradient due to friction by using the Lockhart and Martinelli two-phase pressure drop key parameter:

$$\Phi_v = \left[\frac{\left(\frac{dP}{dz}\right)_f}{\left(\frac{dP}{dz}\right)_v}\right]^{0.5} \qquad (5.29)$$

where the vapor pressure drop is defined as:

$$\left(\frac{dP}{dz}\right)_v = -2f_o \frac{(xG)^2}{\rho_v D_h} \qquad (5.30)$$

f_o is the friction factor for the adiabatic two-phase flow and is estimated here by Colburn's equation as follows:

$$f_o = \frac{0.045}{Re_v^{0.2}} \tag{5.31}$$

Here the Reynolds number of the vapor flow is defined as:

$$Re_v = \frac{xGD_h}{\mu_v} \tag{5.32}$$

Lockhart and Martinelli (1949) analyzed pressure drop data of adiabatic flows of different fluids and obtained the following key multiplier and parameter:

$$\Phi_v = 1 + 2.85\chi_{tt}^{0.523} \tag{5.33}$$

Azer, Abis, and Soliman (1972) and Shao and Granryd (2000) correlated key multipliers for two-phase condensation data instead of adiabatic flow data. Azer's correlation was as follows:

$$\Phi_v = 1 + 1.09\chi_{tt}^{0.039} \tag{5.34}$$

whereas Shao's correlation was as follows:

$$\Phi_v = 1 + 0.8\chi_{tt}^{0.1} \tag{5.35}$$

The contribution of momentum transfer to the total pressure drop is negligible in adiabatic two-phase flows (Shao & Granryd, 2000). However, the momentum transfer contribution becomes more noticeable in condensation heat transfer due to the mass transfer present at the vapor-liquid interface and also due to the change in kinetic energy, which is defined as

$$\left(\frac{dP}{dz}\right)_m = \left[\frac{x^2 G^2}{\varepsilon \rho_v} + \frac{(1-x)^2 G^2}{\rho_l (1-\varepsilon)}\right]_{x=0}$$

$$+ \left[\frac{x^2 G^2}{\varepsilon \rho_v} + \frac{(1-x)^2 G^2}{\rho_l (1-\varepsilon)}\right]_{x=1}$$

(5.36)

Here the void fraction ε was developed by Smith (1971) as

$$\varepsilon = \left(1 + \left(\frac{\rho_v}{\rho_l}\right)\left(\frac{1-x}{x}\right)\left[0.4\right.\right.$$

$$\left.\left. + 0.6 \left(\frac{x(\rho_l/\rho_v) + 0.4(1-x)}{x + 0.4(1-x)}\right)\right]^{0.5}\right)^{-1}$$

(5.37)

After obtaining the frictional and momentum terms, the total pressure drop

was calculated and then compared with the current data. Figure 5-14 and Figure 5-15

show the comparison of classical pressure drop correlation with the three different

key multipliers, Φ_v, which were introduced above, against the current data. The key

multiplier developed by Lockhart-Martinelli shows more agreement and consistency

with the current data for both refrigerants than the key multipliers developed by Shao,
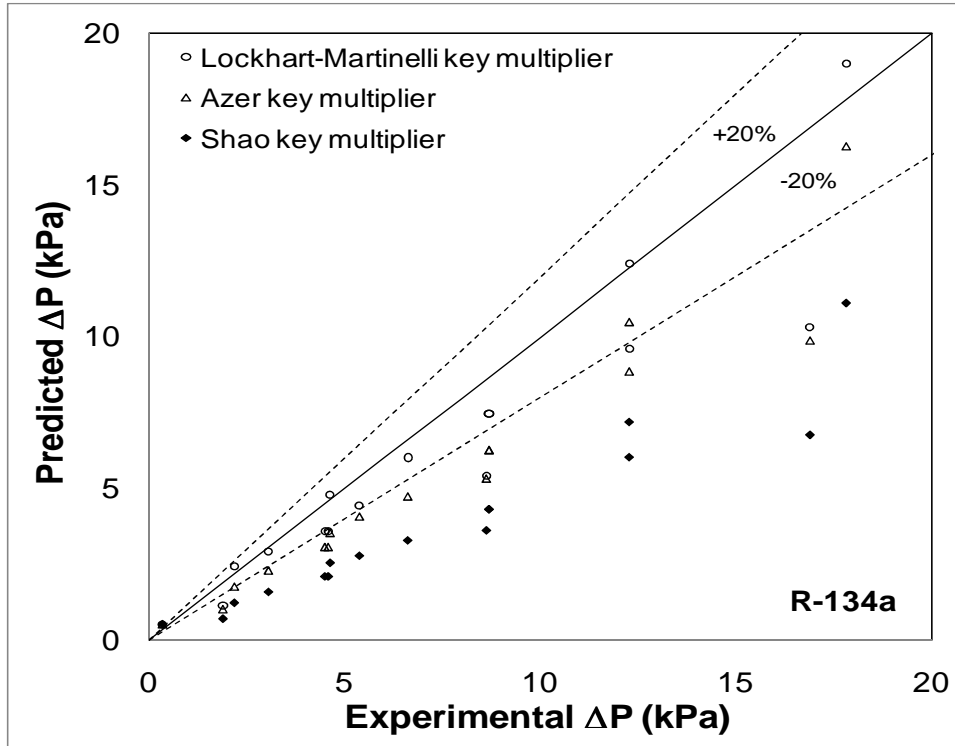
and Azer.

Figure 5-14 Comparison of the classical pressure drop model using three different key multipliers against the present data of R134a
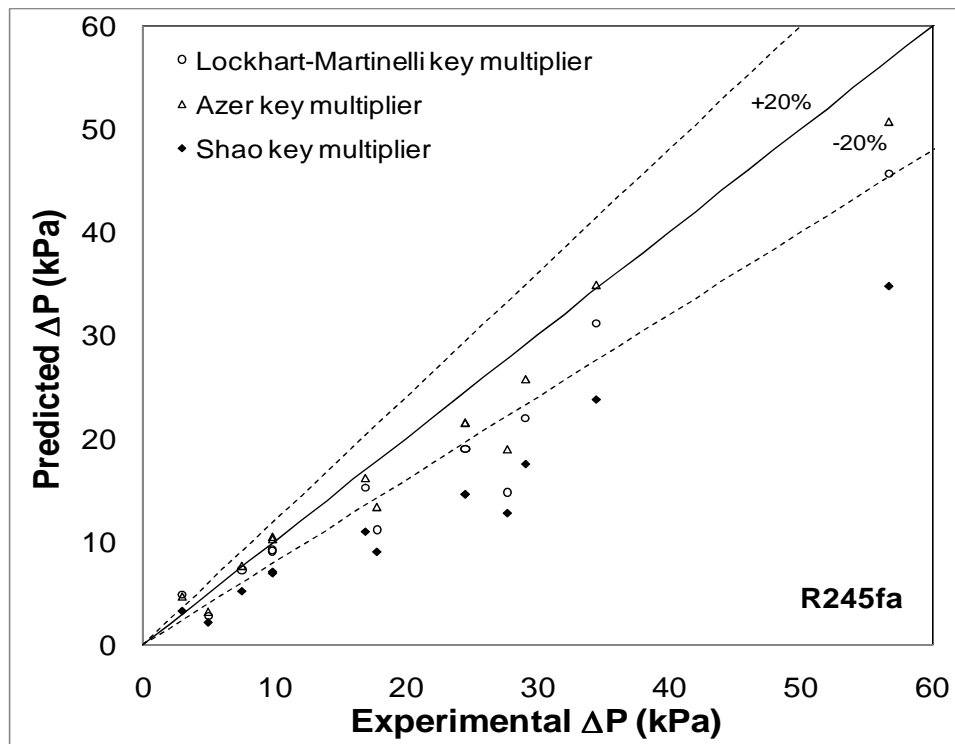
Figure 5-15 Comparison of the classical pressure drop model using three different key multipliers against the present data of R245fa

To reach a better agreement between the correlation and the data for this study, the key multiplier was modified. The newly modified key multiplier is defined as follows:

$$\Phi_v = [1 + 0.25\chi_{tt}^{-0.055}]^{1.98}$$

(5.38)

Figure 5-16 shows the comparison between the current data and the correlation using the newly developed key multiplier, where a better fit is apparent.
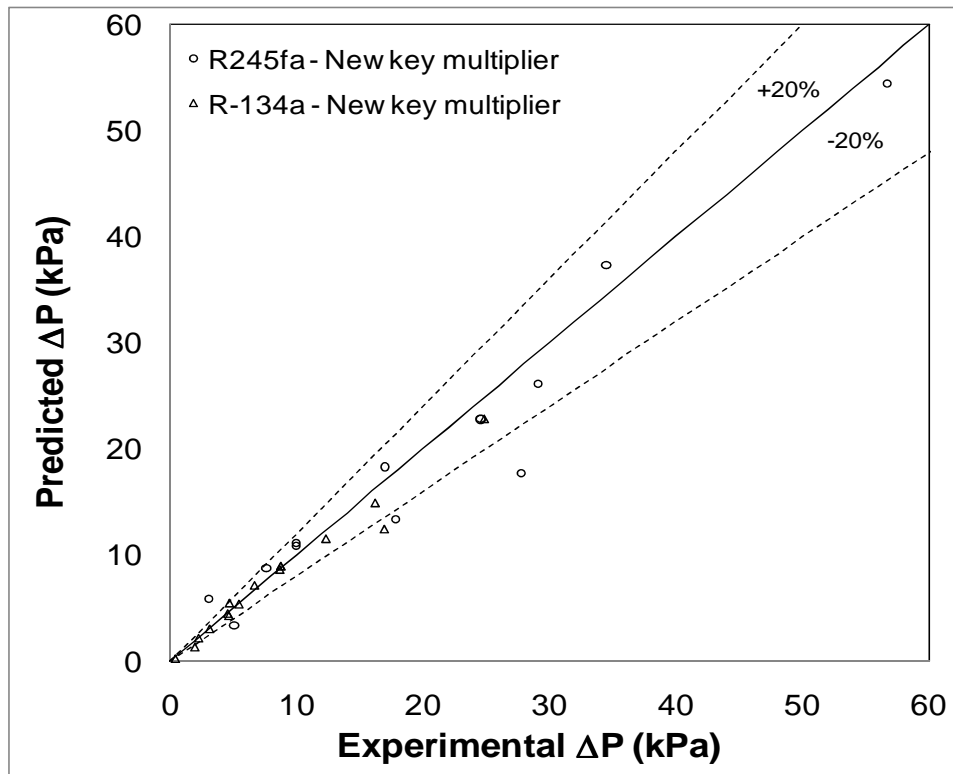
Figure 5-16 Comparison of the classical pressure drop model using the newly modified key multiplier with the current data of R134a & R245fa

By changing the power of χ_{tt} and the whole power of the right hand side of equation (5.38), the effect of pressure drop due to friction to the pressure drop due to vapor flow inside the channel changes, which is the definition of the two-phase pressure drop key multiplier. Although Figure 5-16 shows a good fit; however, when

108

comparing the values of new key multiplier Φ_v, equation (5.38), with the other three

key multipliers presented previously, Figure 5-17, shows that the values of the new

key multiplier from equation (5.38) are lower than that the values of the other key

multiplier for similar conditions. And since Φ_v is the ratio of pressure drop due to

friction to pressure drop due to vapor flow in the channel, then this means that the

pressure drop due to friction is smaller in this high aspect ratio micro-channel than in

the macro-channels. This statement contradicts a wide range of studies of pressure

drop in micro-channels that have concluded that surface tension and frictional

pressure drop are large contributors to the total pressure drop inside the channel. In

order to verify the results, I decided to conduct further studies on pressure drop by

measuring the local pressure drop and then comparing the results with the available

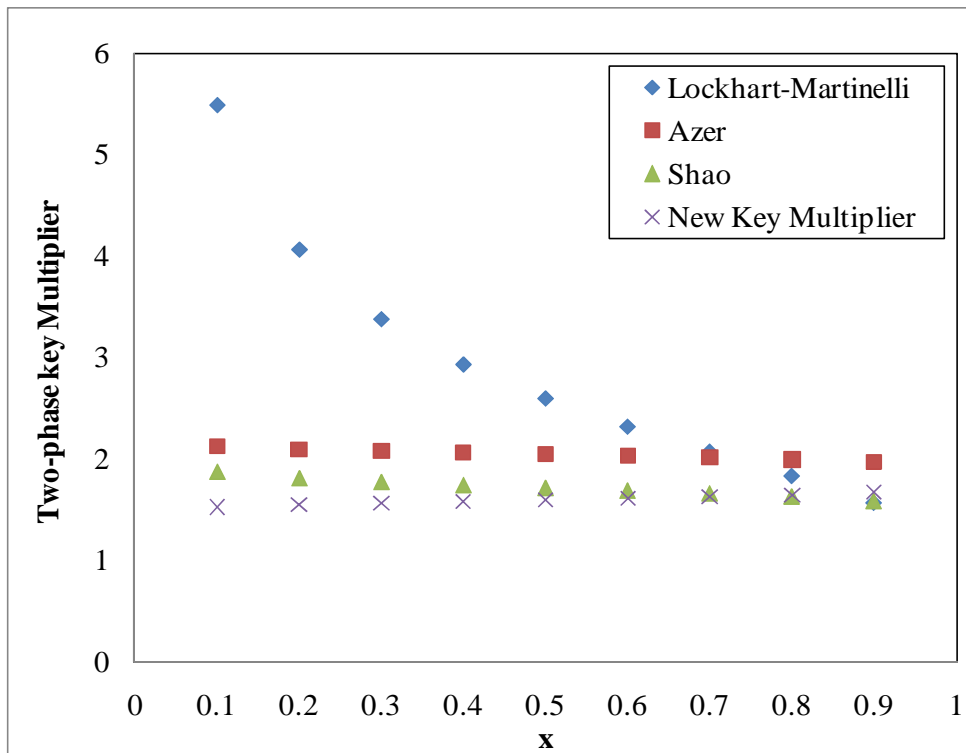pressure drop correlations. The study is presented in details in section 5.3.

Figure 5-17 Comparison of the new key multiplier with the other three key multiplier used in this study

The empirical correlations developed in this report introduce higher accuracy than the original correlation. The accuracy of the correlations is dependent on the accuracy of the data collected from experiments and since the data in this investigation were within 12% for heat transfer coefficient and 5% for pressure drop, these new empirical correlations are more accurate.

5.3 *Local Pressure Drop Correlation*

The analysis presented above of average pressure drop correlation for condensing refrigerants inside a micro-channel, did not results in a model that could be depended upon to include a high percentage of the data collected. Therefore, as a step towards verifying and improving on the models presented above, local pressure drop tests were conducted to evaluate the models as well as other new local pressure drop models. Table 3-5 shows the test matrix for the local pressure drop study. This section will evaluate some of the models available in the literature in addition to the models presented in the previous section. Some of these models are: the homogenous flow model, the Lockhart and Martinelli models, the Friedel model, the Garimella pressure drop model, the Kosky and Staub model, and the Chisholm model.

5.3.1 **Homogenous Flow Model**

The homogenous flow model was developed by Bo Pierre in 1964 to predict the evaporation pressure drop of R12 in 12 mm and 18 mm diameter smooth tubes. It is often used to validate test results because of its simplicity. The model assumes that liquid and vapor travel at the same velocity, which could be true in some regimes than

others, like intermittent flow, where the vapor phase and liquid phase do travel at close velocities.

Equation (5.20) is used to obtain the two-phase frictional pressure drop. The liquid-phase frictional pressure drop uses the Blasius friction factor, defined as:

$$f = 0.316 Re^{-0.25} \tag{5.39}$$

where the liquid-phase frictional pressure drop is defined as:

$$\left(\frac{dP}{dz}\right)_l = \frac{2fG^2}{D_h \rho_l} \tag{5.40}$$

In this model the Lockhart and Martinelli key multiplier is expressed in terms of average density and viscosity of liquid and vapor. The Lockhart and Martinelli key multiplier in this case is defined as:

$$\Phi_l^2 = \frac{\rho_l}{\rho_{2\emptyset}} \left(\frac{\mu_{tp}}{\mu_l}\right)^{0.25} \tag{5.41}$$

where μ_{tp} and ρ_{tp} are the two-phase viscosity and density, respectively. They are expressed as follow:

$$\frac{1}{\mu_{tp}} = \frac{x}{\mu_v} + \frac{(1-x)}{\mu_l} \tag{5.42}$$

$$\frac{1}{\rho_{tp}} = \frac{x}{\rho_v} + \frac{(1-x)}{\rho_l} \tag{5.43}$$

Using the Lockhart and Martinelli multiplier the total two-phase frictional pressure drop can be evaluated by using the following equation:

$$\left(\frac{dP}{dz}\right)_{tp} = \left(\frac{dP}{dz}\right)_l \Phi_l^2 \tag{5.44}$$

It is evident from Figure 5-18 and Figure 5-19 for refrigerant R134a and R245fa, respectively, that the homogenous pressure drop model over predicted the two-phase pressure drop data collected in this investigation by about 20%.

5.3.2 Friedel Correlation

The pressure drop correlation presented below was developed by Friedel in 1979. The correlation consists of a two-phase multiplier and takes into account the Froude number, the gravity effect, the Weber number and the surface tension effect as well. He used 25,000 data points of horizontal and upward flows and fit them in his correlation. The smallest tube diameter was 4 mm. Therefore, his correlation is quite poor in predicting two-phase pressure drop in micro-channels. The correlation is as follows:

$$\Phi_{lo}^2 = E + \frac{3.24 \, FH}{Fr^{0.045} We^{0.035}} \tag{5.45}$$

$$Fr_h = \frac{G^2}{g D_h \rho_h^2} \tag{5.46}$$

$$E = (1 - x)^2 + x^2 \frac{\rho_l f_v}{\rho_v f_l} \tag{5.47}$$

$$F = x^{0.78}(1 - x)^{0.224} \tag{5.48}$$

$$H = \left(\frac{\rho_l}{\rho_v}\right)^{0.91} \left(\frac{\mu_v}{\mu_l}\right)^{0.19} \left(1 - \frac{\mu_v}{\mu_l}\right)^{0.7} \tag{5.49}$$

where the Weber number We_l is defined as:

$$We_l = G^2 D_h / \sigma \rho_h \tag{5.50}$$

ρ_h is the homogenous density and is defined as:

$$\rho_h = \left(\frac{x}{\rho_v} + \frac{1-x}{\rho_l}\right)^{-1} \tag{5.51}$$

where the two-phase frictional pressure drop and the friction factor are as follows:

$$\left(\frac{dP}{dz}\right)_{f,tp} = \left(\frac{dP}{dz}\right)_{lo} \Phi_l^2 \tag{5.52}$$

$$f_{lo} = 0.25 \left[0.86859 \; LN \left(\frac{Re_{lo}}{1.964 \; LN(Re_{lo}) - 3.8215}\right)\right]^{-2} \tag{5.53}$$

It is shown in Figure 5-18 that this model under-predicted the data for R134a especially at high mass fluxes and low saturation temperatures where the pressure drop is larger for both. Whereas for R245fa the model over predicted the data at low mass fluxes and high saturation temperatures and low qualities as well as shown in Figure 5-19. The model was able to predict some points and under predict other points that were taken at low saturation temperature and high mass fluxes and qualities.

5.3.3 Chisholm Correlation

The Chisholm correlation is a well known two-phase pressure drop correlation that is used as a basis for developing pressure drop correlations for two-phase flows. Chisholm developed this correlation in 1973 using conventional tubes. He modified the Lockhart-Martinelli two-phase multiplier to include a coefficient C, which takes into account whether the flow of each phase is laminar or turbulent flow. The correlation also includes the influence of the tube surface roughness on two-phase frictional pressure drop. Chisholm modified the two-phase multiplier defined as:

113

$$\Phi_l^2 = \left[1 + \frac{C}{\chi_{tt}} + \frac{1}{\chi_{tt}^2}\right] \tag{5.54}$$

where C is:

$$C = \frac{1}{S}\sqrt{\frac{\rho_l}{\rho_v}} + S\sqrt{\frac{\rho_v}{\rho_l}} \tag{5.55}$$

where S is the slip ratio, which is the ratio of vapor-phase velocity to liquid-phase velocity.

$$S = \frac{V_v}{V_l} \tag{5.56}$$

Chisholm also introduced a property coefficient as:

$$\Gamma = \sqrt{\frac{\Delta P_{vo}}{\Delta P_{lo}}} = \left(\sqrt{\frac{\rho_l}{\rho_v}}\right)\left(\frac{\mu_v}{\mu_l}\right)^{n/2} \tag{5.57}$$

This makes Chisholm's two-phase multiplier look like the following:

$$\Phi_l^2 = 1 + (\Gamma^2 - 1)\{Bx^{2-n/2}(1-x)^{2-n/2} + x^{2-n}\} \tag{5.58}$$

For rough tubes n=0 and for smooth tubes n=0.25, and where B is defined as:

$$B = \frac{C\Gamma - 2^{n-2} + 2}{\Gamma^2 - 1} \tag{5.59}$$

This correlation over-predicted all our R134a data by a large margin as seen in Figure 5-18. The pressure drop calculated using this correlation was more than twice the values of the pressure drop data from this study. Figure 5-19 also shows that the model over predicted the data by about 30%.

114

5.3.4 Garimella's Correlation

As mentioned in the literature review section, Garimella et al. (2005) developed a comprehensive two-phase pressure drop correlation that addresses all the flow regimes as well as the overlap and transition regimes. The correlation is defined in terms of the interfacial friction factor between the vapor core and the liquid film as follows:

$$\frac{dP}{dz} = \frac{1}{2} f_{int} \frac{G^2 x^2}{\rho_v \alpha^{2.5} D_h}$$

(5.60)

where α is the void fraction developed by Baroczy (1965).

$$\alpha = \left[1 + \left(\frac{1-x}{x} \right)^{0.74} \left(\frac{\rho_v}{\rho_l} \right)^{0.65} \left(\frac{\mu_l}{\mu_v} \right)^{0.13} \right]^{-1}$$

(5.61)

The interfacial friction factor was expressed as a function of the Martinelli parameter, the Reynolds number, a dimensionless surface tension parameter, ψ, and the Darcy friction factor computed using the Churchill equation. The ratio of the interfacial friction factor is defined as:

$$\frac{f_{int}}{f_l} = d \chi^a Re_l^b \psi^c$$

(5.62)

where the empirical constants (d, a, b and c) were obtained by performing regression analysis on data grouped into two regions, whether the flow is laminar or turbulent, by the liquid phase Reynolds number defined as:

- Laminar region ($Re_l < 2100$): d = 1.308×10^{-3}; a = 0.427; b = 0.930; c = -0.121

- Turbulent region ($Re_l > 3400$): d = 25.64; a = 0.532; b = -0.327; c = 0.021

The Martinelli parameter, the Reynolds number, and the dimensionless surface tension parameter are given as:

$$\chi = \left[\frac{\left(\frac{dP}{dz}\right)_l}{\left(\frac{dP}{dz}\right)_v}\right]^{1/2} \tag{5.63}$$

$$Re_l = \frac{GD(1-x)}{(1+\sqrt{\alpha})\mu_l} \tag{5.64}$$

$$Re_v = \frac{GxD}{\mu_v\sqrt{\alpha}} \tag{5.65}$$

$$\psi = \frac{G(1-x)\mu_l}{\rho_l(1-x)\sigma} \tag{5.66}$$

Garemilla's model also over predicted the data of R134a for this investigation as shown in Figure 5-18. It did poorly to predict the data at high mass fluxes (400 kg/m^{2}s). In addition, this model tends to have a large change in value (11%) of pressure drop when changing the flow quality from 80% to 90%. This model also over predicted the majority of the R245fa data, where it also did predict some points, as shown in Figure 5-19.

5.3.5 *Cavallini Model*

Cavallini (2005) developed a frictional pressure drop model for two-phase flow in which he used the liquid-entrained fraction, E, that was developed by Paleev and Filippovich (1966) to calculate the two-phase multiplier. The Cavallini model is defined as follow:

$$\left(\frac{dP}{dz}\right)_f = \Phi_{lo}^2\left(\frac{dP}{dz}\right)_{lo} = \Phi_{lo}^2\frac{2f_{lo}G^2}{D_h\rho_l} \tag{5.67}$$

where

$$\Phi_{lo}^2 = Z + 3.595FH(1 - E)^W \tag{5.68}$$

$$Z = (1 - x)^2 + x^2(\rho_l/\rho_v)(\mu_v/\mu_l)^{0.2} \tag{5.69}$$

$$F = x^{0.9525}(1 - x)^{0.414} \tag{5.70}$$

$$H = (\rho_l/\rho_v)^{1.132}(\mu_v/\mu_l)^{0.44}\left(1 - \frac{\mu_v}{\mu_l}\right)^{3.542} \tag{5.71}$$

$$E = 0.015 + 0.441 \log\left[(\frac{\rho_{gc}}{\rho_l})\left(\frac{\mu_l j_v}{\sigma}\right)^2 10^4\right] \tag{5.72}$$

where

$$\rho_{gc} = \rho_v\left(1 + \frac{(1 - x)E}{x}\right) \tag{5.73}$$

$$W = 1.398p_{red} \tag{5.74}$$

$$f_{lo} = 0.046\left(\frac{GD_h}{\mu_l}\right)^{-0.2} \tag{5.75}$$

Although some data points fall in the 20% error margin, this model over predicted the majority of the data for R134a as can be seen in Figure 5-18. As for the data of R245fa, the model was very poor in predicting the data as it is obvious in Figure 5-19.

5.3.6 *Lockhart-Martinelli Model*

Refer to section 5.2.1 of this thesis.

At low mass fluxes, this model under predicted our results; however, at mass fluxes 300 kg/m^{2}s and 400 kg/m^{2}s the model was able to predict the majority of the data within that mass flux range for both refrigerants. Figure 5-18 and Figure 5-19 show a comparison of the data of both R134a and R245fa versus this model, respectively.

5.3.7 *Classical Pressure drop Model*

Refer to section 5.2.1 of this thesis.

This model was the only model evaluated in this study that accurately predicted the majority of the data for both refrigerants using the Lockhart and Martinelli (1949) two-phase key multiplier (Equation 5.33). It under predicted data at high qualities such as: 80% and 90% vapor qualities.

Figure 5-18 and Figure 5-19 show comparisons of the data versus all the pressure drop correlations considered in this study for refrigerants R134a and R245fa respectively.
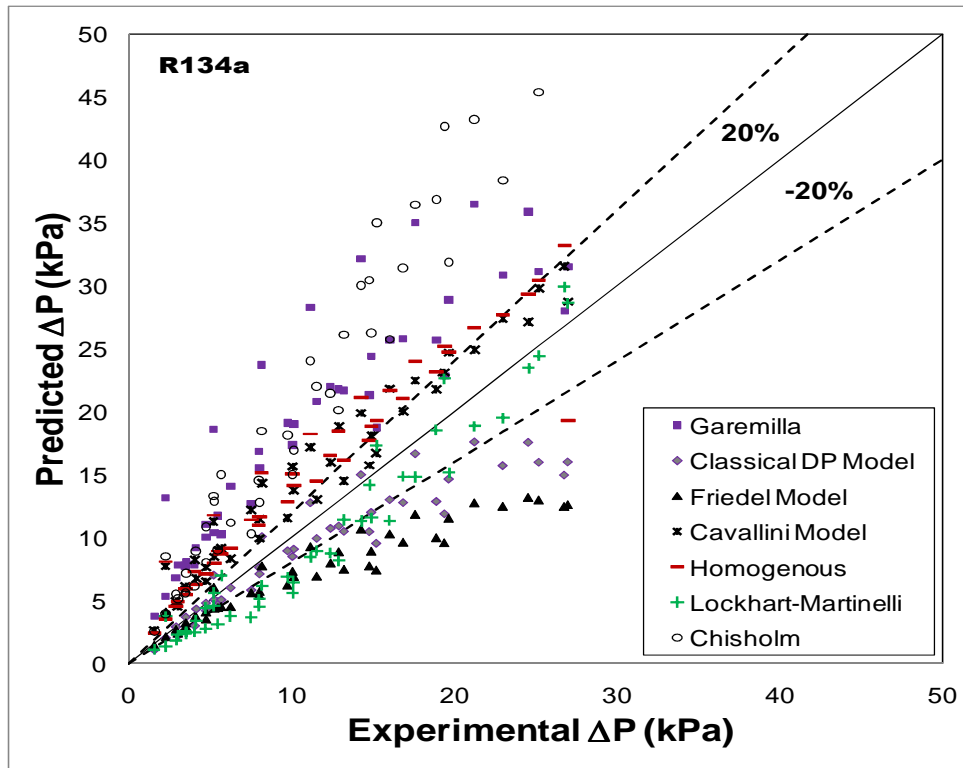
Figure 5-18 Comparison of experimental data with available pressure drop correlations for R134a
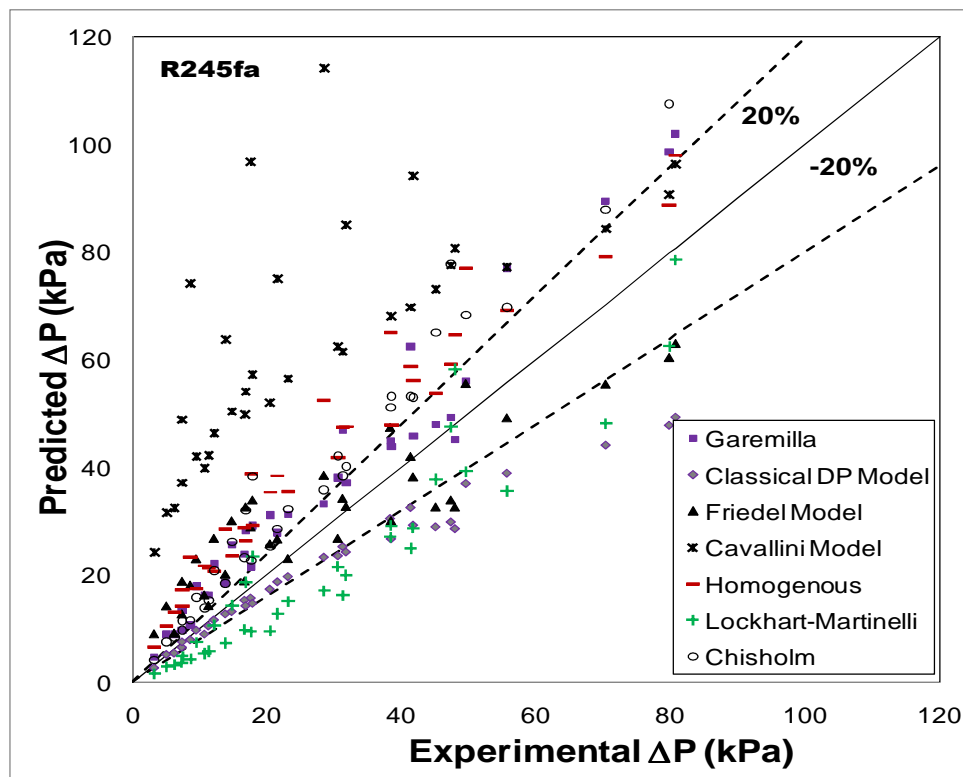

Figure 5-19 Comparison of experimental data with available pressure drop correlations for R245fa

119

Due to the good agreement between the data and the predicted results of the classical pressure drop correlation, the correlation was modified to predict the data more accurately. In order to fit the data, the two-phase key multiplier was modified as follows:

$$\Phi_v = (1 + 1.125\chi_{tt}^{0.356})^{1.85}$$

<div align="right">(5.76)</div>

Figure 5-20 shows a comparison of the data with the original classical pressure drop correlation and with the modified classical pressure drop correlation as well. The modification generated a 17% improvement. The modified model was able to predict 85% of the data points, where the original model only predicted 68% of the data points.
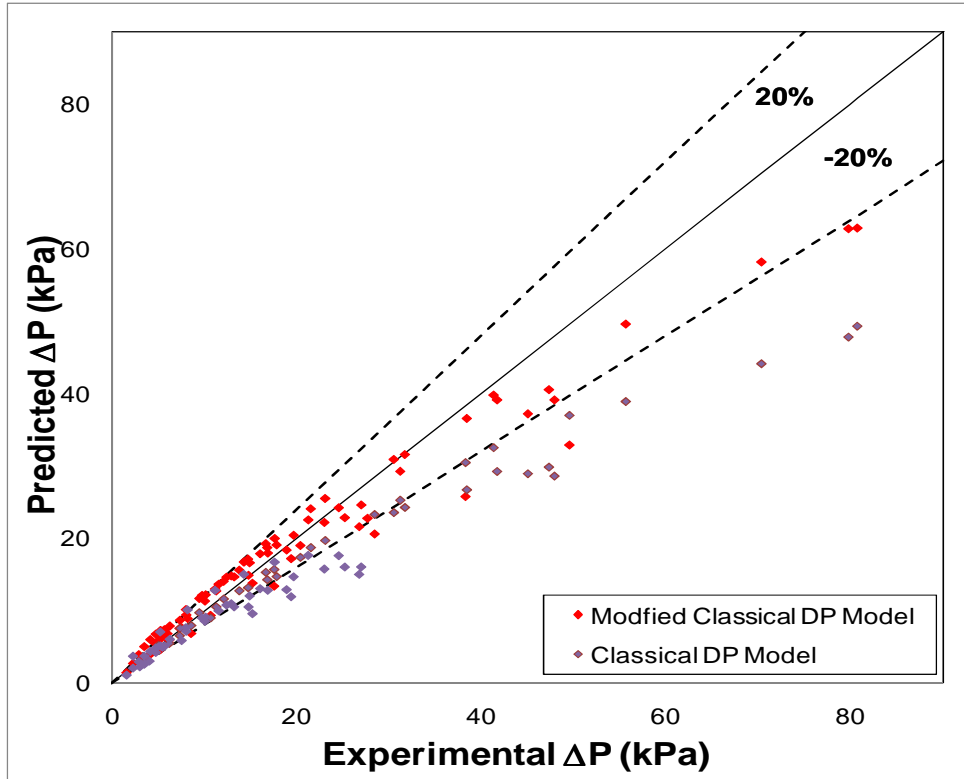
Figure 5-20 Comparison of experimental data with the classical pressure drop model and the modified classical pressure drop model

The modified two-phase key multiplier, equation 5.76, is again compared with Lockhart-Martenilli, Azer and Shao two-phase key multipliers in Figure 5-21. It is obvious from the figure that the values of the new key multiplier modified by Al Hajri, equation (5.76) are higher than the values of the other key multiplier for similar conditions. And since Φ_v is the ratio of pressure drop due to friction to pressure drop due to vapor flow in the channel, then this means that the pressure drop due to friction is higher in this high aspect ratio micro-channel than in the macro-channels. Unlike the statement drawn in section (5.2.2) page 113, which was based on values of average pressure drops, the results of local pressure drop with the new key multiplier (equation (5.76)) show better agreement and make more sense when compared with the classical pressure drop correlation.
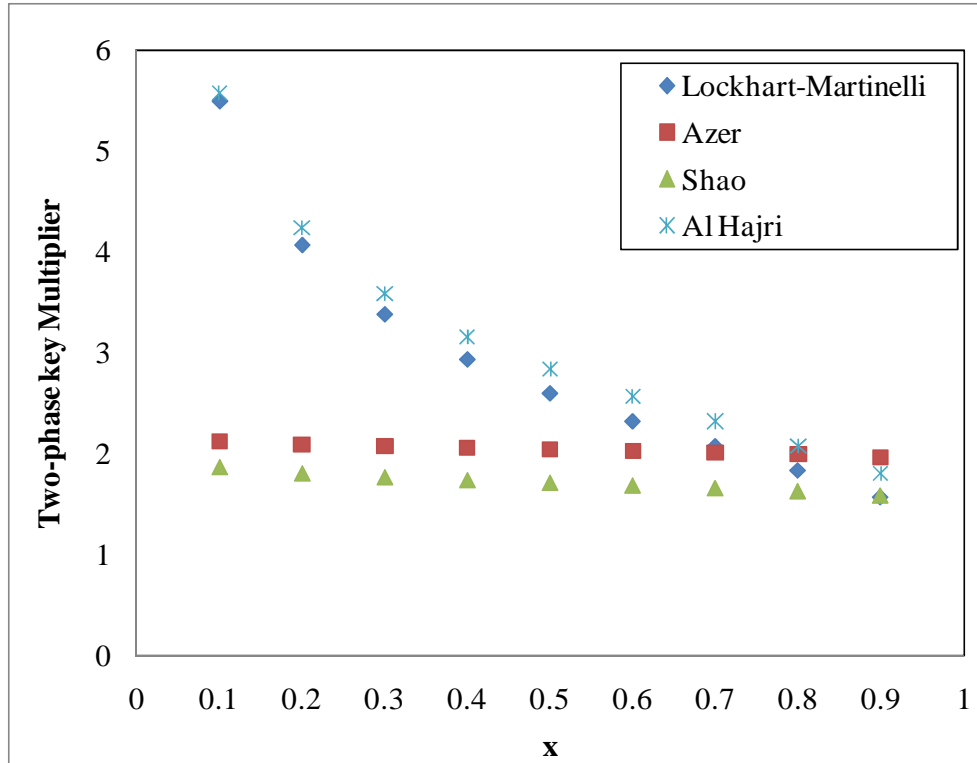
Figure 5-21 Comparison of the two-phase key multiplier modified by Al Hajri with several others key multipliers

It is apparent that the classical pressure drop model to a great extent is capable of predicting pressure drop of two-phase refrigerant flow inside a high aspect ratio rectangular macro-channel. The modified model above is a general model that includes two different refrigerants with different physical properties, whereas the original model did not include R245fa data.

5.3.8 Summary

This chapter presented comparisons of averaged heat transfer coefficient, overall pressure drop and local pressure drop results with the existing correlations of mini and micro-channels available in the open literature and of relevance to the present study. It was shown that, utilizing the experimental data of the present study some existing correlations were successfully modified to fit the data of the present

study for preliminary design and prediction purposes. Additional physical understanding of the phenomena, supported by experimental and analytical/computational work is necessary to further verify the validity of the proposed empirical correlations.

CHAPTER 6: FLOW VISUALIZATION

This chapter presents visual results for two-phase flow inside a high aspect ratio micro-channel. Two channels with similar cross-sectional areas (2.8 mm x 0.4 mm) but different viewing windows were used to collect the visual results. One channel had a viewing window of 2.8 mm (Figure 6-1) and the other had a viewing window of 0.4 mm (Figure 6-2), so that the two-phase flow could be studied from both sides of the cross-sectional area of the channel. The two-phase flow was tested for the conditions shown in Table 6-1. The visualization results presented in this chapter are for R245fa only. R134a was not used in visualization experiments due to its high pressure which may cause the glass cover to break or damage the test section.

It is well understood that both pressure drop and heat transfer coefficients are dependent on the flow regime types that exist in the channel. The visual experiments conducted in this study allowed us to identify the different types of flow regimes in the channel, and then relate their effects on pressure drop. The study has revealed that the majority of the flow regimes (dispersed, intermittent, wavy and annual) were observed in both channels, except the wavy-film flow, which was only seen in the channel with a 2.8 mm viewing window. The results obtained from the visualization were then used to develop flow regime maps, which were compared with the flow regime maps available in the literature as applicable.
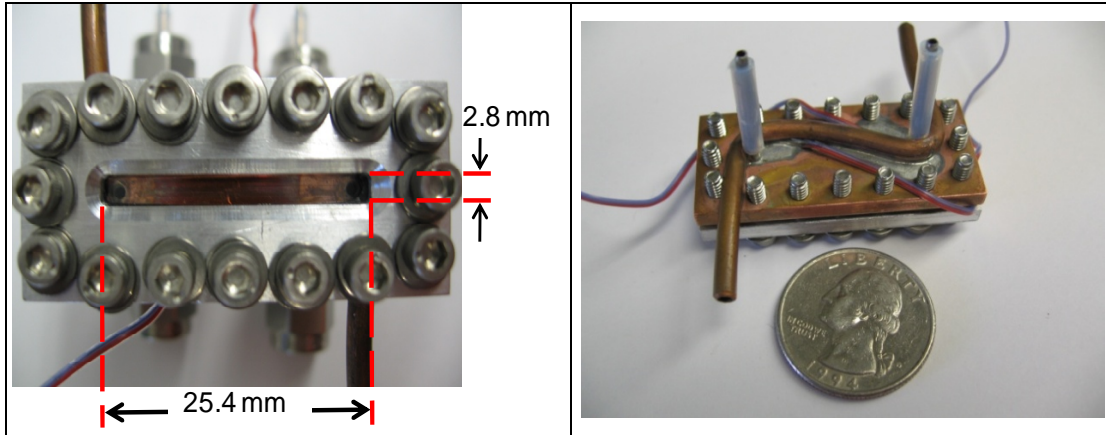
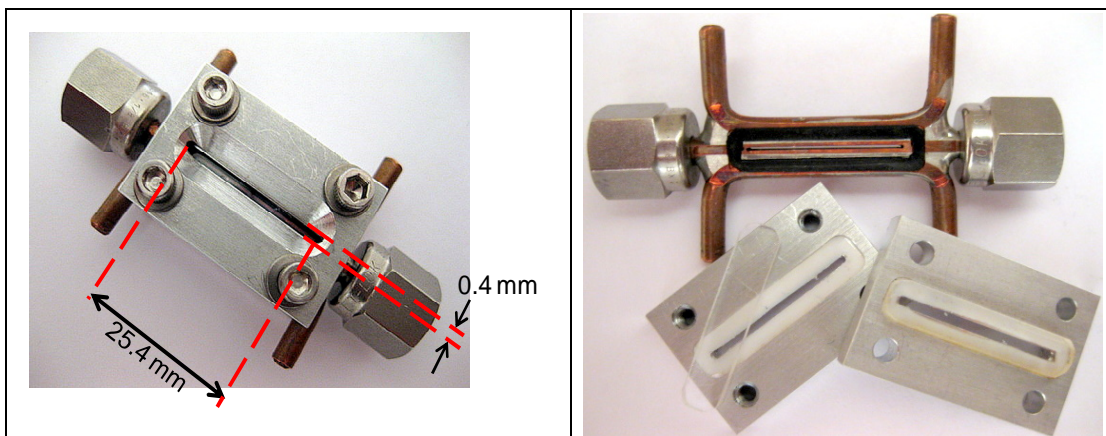Figure 6-1 Visualization tests section with 2.8 mm viewing window and 0.4 mm depth

Figure 6-2 Visualization tests section with 0.4 mm viewing window and 2.8 mm depth

6.1 *Flow Regime Mapping*

This section presents the flow visualization experiments for the two different channels in two different subsections. In each case compares the results of the visualization collected for each channel are compared with applicable flow regime maps available in the open literature. As stated in the literature review section, researchers have developed different ways to present their flow regime maps. In the present work only three types of flow regimes will be taken under consideration: the superficial vapor velocity, j_v, versus the Lockhart-Martinelli parameter, the superficial vapor velocity versus the ratio of liquid and vapor volumes $(1-\sigma)/\sigma$, and the mass flux

versus vapor quality. The test matrix considered for this part of the investigation is presented in Table 6-1.

Table 6-1 Visualization test matrix

Test Set	Mass flux (kg/m^{2}s)	Saturation Temp (^{o}C)	Quality	Study
1			0.1	
2		30	0.2	
3			0.3	
4			0.4	***Effect of***
5	300	40	0.5	***Saturation***
6			0.6	***Temperature***
7			0.7	
8		50	0.8	
9			0.9	
10			0.1	
11	200		0.2	
12			0.3	
13			0.4	***Effect of***
14	300	50	0.5	***Mass Flux***
15			0.6	
16			0.7	
17	400		0.8	
18			0.9	

6.1.1   *The 2.8 mm x 0.4 mm channel*

Figure 6-3 shows the channel with the viewing window of 2.8 mm, used for light access and visualization, which was positioned in the horizontal plane (xy-plane) with channel depth of 0.4 mm in the (z) axis direction as shown in the figure. This channel was intentionally designed with a 90° entrance to the channel to simulate a practical heat exchanger where in most of the times heat exchangers have a 90° entrance. The high-speed camera was placed such that it was looking from the top, down to the channel as demonstrated in the figure. It is worth clarifying that the top of the channel was covered with glass and the channel was made out of a copper block.
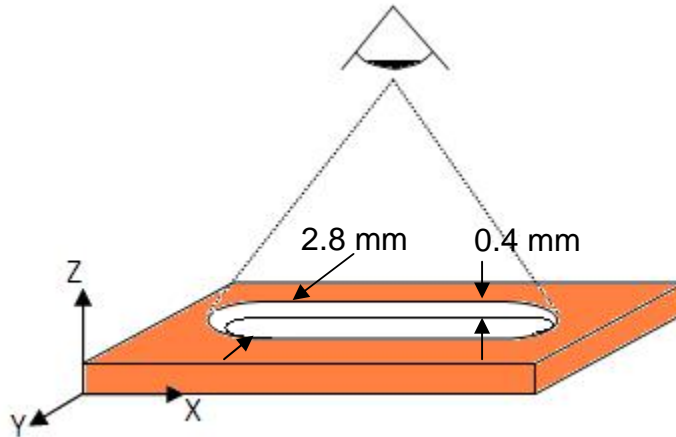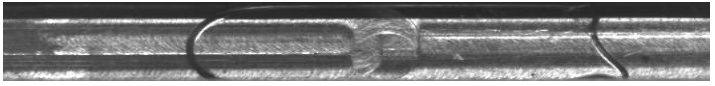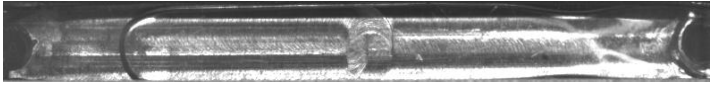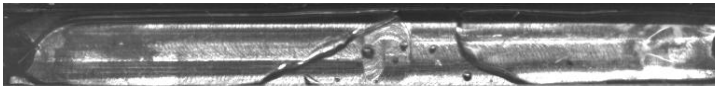
126
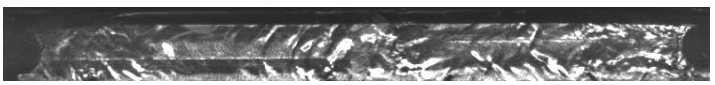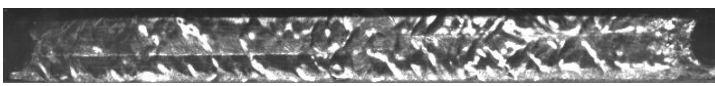
Figure 6-3 Diagram of the visualization channel with 2.8 mm viewing window and 0.4 mm depth

The digital visualization videos collected for each test were used to identify the different flow regimes present in each test. The flow regimes were classified into two major categories: plug/slug and wavy film. These major flow regimes were then classified further as follows: within the plug/slug flow regimes we identified plug flow, elongated bubble/slug flow and elongated bubble/bubbly/slug flow; within the wav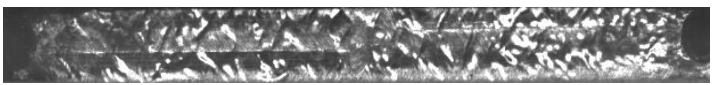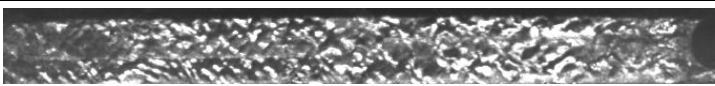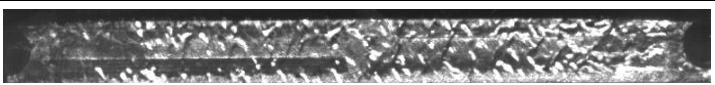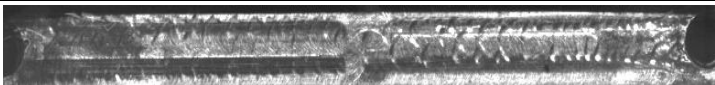y film flow regime we identified discrete wavy and disperse wavy flows. The bubbly flow is identified here as small bubbles that are smaller than the average bubble size that flow in the slug between two large bubbles. The flow regime changed from plug to gated bubble/slug flow to elongated bubble/bubbly/slug flow to discrete wavy film flow to disperse wavy film flow. It is worth noting here that at moderate qualities (10%-30%) it was difficult to identify whether there was liquid flowing on the surface of the glass; however, it seemed that there was a buoyancy effect, particularly in the channel with viewing window of 2.8 mm. In other words, after the elongated bubble/bubbly/slug flow, the vapor would flow on top on a liquid film. The film thickness would decrease as the quality of vapor increased. In addition, as the vapor quality increased, the velocity of the vapor increased; therefore, the vapor

flowed faster at high vapor qualities than at low vapor qualities, creating a non-uniform wavy pattern on the liquid film, which is classified as the disperse wavy film flow regime in the present work. Table 6-2 depicts some of the digital images of the flow regimes that were observed at mass flux of 200 kg/m^{2}s and at 50 ^{o}C saturation temperature.

Table 6-2 Digital Images of two-phase flow inside the 2.8 mm viewing window micro-channel at mass flux of 200 kg/m^{2}s and Tsat = 50 ^{o}C

x	Flow Regime	Image of the regime
0.02	Plug	
0.05	Plug	
0.08	Elongated Bubble/Bubbly/Slug	
0.1	Elongated Bubble/Bubbly/Slug	
0.2	Discrete Wavy Film	
0.3	Discrete Wavy Film	
0.4	Disperse Wavy Film	
0.5	Disperse Wavy Film	
0.6	Disperse Wavy Film	
0.7	Disperse Wavy Film	
0.8	Disperse Wavy Film	

It was observed in this channel that as soon as the two-phase flow enters the channel, vapor starts traveling on top of the liquid due to the buoyancy affect

128

combined with the 90° entrance. The reason is that as the two-phase flow enters the channel and collides with the glass, the flow separates and due to bouncy the vapor flows on top of the liquid. The observation was not as obvious at flows with vapor quality lower than 10% where the plug/slug regime was present. After vapor qualities higher than 10%, the observation became more obvious, where vapor travels over a liquid layer.

All the visualization results from all the testing conditions in Table 6-1 are shown in the test matrix table are presented in the flow regime map below, Figure 6-4. Each flow regime is presented in the figure by a different mark in order to identify flow regimes and transition regimes easily. The flow map in Figure 6-4 uses the superficial vapor velocity in the vertical axis and the Lockhart-Martinelli parameter in the horizontal axis. The solid and dashed lines in the figure show where the transition occurred from one flow regime to another. It was observed that the transition from the plug/slug regime to the wavy film regime occurred at vapor qualities ranging from 10% to 20% while the transition from discrete wavy film to disperse wavy film occurred between vapor qualities of 30% to 40%.
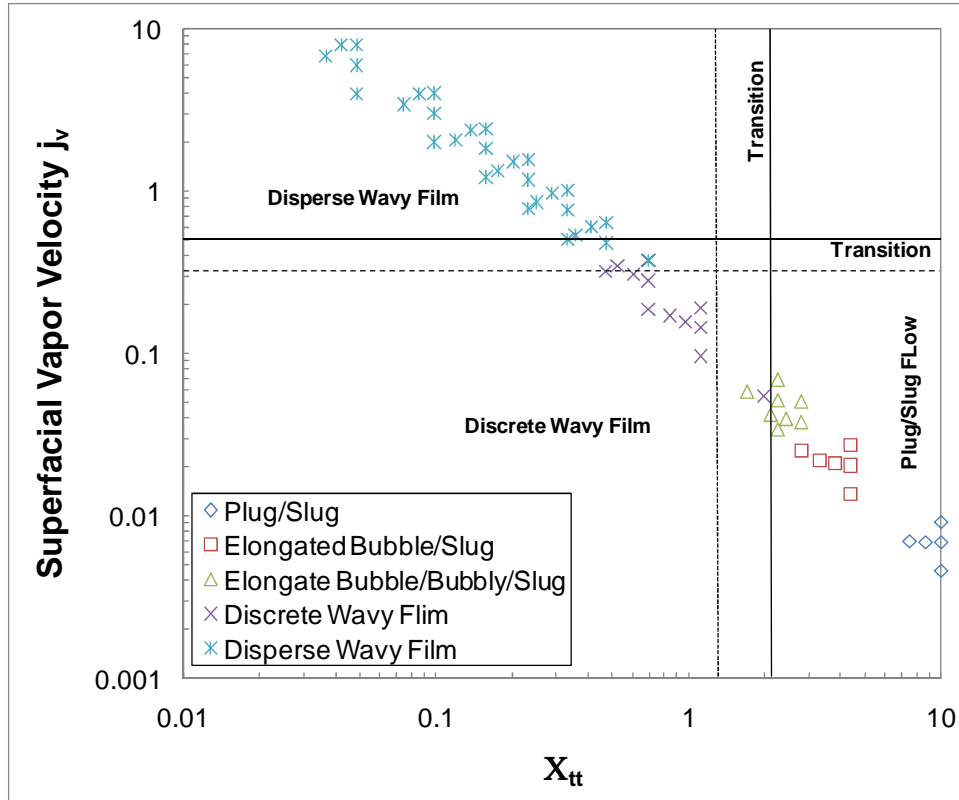
Figure 6-4 Visualization results of the 2.8 mm viewing window micro-channel plotted in a flow regime map

Figure 6-5 shows the visualization data from this study on a flow regime map developed by Wang et al. (1999). They developed this flow regime map using R134a as the working fluid flowing in 10 micro-channels with a hydraulic diameter of 1.46 mm. They conducted tests with mass flux ranging from 75 to 750 kg/m^{2}s and inlet temperatures ranging from 64 to 80.5 $^{\circ}$C. It is clear from the figure that there is some agreement between the Wang et al. (1999) flow regime map and the current data. Particularly, the plug/slug flow of our observation agrees with their slug/churn flow and the discrete wavy film agrees with their stratified wavy flow. As for the dispersed wavy flow points, they fall into the transition region from stratified wavy to annular flow regions. Similar results are also seen in the comparison of our data points when plotted on the Breber et al. (1980) flow regime map, Figure 6-6.
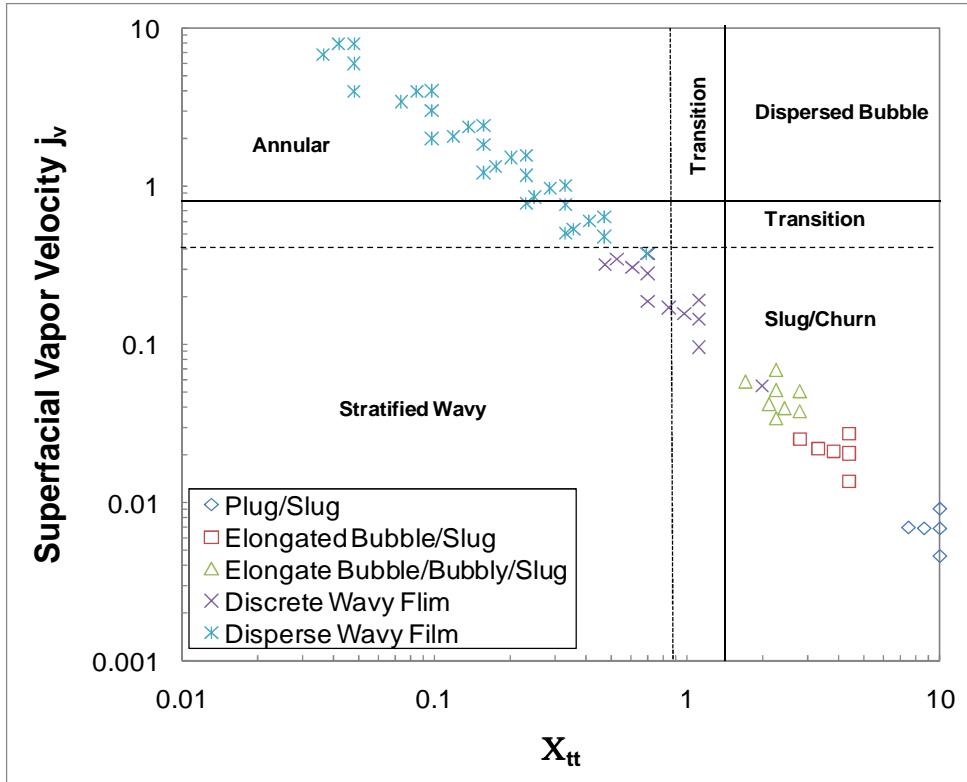
Figure 6-5 Visualization results of the 2.8 mm viewing window micro-channel plotted in a flow regime map developed Wang et al. (1999)
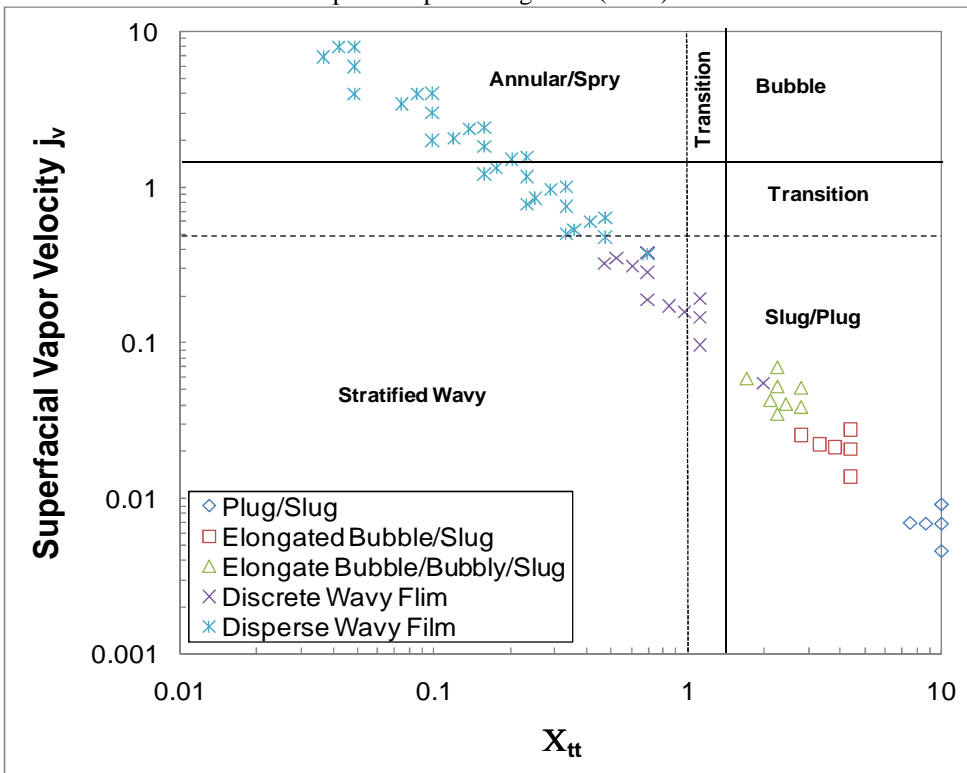

Figure 6-6 Visualization results of the 2.8 mm viewing window micro-channel plotted in a flow regime map developed Breber et al. (1980)

It is worth mentioning that the transition from plug/slug regime to the wavy

film regime in this channel (Figure 6-4) occurs earlier than the transition from

plug/slug regime to the stratified wavy regime in Wang et al. (1999) (Figure 6-5) map

and Breber et al. (1980) map (Figure 6-6). This is again due to the fact that the two-

phase flow in the present study enters the channel at 90° angle which cause the vapor

to travel above the liquid due to the bouncy affect. Therefore, the regime occurs

earlier in this channel compared to the work done by Wang et al. (1999) and Breber et

al. (1980)

The second type of flow regime maps was developed by Tandon et al. (1982),

which uses the superficial vapor velocity, j_v, on the vertical axis and the ratio of liquid

and vapor volumes $(1-\sigma)/\sigma$ on the horizontal axis, where σ is the void fraction. The

void fraction that Tandon et al. (1982) used was the Smith (1969) void fraction,

which is defined as:

$$\sigma = \left[1 + A_{SM}\left(\frac{1-x}{x}\right)\left(\frac{\rho_v}{\rho_l}\right)\right]^{-1}$$

(6.1)

where A_{SM} is defined as:

$$A_{SM} = 0.4 + 0.6\sqrt{\left[\frac{\rho_l}{\rho_v} + 0.4\left(\frac{1-x}{x}\right)\right]\Big/\left[1 + 0.4\left(\frac{1-x}{x}\right)\right]}$$

(6.2)

When comparing the data of this work to the Tandon et al. (1982) flow regime

map, the comparison resulted in some agreement for some regimes and poor

prediction for other regimes. Figure 6-7 shows all the visualization results of the

present study plotted on the Tandon et al. (1982) flow regime map. It is obvious from

the figure that the plug/slug regime from the present study falls within the slug regime

indicated in the Tandon et al. (1982) flow regime map. However, the discrete wavy

film data points also fall within the slug flow regime of the map. As for the dispersed wavy film regime data points, they are scattered between the wavy, annular/semiannular and spray flow regime.
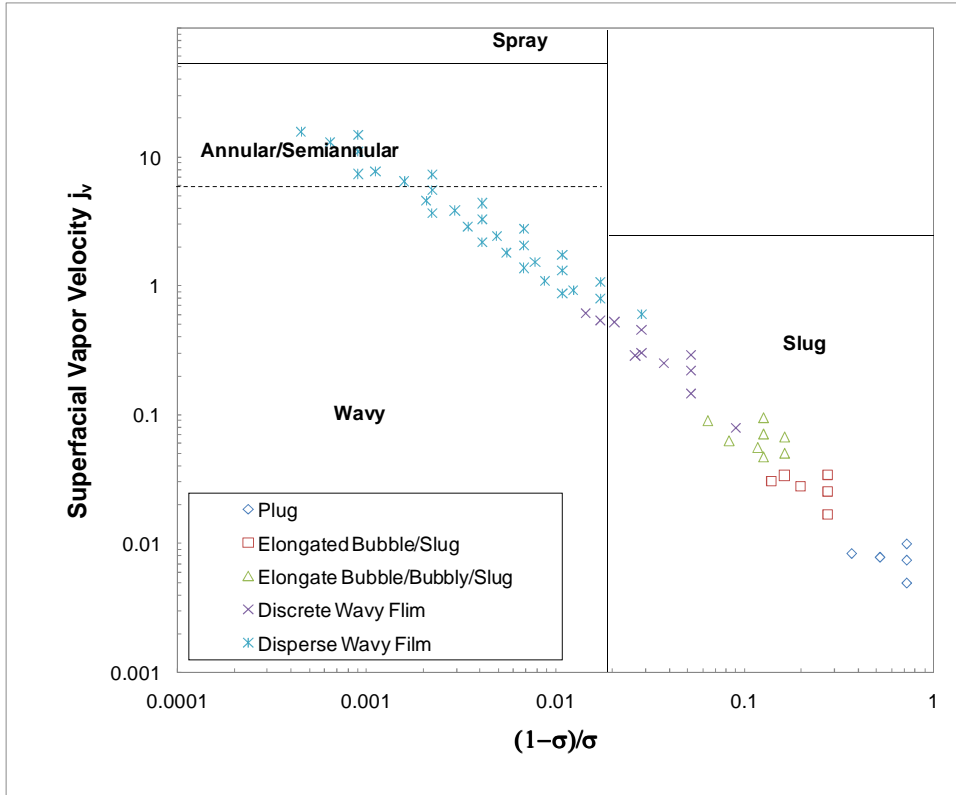

Figure 6-7 Visualization results of the 2.8 mm viewing window micro-channel plotted in a flow regime map developed Tandon et al. (1982)

The third type of flow regime map with which we compared our data is that which uses the mass flux on the vertical axis and the quality on the horizontal axis. Figure 6-8 shows the visual data from this investigation on a flow regime map developed by Coleman and Garimella (2000, 2003). The flow map was developed using R134a as the working fluid flowing in a circular tube of hydraulic diameter 0.76 mm at mass fluxes ranging from 150 to 750 kg/m^{2}s. It is clear from the figure that there is fair agreement between the data and the map in the plug/slug regime. All the discrete wavy film data points fall within the plug/slug and annular film flow

133

regime of the map, while the rest of the data points fall in the annular film flow and the annular film and mist flow regime of the map.

Figure 6-8 Visualization results of the 2.8 mm viewing window micro-channel plotted in a flow regime map developed Coleman and Garimella (2000, 2003)

Cavallini et al. (2002) also developed a flow regime map after an intensive analysis on flow regimes found in the literature. His flow map consists of three major regimes: slug, transition and wavy stratified flow, and annular flow. When our results were plotted on the Cavallini et al. (2002) flow regime map, all the plug/slug data and two point of the discrete wavy film fell in the slug flow regime on the map, whereas the rest of the data fell in the annular flow regime on the map, as shown in Figure 6-9.
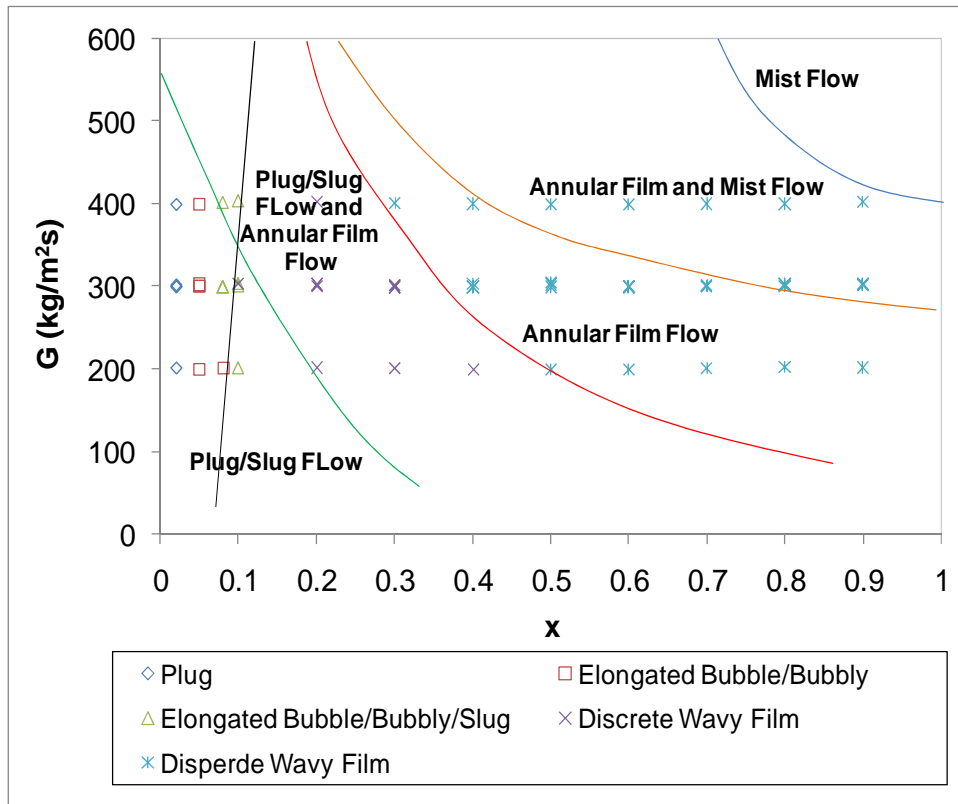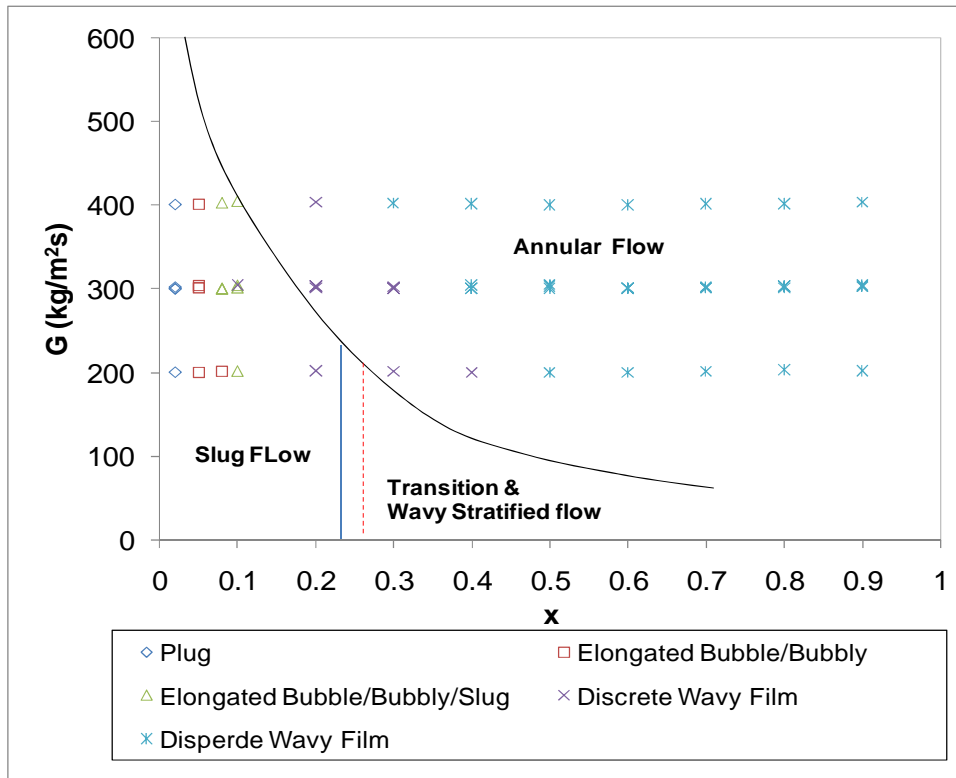
Figure 6-9 Visualization results of the 2.8 mm viewing window micro-channel plotted in a flow regime map developed Cavallini et al. (2002)

Amongst the noticeable differences the above comparison reveals, one significant difference is that none of the maps included regimes in which a liquid film flows on the tube surface and the vapor flows on top of the liquid film, as was the case here. This could be due to the 90° entrance angle of the mixture to the channel in the present work, Figure 6-1. A liquid and vapor mixture flows from the evaporator inside a 1/8" diameter circular tube where liquid flows on the surface of the tube and the vapor flows in the middle of the tube forming a vapor core. When this mixture enters the channel, it hits the cover glass and due to buoyancy forces, the vapor flows on the top of the liquid. This creates a regime of liquid film with waves created by the vapor flowing on top of it, instead of an annular flow. This shows the importance of the entrance effect and how it can change the flow dynamics, which in turn affects the

pressure drop and the heat transfer. Due to the difference in flow patterns of the data studied in this section from other flow regimes, it was necessary to develop a flow regime map that included the regimes observed in this work, such as the discrete wavy film and the disperse wavy film flows. Figure 6-10 shows the newly developed flow regime map for a channel with a hydraulic diameter of 0.7 mm using R245fa as the working fluid at saturation temperatures ranging from 30 to 40 ^{o}C and mass fluxes between 200 and 400 kg/m^{2}s. It is obvious when comparing Figure 6-9 and Figure 6-10 the transition from plug/slug flow regime to the wavy film occurs earlier with the data obtained from the present work than those of Cavallini et al. (2002).
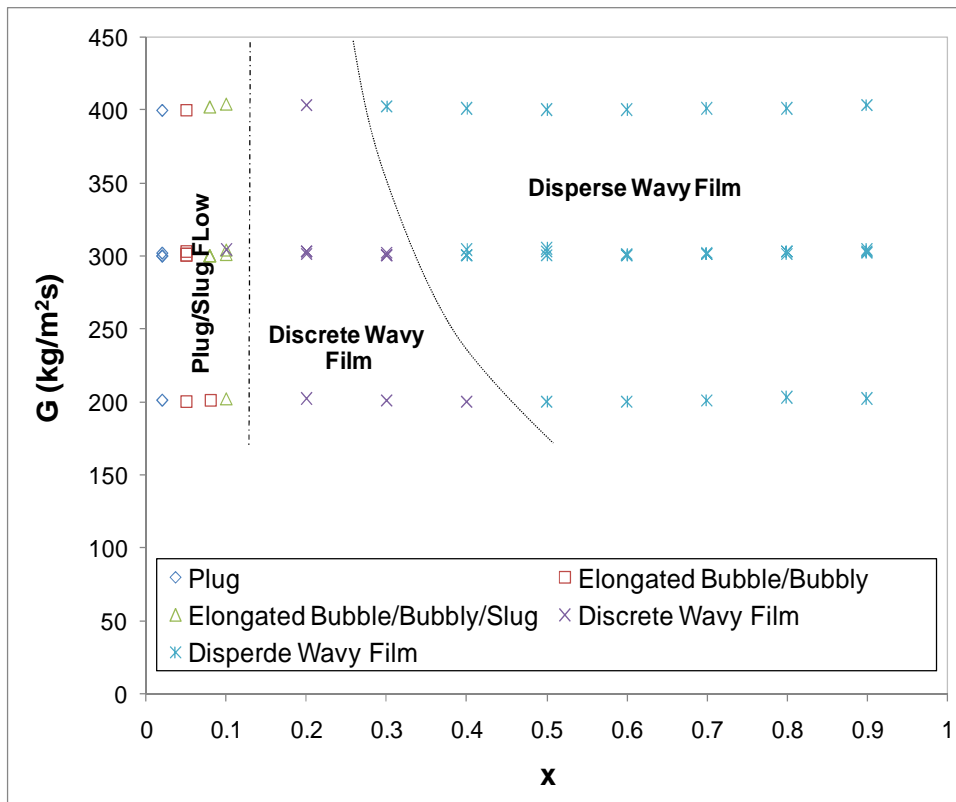

Figure 6-10 Newly developed flow regime map for data collected from the 2.8 mm viewing window micro-channel

6.1.2 The 0.4 mm x 2.8 mm channel

This channel had two viewing windows of 0.4 mm, one from the top for flow

visualization and the other from the bottom for the light access. The windows were

positioned in the horizontal plane (xy-plane) as shown in the Figure 6-11 below,

where the channel depth was 2.8 mm in the (z) axis direction. The high-speed camera

was placed in a position such that it was looking from the top, down to the channel, as

demonstrated in the graph below, Figure 6-11. Glass was used to cover the open side

of the channel, whereas the channel was made out of copper.
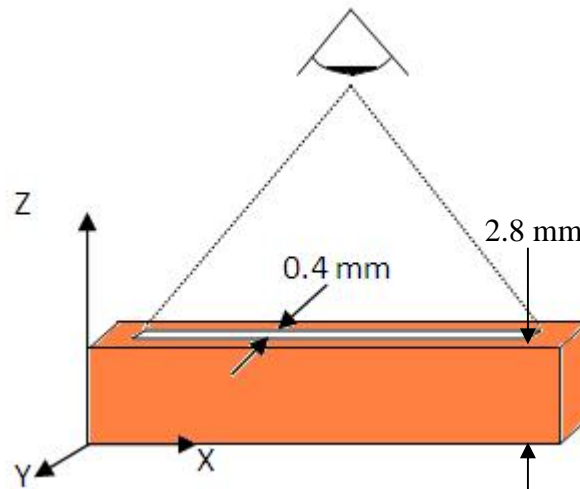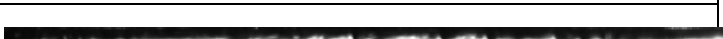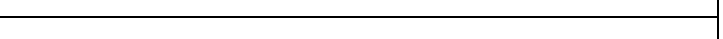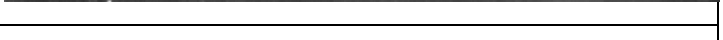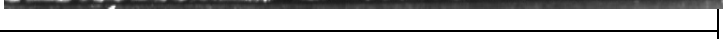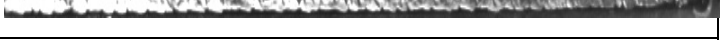
Figure 6-11 Diagram of the visualization channel with 0.4 mm viewing window and 2.8 mm depth

Table 6-3 shows the flow regimes observed during a test with mass flux of

300 kg/m^{2}s and saturation temperature 30 ^{o}C. At low vapor qualities up to 10%, the

regimes are similar to those seen in the previous channel; however, after the vapor

quality increases beyond 10%, the flow becomes annular wavy flow. The major

regimes that were identified using this micro-channel were the plug/slug and the

annular flow regimes. The plug/slug flow regime was also classified into three

different flow regimes: plug flow, elongated bubble/slug flow and elongated

bubble/bubbly/ slug flow. As the vapor quality was increased, the flow regime

changed from plug flow to elongated bubble/slug flow to elongated

bubble/bubbly/slug flow and then finally to annular flow.

Table 6-3 Digital Images of two-phase flow inside the 0.4 mm viewing window micro-channel at mass
flux of 300 kg/m^{2}s and Tsat = 30 ^{o}C

x	Regime	Image of the regime
0.02	Plug/Slug	
0.05	Plug/Slug	
0.08	Elongated Bubble/Bubbly/Slug	
0.1	Elongated Bubble/Bubbly/Slug	
0.2	Annular Wavy	
0.3	Annular Wavy	
0.4	Annular Wavy	
0.5	Annular Wavy	
0.6	Annular Wavy	
0.7	Annular Wavy	
0.8	Annular Wavy	

It is worth mentioning that wavy film flow was not observed in this channel as

it was in the previous channel presented in this chapter. This is possibly due to the

way the two-phase flow enters to this channel compared to the other channel

presented previously in this chapter. As it can be seen in Figure 6-11 the entrance to

the channel is aligned with the channel. The two-phase flow prior to the channel

entrance takes a shape of a thin film on the inter surface of the channel and a vapor

core formed in the middle of the channel and traveling at a higher velocity than the

liquid layer. Since the entrance is aligned with the channel, then the liquid layer

remains flowing on the inter surface of the channel and the vapor core in the middle

of the channel forming an annular flow.

The visual data collected from testing the two-phase flow using this channel

are plotted in a flow regime map below, Figure 6-12. The flow regime map below

uses the superficial vapor velocity, j_v, on the vertical axis and Lockhart-Martinelli

parameter on the horizontal axis. The transition from plug/slug regime to annular

wavy regime occurs at vapor qualities ranging from 10% to 20%.
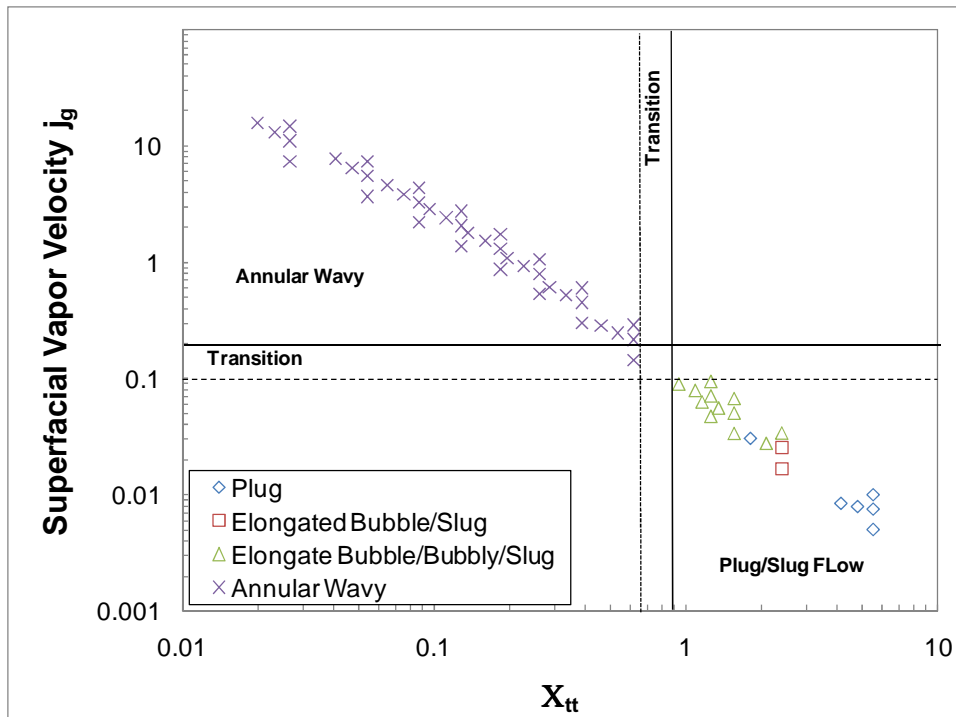
Figure 6-12 Visualization results of the 0.4 mm viewing window micro-channel plotted in a flow regime map

Figure 6-13 shows the visual data of this work plotted on a flow regime map developed by Wang et al. (1999). It is obvious from the figure that about 30% of the plug/slug regime data fell in the transition regime of the map. As for the annular flow data points, they fell in the stratified wavy regime and the annular regime of the map. Similar results to the Wang et al. (1999) flow regime map are shown in the Breber et al. (1980) flow regime map, Figure 6-14.

Figure 6-13 Visualization results of the 0.4 mm viewing window micro-channel plotted in a flow regime map developed Wang et al. (1999)
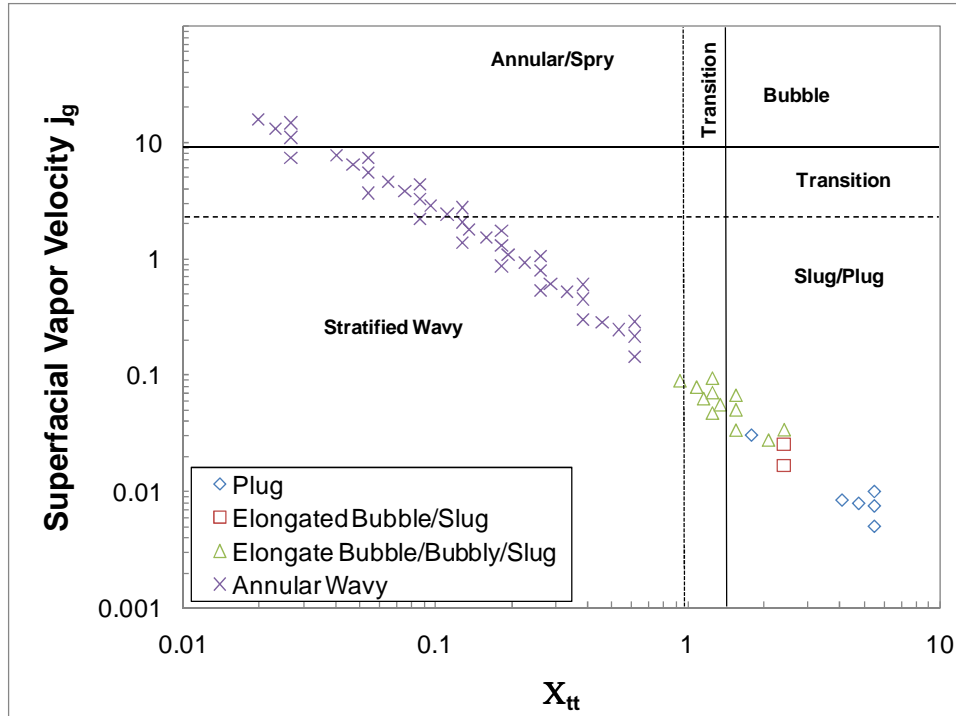
Figure 6-14 Visualization results of the 0.4 mm viewing window micro-channel plotted in a flow regime map developed Breber et al. (1980)

It is obvious when comparing the newly developed flow regime map of the present channel (Figure 6-12) to the flow regime maps presented in Figure 6-13 and Figure 6-14 that the transition from the plug/slug flow regime to the annular flow regime in Figure 6-12 occurs later than the transition from slug to stratified wavy in Figure 6-13 and Figure 6-14. This can be explained by the diagram (Figure 6-15) below. In addition to the fact that surface tension forces at the liquid-vapor interface pull the interfacial liquid waves in the annulus towards the tube center that eventually block the vapor passage, and hence form slugs. In other words, in high aspect ratio channel such as the one used in this study, the liquid layers in the larger surfaces of the channel are very close to each other (Figure 6-15 (c)); therefore, at low vapor qualities (in this case between 10% and 20% vapor qualities) any occurrence of large waves can cause the liquid layers to collapses; thus, forming a bubble or elongated

bubble in this case. On the other hand, this effect can occur in circular and rectangular channels at even lower vapor qualities (qualities lower than 10%) for the same operating conditions. This conclusion agrees with that reached by Griffith and Lee (1964) investigation.

(a)   (b)

(c)
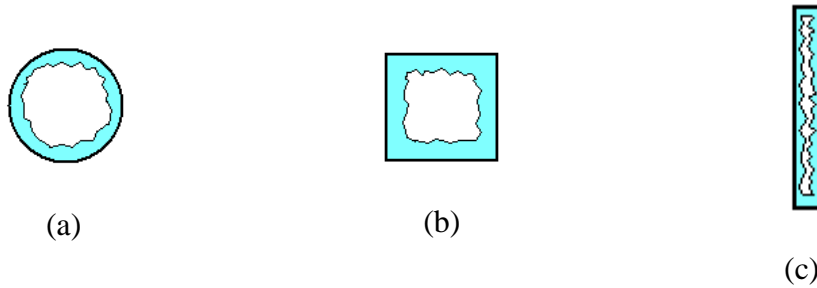
Figure 6-15 Demonstration of liquid layer distribution inside (a) Circular tube, (b) high aspect ratio rectangular channnel

Figure 6-16 shows the visual data plotted on the Tandon et al. (1982) flow regime map; it is clear from Figure 6-16 that there is good agreement between the data and the map at the slug regime; however, there are some annular flow data points in the slug flow regime of the map where the rest of the data of the annular flow regime fall in the wavy and annular flow regimes of the map.
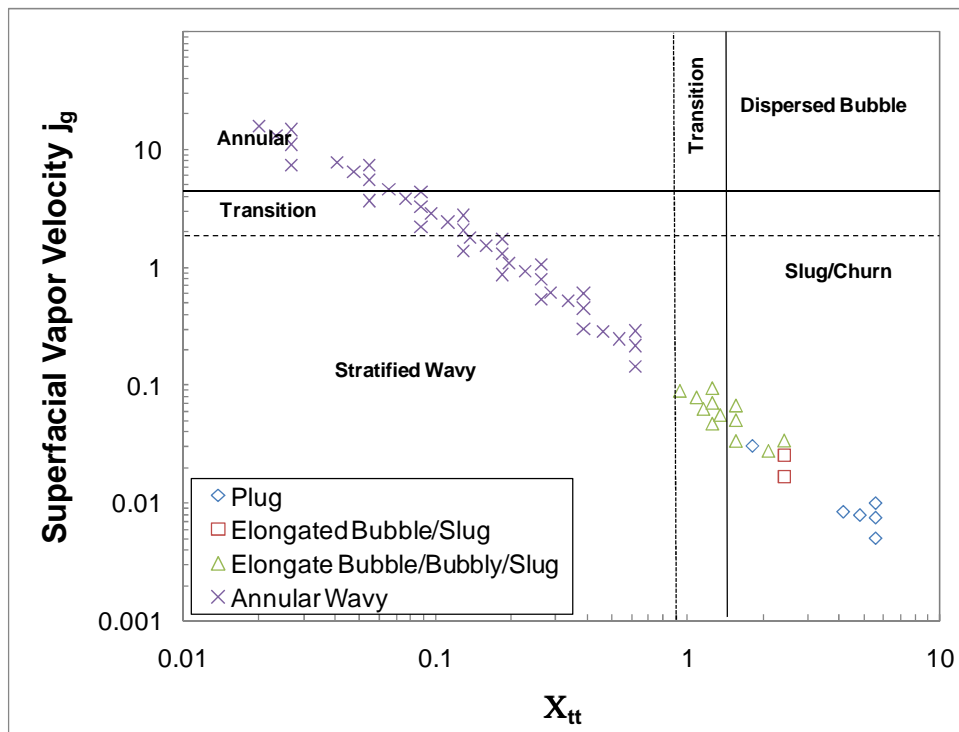
Figure 6-16 Visualization results of the 0.4 mm viewing window micro-channel plotted in a flow regime map developed Tandon et al. (1982)

All of the above three comparisons have a wavy flow regime before the annular flow regime, whereas for the particular channel studied here, such regime was not observed in the visual tests. This is possibly due to the difference in channel diameters. In the case of Wang et al. (1999), the channel hydraulic diameter was twice as large as the channel tested in this work. In addition, the Wang et al. (1999) study was conducted on a multi-port (10 channels) test segment where flow mal-distribution can occur, which may promotes a wavy flow.

When the data is compared to a micro-channel type of flow regime maps, as represented in the case shown in Figure 6-17 below, it is clear that the agreement is very good. Figure 6-17 presents the visual data points of this study on Coleman and Garimella's (2000, 2003) flow regime map. Their flow regime was generated from

two-phase flow tests conducted on a 0.76 mm circular micro-channel using R134a as the working fluid and for mass fluxes ranging from 150 to 750 kg/m^{2}s at reduced pressure lower than 0.35. The size of the channel used to generate their flow regime is comparable to the channel size used in this study and some testing conditions are also similar; thus, the flow map and the data agree to a great extent. It is also worth mentioning that Coleman and Garimella were able to observe the annular film and mist flow because the channel they used was glass where as in this study the narrowness of the viewing window made it difficult to see the vapor core and to determine whether there was a mist flow with the annular flow.
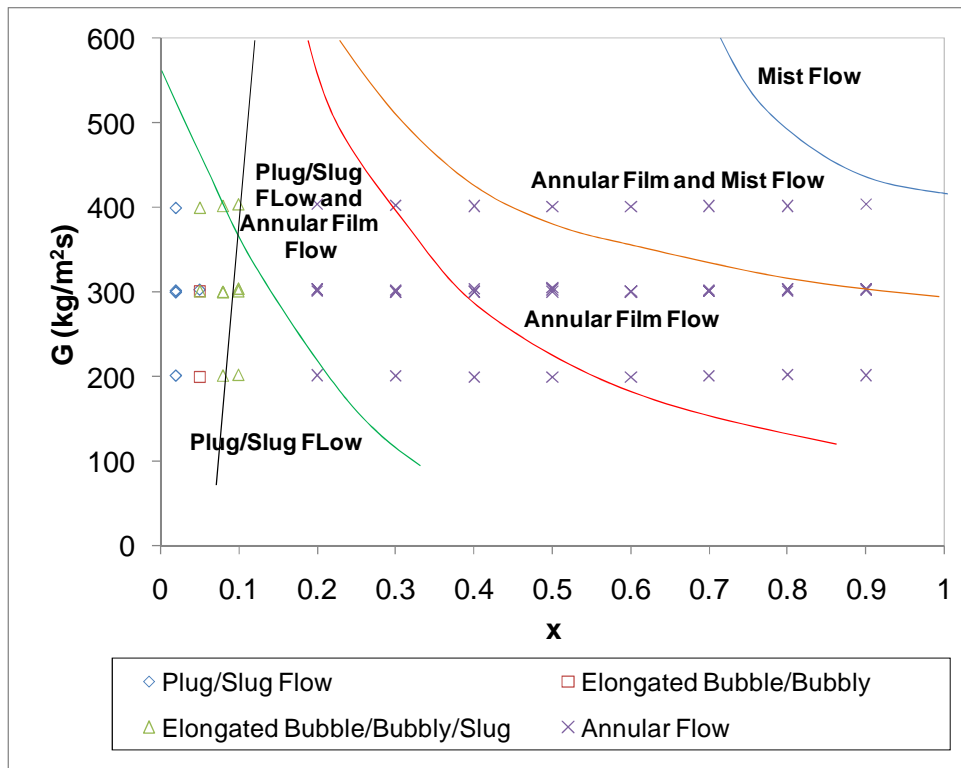
Figure 6-17 Visualization results of the 0.4 mm viewing window micro-channel plotted in a flow regime map developed Coleman and Garimella (2000, 2003)

The visual data of this tested channel showed a great agreement with the flow regime map developed by Cavallini et al. (2002). Figure 6-18 shows this comparison,

144

in which the plug/slug data points fell in the slug flow regime of the map and all

except one data point of the annular flow data fell in the annular flow regime of the
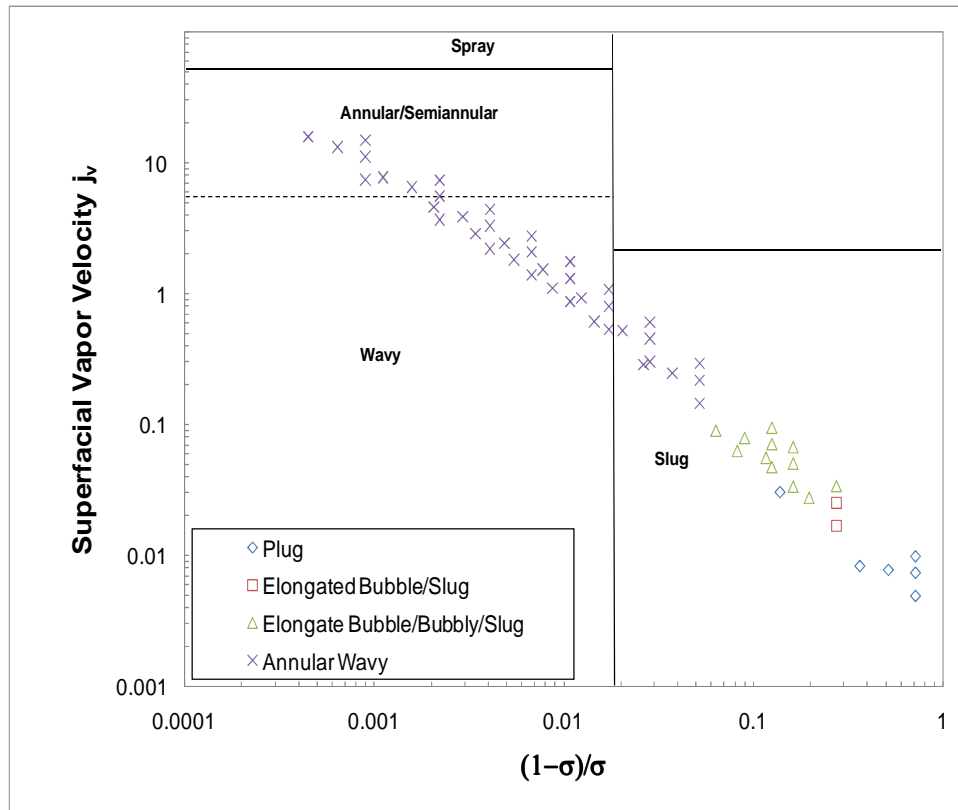
map.
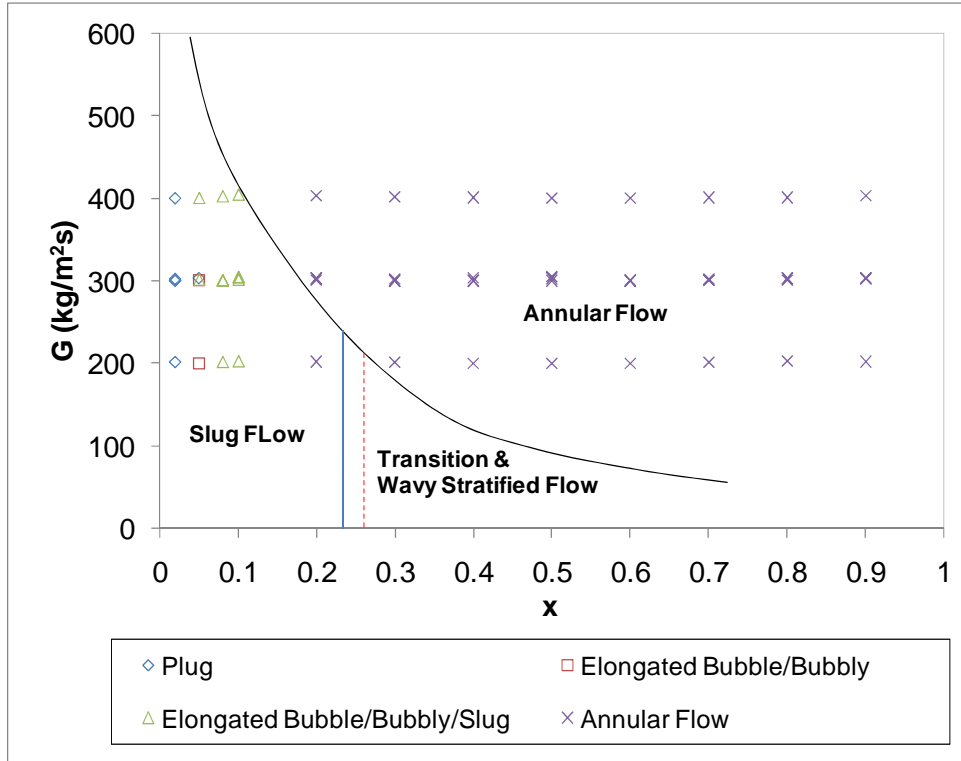
Figure 6-18 Visualization results of the 0.4 mm viewing window micro-channel plotted in a flow regime map developed Cavallini et al. (2002)

From the visualization results and the flow regime maps evaluated in this

study, we observed that the annular flow occurs at lower vapor qualities when the

mass flux increases causing the plug/slug flow regime to become narrower at high

mass fluxes, whereas the opposite happens when mass flux is decreased. Utilizing the

visualization data of the present study, a new flow regime map was developed. In this

study, only three mass fluxes were considered (200, 300 and 400 kg/m^{2}s). Thus, when

developing a flow regime map using the data collected the transition line became a

straight vertical line, as shown in Figure 6-19.
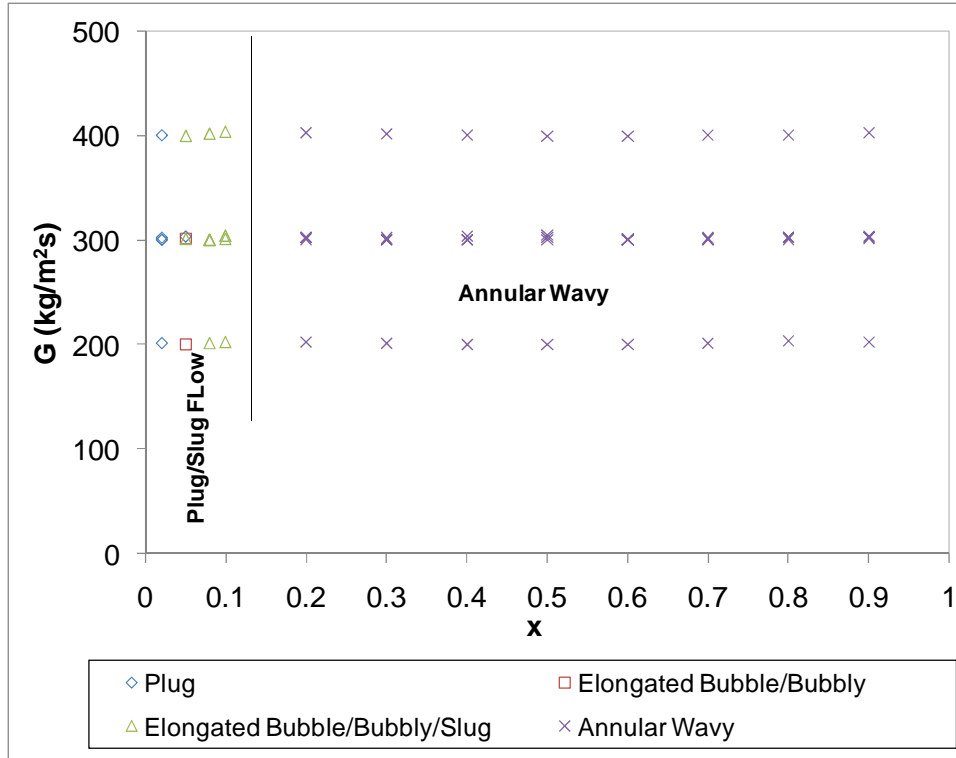
Figure 6-19 Newly developed flow regime map for data collected from the 0.4 mm viewing window micro-channel

6.1.3 Summary

This chapter shows the results of the visualization channels used to study the two-phase flow inside the channel. The results of the tests are presented in the form of pictures of the different flows and flow regime maps. A flow regime map was developed for each of the two visualization channel used in this study. The results were also compared with three different flow regime map types obtained from the literature. Comparison of the flow visualization maps with previous data and against the two channels studied here revealed improved understanding of the role of high aspect ratio micro-channels in condensation process.

CHAPTER 7: CONCLUSIONS AND RECOMMENDATIONS FOR FUTURE WORK

7.1 Conclusions

To characterize condensation heat transfer and pressure drop coefficients in micro channels with a small hydraulic diameter and high aspect ratio, a single micro-channel made of copper with the dimensions of 190 mm $\times$ 2.8 mm $\times$ 0.4 mm was fabricated. The study began with detailed survey of the open literature. Next, a testing apparatus was designed, built and equipped with all the necessary instrumentations to obtain accurate data. Then, parametric tests were conducted and analyzed for two selected refrigerants, R134a and R245fa. Utilizing a linear regression analysis, the effect of various operation parameters on both pressure drop and heat transfer coefficients was studied. Correlations of average heat transfer coefficients, average pressure drops and local pressure drops were developed by modifying the available correlations utilizing the experimental results of the present study. Finally, visualization tests of two-phase flow were conducted in two different channels. From the obtained visual data several flow regimes were characterized and the corresponding flow maps were developed.

From the analysis of the results the following conclusions can be drawn:

- The present research represents the first study of its kind to investigate condensation heat transfer in a single high-aspect ratio micro channel, combined with flow visualization experiments.

- Two refrigerants were selected for this study, on ehigh pressure (R-134a) and one new low pressure refrigerant (R-245fa). While, there are some previous study on condensation of R-134a, there has been no previous work on condensation of R-245fa in micro channels

- For both refrigerants, the heat transfer and pressure drop coefficients decreased with an increase in the saturation temperature.

- As expected, with increase in the mass flow, both heat transfer and pressure drop coefficients increased.

- The effect of inlet superheat on heat transfer and pressure drop coefficients was insignificant and for the most part within the experimental uncertainties. That is because for the range of inlet super heat studied the the fully developed condensation flow regime was hardly affected, thus negligible effect on heat transfer and pressure drops.

- Refrigerant R245fa on average demonstrated a 15%-better heat transfer performance than that of R134a, whereas the pressure drop for R245fa on average is almost three times higher than that of R134a for the same operating conditions. The reasons for this trend were documented in the thesis.

- The obtained heat transfer coefficients as well as pressure drop in high aspect ratio micro-channel studied are considerably higher than those in the corresponding macro and mini-channels. The main reasons for the better performance are documented in the thesis.

- Among the correlations available for micro and mini-channels, the best match model for heat transfer is the void fraction model and the classical pressure model for the average and local pressure drops. The said correlations were modified to better match the experimental data of the present work.

- The visualization test sections are unique and very innovative in terms of design and fabrication. Also the visualization results obtained in this present work are one of its kinds. They open wide doors for researchers to further investigate the two-phase flow in high aspect ratio micro-channels.

- Several flow regimes were identified in the flow visualization experiments, including plug/slug, wavy film and annular flow regimes.

- The various flow regime maps identified in the present study were compared with those available in the literature. While the flow maps for studies in micro-channels were for the most part in good agreement with the present experiments. It is difficult to draw definitive conclusions on any deviations in the fundamental physics between the high aspect ratio micro-channel tested in this study and those of the mini-channels. In particular, effect of aspect ratio on condensation in micro-channels needs to be further studied.

7.2 *Recommendations for Future Work*

- Design and test a multi-channel heat exchanger with channels of similar size to the ones tested in this study for further verification and improvement of the correlations to include multi-passage channels. Potential flow misdistribution for condensation in a practical heat exchanger of this nature might be a serious problem and should be studied.

- Conduct experiments in channels with hydraulic diameter similar to that of the present study, but with different shapes to characterize the effect of channel shape.

- Evaluate a channel with aspect ratio higher than that of the current channel and another with lower aspect ratio to further quantify the effect of aspect ratio for condensation in the current micro-channel geometry.

- Accompany each of the above recommended tests with visualization tests and combine the results with the current study to develop a more general flow regime map.

- The results of the above additional recommended tests and the associated visualization results can be used to develop more reliable correlations for condensation in high aspect ratio micro-channels.

Bibliography

Azer, N.Z., L. V. Abis, and H. M. Soliman. "Local Heat Transfer Coefficient During Annular Flow Condensation." *ASHRAE Transactions* 78, no. 2 (1972): 135-134.

Baird, J.R., D.F. Fletcher, and B.S. Haynes. "Local Condensation Heat Transfer Rate in Fine Passages." Edited by 4466. *Int. J. of Heat and Mass Transfer* 46 (2003): 4453.

Baker, O. "Simultaneous Flow of Oil and Gas." *Oil and Gas Journal* 53 (1954): 185-195.

Bergles, Arthur E., H. John Lienhard V, Gail E. Kendall, and Peter Griffith. "Boiling and evaporation in small diameter channels." *Heat Transfer Engineering* 24, no. 1 (2003): 18-40.

Bontemps, A. "Measurements of single-phase pressure drop and heat transfer coefficient in micro and minichannels." *Microscale Heat Transfer* (Springer), 2005: 25-48.

Breber, G, J W Palen, and J Taborek. "Prediction of Horizontal Tubeside Condensation of Pure Components Using FLow Regime Criteria." *Journal of Heat Transfer, Transactions ASME* 102, no. 3 (1980): 471-476.

Cavallini, A., G. Censi, D. Del Col, L. Doretti, G.A. Longo, and L. Rossetto. "Condensation of Halogenated Refrigerants inside Smooth Tubes." *HVAC&R Research* 8, no. 4 (2002): 429-451.

Chen, I. Y. "Two-Phase Pressure Drop of Air-Water and R410 in Small Horizontal Tubes." *Int. J. Multiphase Flow* 27 (2001): 1293-1299.

Chen, J. "Correlation for Boiling Heat Transfer for Saturated Fluid in Convective Flow." *Ind. Eng. Chem. Process Des. Dev.* 5, no. 3 (1966): 322-329.

Chisholm, D. "Pressure Gradients Due to Friction During the Flow of Evaporationg Two-Phase Mixtures in Smooth Tubes and Channels." *International Journal of Heat and Mass Transfer* 16, no. 2 (1973): 347-358.

Coleman, J W. "Flow Visualization and Pressure Drop in Small Hydraulic Diameter Geometries During Phase Change of Refrigerants." *Mechanical Engineering* Ph.D Thesis (2000).

Coleman, J. W., and S. Garimella. "Charactaristic of Two-Phase Patterns in Small Diameter Round and Rectangular Tubes." *Int. J. Heat Mass Transfer* 42 (1999): 2869-2881.

Coleman, J.W., and S. Garimella. "Two-Phase Flow Regime Transitions in Microchannel Tubes: The Effect of Hydraulic Diameter." *In: Procedings of ASME Heat Transfer Division* (ASME IMECE2000) 4 (2000-I): 71-83.

Coleman, J.W., and S. Garimella. "Two-Phase Flow Regimes in Round, Square and Rectangular Tubes During Condensation of Refrigerant R134a." *International Journal of Refrigeration* 26, no. 1 (2003): 117-128.

Coleman, J.W., and S. Garimella. "Visualization of Two-Phase Refrigerant Flow During Phase Change." *In: 34th National Heat Transfer Conference*, 2000-II: nHTC2000-12115.

Cornwell, K, and P A Kew. "Boiling in small parallel channels." In *Energy Efficiency in Process Technology*, by P A Pilavachi, 624-638. New York: Elsevier, 1993.

Dobson, M. K., and J. C. Chato. "Condensation in Smooth Horizontal Tubes." *ASME Journal of Heat Transfer* 120 (1998): 193-213.

El Hajal, J., J. Thome, and A. Cavallini. "Condensation in Horizontal Tubes, Part I: Two-Phase Flow Pattern Map." *International Journal of Heat and Mass Transfer* 46 (2003): 3349-3363.

Friedel, L. "Improved Friction Pressure Drop Correlations for Horizontal and Vertical Two Phase Flow." *3R International* 18, no. 7 (July 1979): 485-491.

Garimella, S., A. Agarwell, and J. D. Killion. "Condensation Presssure Drop in Circular Micro-Channels." *Heat Transfer Engineering* 26, no. 3 (2005): 28-35.

Garimella, S., J. D. Killion, and J. W. Coleman. "An Experimentally Validated Model for Two Phase Pressure Drop in the Intermittent Flow Regime for Noncircular Micro-Channels." *Journal of Fluid Engineering* 125 (2003): 887-894.

Garimella, Srinivas. "Condensation Flow Mechanisms in Microchannels Basis for Pressure Drop and Heat Transfer Models." *Heat Transfer Engineering*, 2004: 104-116.

Griffith, P, and K S Lee. "Stability of Annulus of Liquid in Tube." *Journal of Basic Engineering, Transactions ASME* 86, no. 4 (1964): 666-668.

Jassim, E W, and T A Newell. "Prediction of Two-Phase Pressure Drop and Viod Fraction in Microchannels using Probabilistic Flow Regime Mapping." *International Journal of Heat and Mass Transfer* 49 (2006): 2446-2457.

Jund, D., K. Song, Y. Cho, and S. Kim. "Flow Condensation Heat Transfer Coefficient of Pure Refrigerants." *Int. J. of Refrigeration* 26 (2003): 4-11.

Jung, D S, and R Radermacher. "Prediction of Pressure Drop During Horizontal
Annular Flow Boiling of Pure and Mixed Refrigerants." *International Journal
of Heat and Mass Tranfer* 32, no. 12 (1989): 2435-2446.

Kattan, N., J. R. Thome, and D. Favrat. "Flow Boiling in Horizontal Tubes: Part I -
Development of a Diabatic Two-Phase Flow Pattern Map." *Joutnal of Heat
Transfer, Transactions ASME* 120, no. 1 (1998-I): 140-147.

Kattan, N., J. R. Thome, and D. Favrat. "Flow Boiling in Horizontal Tubes: Part II -
New Heat Transfer Data for Five Refrigerants." *Journal of Heat Transfer,
Transactions ASME* 120, no. 1 (1998-II): 148-155.

Kattan, N., J. R. Thome, and D. Favrat. "Flow Boiling in Horizontal Tubes: Part III
Developement of a New Heat Transfer Model Based on Flow Pattern."
Journal of Heat Transfer 120, no. 1 (1998-III): 156-165.

Kim, M H, J S Shin, C Huh, T J Kim, and K W Seo. "A Study of Condensation Heat
Transfer in a Single Mini-Tube and a Review of Korean Micro- and Mini-
Channels Studies." *Proc. of the First Int. Conference on Microchannels and
Minichannels*, April 2003: 47-58.

Lee, H J, and Y Lee. "Pressure Drop Correlations for Two-Phase Flow within
Horizontal Rectangular Channels with Small Heights." *International Journal
of Mulitiphase flow* 27, no. 5 (2001): 783-796.

Lockhart, R. W., and R. C. Martinelli. "Proposed Correlation of Data for Isothermal
Two-Phase, Two Component Flow in Pipes." *Chem. Eng. Prog.* 45, no. 1
(1949): 39-48.

Mandhane, J M, G A Gregory, and K Aziz. "A flow Pattern Map for Gas-Liquid Flow in Horizontal and Inclined Pipes." *International Journal of Multiphase Flow* 1 (1974): 537-553.

Martinelli, R. C., and B. Nelson. "Prediction of Pressure Drop During Forced-Circulation Boiling Water." *Trans. ASME* 70 (1948): 695-702.

Mishima, K, and M Ishii. "Flow Regime Transition Criteria for Upward Two-Phase Flow in Vertical Tubes." *International Journal of Heat Transfer and Mass Transfer* 27, no. 5 (1984): 723-737.

Mishima, K, and T Hibiki. "Some Characteristics of Air-Water Two-Phase Flow in Small Diameter Vertical Tubes." *International Journal of Multiphase Flow* 22, no. 4 (1996): 703-712.

Mitra, B. "Supercritical Gas Cooling and Condensation of Refrigerant R410a at near-Critical Pressures." *Mechanical Engineering* , 2005.

Paleev, J. J., and B. S. Filippovich. "Phenomena of Liquid Transfer in Two-Phase Dispersed Annular Flow." *Int. J. Heat Transfer* 9 (1966): 1089-1093.

Pierre, Bo. "Flow Resistance With Boiling Refrigerants. Part I." *ASHRAE Journal*, 1964: 58-65.

Riehl, R. R., P M Seleghim Jr., and J. M. Ochterbeck. "Comparison of Heat Transfer Correlations for Single- and Two-Phase Microchannel Flows for Microelectronics Cooling." *ITherm'98 – Sixth Intersociety Conference on Thermal and Thermomechanical Phenomena in Electronic Systems*, May 1998: 409-416.

Riehl, R., and Jay M. Ochterbeck. "Experimental Invertigation of the Convective Condensation Heat Transfer in Microchannel Flows." *Proceedings of the ENCIT*. Caxambu-MG, Brazil, 2002. CIT02-0495.

Rouhani, Z., and E. Axelsson. "Calculation of Void Fraction in the Sub-cooled and Quality boiling Regions." *International Jouranl of Heat and Mass Transfer* 13 (1970): 383-393.

Saho, D. W., and E. G. Granryd. "Flow Pattern Heat Transfer and Pressure Drop in Flow Condensation Pat I: Pure and Azeotropic Refrigerants." *International Journal of HVAC&R Research* 6, no. 2 (2000): 175-195.

Shah, M. "A general Correlation of Heat Transfer During Film Condensation Inside Pipes." *International Journal of Heat Transfer* 22 (1978): 547-556.

Shah, M. "A New Correlation for Heat Transfer During Boiling Flow Through Pipes." *ASHRAE Transactions* 82, no. 2 (1976): 66-86.

Shin, J. S., and M. H. Kim. "An Experimental Study of Condensation Heat Transfer Inside t techniquea Mini-Channel With a New Measureme." *Int. J. Multiphase Flow* 30 (2004): 311-325.

Smith, S. L. "Void Fraction in Tow-phase Flow: A Correlation Based Upon an Equal Velocity head Model." *Heat Fluid Flow* 1 (1971): 22-39.

Smith, S. L. "Void Fractions in Two-Phase FLow: A Correlation Based Upon an Equal Velocity Head Model." *Proc. Instn. Mech. Engrs.* 184, no. Part 1(26) (1969): 647-664.

Souza, A L, J C Chato, J P Wattelet, and B R Christoffersen. "Pressure drop during two-phase flow of pure refrigerants and refrigerant-oil mixture in horizontal

smooth tubes." *Heat Transfer with Alternate Refrigerants (ASME), HTD* 243 (1993): 35-41.

Steiner, D. "Heat Transfer to Boiling Saturated Liquids." *VDI-Heat Atlas*, 1993: 1-33.

Suo, M, and P Griffith. "Two-Phase Flow in Capillary Tubes." *Journal of Basic Engineering, Transaction ASME* 86, no. 3 (1964): 576-582.

Taitel, Y, and A E Dukler. "A Model for Predicting Flow Regime Transitions in Horizontal and Near Horizontal Gas-Liquid Flow." *American Institute of Chemical Engineering Journal* 22 (1976): 47-55.

Tandon, T. N., H. K. Varma, and C. P. Gupta. "A New Flow Regimes Map for Condensation Inside Horizontal Tubes." *Journal of Heat Transfer, ASME* 104 (1982): 763-768.

Thome, J. R., J. El Hajal, and A. Cavallini. "Condensation in Horizontal Tubes Part II: New Heat Model Based on Flow Regimes." *International Journal of Heat and Mass Transfer* 46 (2003): 3365-3387.

Tran, T N, M C Chyu, M W Wanbsganss, and D M France. "Two-phase pressure drop of refrigerants during flow boiling in small channels: An experimental investigation and correlation development." *International journal of Multiphase Flow* 26 (2000): 1739-1754.

Triplett, K A, S M Ghiaasiaan, S I Abdel-Khalik, A LeMouel, and B N McCord. "Gas=Liquid Two-phase Flow in Microchannels. Part 2: Void Fraction and Pressure Drop." *International Journal of Multiphase Flow* 25, no. 3 (1999): 395-410.

Troniewski, L, and R Ulbrich. "Two-Phase Gas-Liquid Flow in Rectangular
   Channels." *Chemical Engineering Science* 39, no. 4 (1984): 751-765.

Wang, W. W. W. "Condensation and Single-Phase Heat Transfer Coefficient and
   Flow Regime Visualization in Microchannel Tubes for HFC-134a." *The Ohio
   State University*, 1999: Ph.D. Thesis 194 pp.

Wang, W.W., T.D. Radcliff, and R.N. Christensen. "A Condensation Heat Transfer
   Correlation for Millimeter-Scale Tubing With Flow Regime Transition." *Exp.
   Thermal Fluid Sci.* 26 (2002): 472-485.

Webb, R L, and R N Zhang. "Condensation Heat Transfer in Small Diameter Tubes."
   Proceedings of the 11th International Heat Transfer Conference 6 (1998):
   403-408.

Weisman, J, D Duncan, J Gibson, and T Crawford. "Effects of Fluid Properties and
   Pipe Diameter on Two-Phase Flow Patterns in Horizontal Lines." *Int. J.
   Multiphase Flow* 5, no. 6 (1979): 437-462.

Wheeler, M W, F R Best, and T R Reinarts. "An investigation of two phase flow
   pressure drops in a reduced acceleration environment." *AIP Conference
   Proceedings* 271, no. 3 (1993): 987-992.

Wilson, M J, T A Newell, J C Chato, and C A Infante Ferreira. "Refrigerant Charge,
   Pressure Drop, and Condensation Heat Transfer in Flattened Tubes."
   International Journal of Refrigeration 26, no. 4 (2003): 442-451.

Wojtkowiak, J., and Cz. O. Poiel. "Viscosity Correlation Fractor for Rotameter." *J.
   Fluids Eng.* 118, no. 3 (1996): 569-574.

Yang, C. Y., and C. C. Shieh. "FLow Pattern of AIr -Water and Two-Phase R-134a in Small Circular Tibes." *Int. J. Multiphase Flow* 27 (2001): 1163-1177.

Zhang, M, and R L Webb. "Correlation of Two-Phase Friction for Refrigerants in Small-Diameter Tubes." *Experimental Thermal and Fluid Science* 25, no. 3-4 (2001): 131-139.

Zhang, M, and S L Kwon. "Two-phase frictional pressure drop for refrigerants in small diameter tubes." In *Compact Heat Exchangers and Enhancement Technology for the Process Industries*, by M Zhang and N D Kwon, edited by R K Shah. New York: Begall House, 1999.

Zhang, M., and R. L. Webb. "Correlation of Two-Phase Friction for Refrigerats in Small-Diameter Tubes." *Exp. Therm. Fluid Sci.* 25 (2001): 131-139.

Zhao, T S, and Q Liao. "Theoretical Analysis of Film Condensation Heat Transfer Inside Vertical Mini Triangular Channels." *Int. J. Heat and Mass Transfer* 45 (2002): 2829-2842.